AD-A059 960 VARIAN ASSOCIATES PALO ALTO CALIF F/G 17/5
1.06-MICRON III-V PHOTOCATHODE DEVELOPMENT.(U)
MAY 78 J S ESCHER, P E GREGORY, S B HYDER F33615-76-C-1351
UNCLASSIFIED AFAL-TR-78-78 NL

1 OF 2
ADA
059960

AFAL-TR-78-78

LEVEL II

1.06 - MICRON III-V PHOTOCATHODE DEVELOPMENT

J. S. ESCHER
P. E. GREGORY
S. B. HYDER
R. R. SAXENA
VARIAN ASSOCIATES, INC.
PALO ALTO, CALIFORNIA 94303

MAY 1978

TECHNICAL REPORT AFAL-TR-78-78
Interim Report – November 1976 - November 1977

Approved for public release; distribution unlimited.

AIR FORCE AVIONICS LABORATORY
AIR FORCE WRIGHT AERONAUTICAL LABORATORIES
AIR FORCE SYSTEMS COMMAND
WRIGHT-PATTERSON AIR FORCE BASE, OHIO 45433

NOTICE

When Government drawings, specifications, or other data are used for any purpose other than in connection with a definitely related Government procurement operation, the United States Government thereby incurs no responsibility nor any obligation whatsoever; and the fact that the government may have formulated, furnished, or in any way supplied the said drawings, specifications, or other data, is not to be regarded by implication or otherwise as in any manner licensing the holder or any other person or corporation, or conveying any rights or permission to manufacture, use, or sell any patented invention that may in any way be related thereto.

This report has been reviewed by the Information Office (OI) and is releasable to the National Technical Information Service (NTIS). At NTIS, it will be available to the general public, including foreign nations.

This technical report has been reviewed and is approved for publication.

Donald J Peacock

DONALD J. PEACOCK
Project Engineer

Donald R. Locker

DONALD LOCKER
Acting Group Leader
Electro-Optic Detectors

FOR THE COMMANDER

William C Schoonover

William C. Schoonover, Chief
Electro-Optics Technology Branch
Electronic Technology Division

"If your address has changed, if you wish to be removed from our mailing list, or if the addressee is no longer employed by your organization please notify AFAL/DHO *, W-PAFB, OH 45433 to help us maintain a current mailing list".*

Copies of this report should not be returned unless return is required by security considerations, contractual obligations, or notice on a specific document.

AIR FORCE/56780/7 September 1978 — 100

SECURITY CLASSIFICATION OF THIS PAGE (When Data Entered)

REPORT DOCUMENTATION PAGE

READ INSTRUCTIONS BEFORE COMPLETING FORM

1. REPORT NUMBER: AFAL-TR-78-78	2. GOVT ACCESSION NO.
3. RECIPIENT'S CATALOG NUMBER	Annual technical rept. no. 1,
4. TITLE (and Subtitle): 1.06-MICRON III-V PHOTOCATHODE DEVELOPMENT.	5. TYPE OF REPORT & PERIOD COVERED: Interim Report Nov 1976 — Nov 1977
	6. PERFORMING ORG. REPORT NUMBER
7. AUTHOR(s): J. S. Escher, P. E. Gregory, S. B. Hyder, and R. R. Saxena	8. CONTRACT OR GRANT NUMBER(s): F33615-76-C-1351
9. PERFORMING ORGANIZATION NAME AND ADDRESS: Varian Associates, Inc. 611 Hansen Way Palo Alto, CA 94303	10. PROGRAM ELEMENT, PROJECT, TASK AREA & WORK UNIT NUMBERS: Project 2001 Task 200103 Work Unit 20010360 03
11. CONTROLLING OFFICE NAME AND ADDRESS: Air Force Avionics Laboratory (DHO) AF Wright Aeronautical Laboratories, AFSC Wright-Patterson AFB, Ohio 45433	12. REPORT DATE: May 1978
	13. NUMBER OF PAGES: 103
14. MONITORING AGENCY NAME & ADDRESS (if different from Controlling Office): DCASMA San Francisco 1250 Bayhill Drive San Bruno, CA 94066	15. SECURITY CLASS. (of this report): Unclassified
	15a. DECLASSIFICATION DOWNGRADING SCHEDULE

16. DISTRIBUTION STATEMENT (of this Report)

Approved for public release; distribution unlimited.

17. DISTRIBUTION STATEMENT (of the abstract entered in Block 20, if different from Report)

18. SUPPLEMENTARY NOTES

Annual Technical Report No. 1

19. KEY WORDS (Continue on reverse side if necessary and identify by block number)

transferred-electron photoemission
heterojunctions
III-V compounds
1.06-micron detector
Schottky barriers

20. ABSTRACT (Continue on reverse side if necessary and identify by block number)

The design, fabrication, and initial evaluation of three transferred-electron (field assisted) photocathodes for high performance 1.06-micron detection are reported. 2.7% and 2.8% yields at 1.06 have been achieved from a direct emitter and a hybrid InP/InGaAsP heterojunction cathode, respectively. Feasibility of p-InGaP as a transferred-electron emitter has been demonstrated.

DD FORM 1 JAN 73 1473 EDITION OF 1 NOV 65 IS OBSOLETE

SECURITY CLASSIFICATION OF THIS PAGE (When Data Entered)

PREFACE

The work reported here was supported by the Air Force Avionics Laboratory, Wright-Patterson Air Force Base, Ohio, under contract F33615-76-C-1351. The Monitoring Engineer is Mr. Donald J. Peacock. The program is aimed at the development of III-V high performance bias-assisted photocathodes for 1.06-micron detection.

The work was carried out in the Varian Corporate Research Solid State Laboratory. Contributions to this work were made by J. S. Escher, P. E. Gregory, S. B. Hyder, and R. R. Saxena. The Program Manager is R. L. Bell.

TABLE OF CONTENTS

LIST OF ILLUSTRATIONS

LIST OF ILLUSTRATIONS (Contd.)

LIST OF ILLUSTRATIONS (Contd.)

LIST OF ILLUSTRATIONS (Contd.)

SUMMARY

It is the general purpose of this work to significantly improve the state-of-the-art in 1.06-micron photocathode devices for use in active laser communications and imaging systems. The overall goal of the program is to develop a high sensitivity III-V semiconductor 1.06-micron photocathode utilizing field-assisted, transferred-electron (TE) photoemission. The cathode structure should be capable of 20% quantum efficiency, large active area, and sealed-off tube operation.

The most sensitive 1.06-micron photocathodes available today are the negative electron affinity (NEA) III-V semiconductor cathodes. Yields of 0.5 to 3.0% at 1.06 microns are commercially available in a photomultiplier tube from Varian Associates, Inc. Achieving a high quantum efficiency from a single-crystal III-V photoemitter is largely a question of electron surface escape probability since the processes of photon absorption and electron diffusion to the surface can be quite efficient. Work function and surface barrier effects at the vacuum-semiconductor interface limit the successful transport of photoexcited electrons into vacuum. In order to overcome the surface barrier effects, various externally-biased cathodes have been studied over the years. A number of p-n junction, MOS, field-emission, and heterojunction bias-assisted photocathodes have been proposed and experimentally studied but none has shown reasonably efficient photoemission combined with low dark current emission to be of practical interest.

In 1974 however, Bell, James, and Moon of this laboratory demonstrated a bias-assisted p-InP cathode using for the first time the mechanism of TE photoemission. TE photoemission is based on the fact that for certain III-V semiconductors such as InP, InGaAsP alloys, and GaAs, electrons can be promoted to the upper conduction band valleys with reasonable efficiency by applying modest electric fields. Photogenerated electrons with successfully transfer to the upper valleys have a good probability of

being emitted over the work function and surface energy barriers into vacuum. Encouraged by this initial result, work at Varian on TE photocathodes has progressed steadily over the past three years with a major emphasis being made on both 1-2 micron passive night vision detectors and this work on high performance 1.06-micron detectors.

There are three TE photocathode designs under current evaluation for high efficiency 1.06-micron detection. The first of these is a p-InGaAsP direct emitter cathode in which the processes of photogeneration and electron emission are confined (as in a NEA cathode) to a single active layer. This is the simplest of designs and from a materials standpoint the most straightforward and highly developed. Vacuum photoemission experiments from direct emitter cathodes have demonstrated 1.06-micron yields up to 2.7% under full bias conditions. This represents a factor of 10 to 20 improvement over a conventional S-1 cathode and is comparable to a good NEA cathode. The second approach is that of a hybrid p-InP/p-InGaAsP TE heterojunction cathode. The heterojunction cathode separates the functions of photoelectron generation (p-InGaAsP) and electron emission (p-InP) into distinct layers. In principle, the heterojunction approach should achieve a higher efficiency device since each function can in principle be separately optimized. 2.8% reflection-mode yield at 1.06 microns has been achieved from a hybrid heterojunction cathode during this reporting period.

The third cathode design, which offers the highest potential 1.06-micron sensitivity, is a p-InGaP/p-InGaAs heterojunction TE cathode. The electron emitting layer (p-InGaP) has a higher bandgap than that of p-InP, 1.7 eV vs 1.35 eV. Therefore it is anticipated (based on experimental NEA work) that the surface escape probability from a p-InGaP emitter would be superior to that of p-InP, and hence offer improved performance over that of either the p-InGaAsP direct emitter cathode or the p-InP/p-InGaAsP

heterojunction cathode. An all vapor phase epitaxy system has been designed, debugged, and made operational to grow the InGaP/InGaAs structure. Details of this system are discussed, along with some initial photoemission experiments from p-InGaP emitter cathodes. Feasibility of p-InGaP as a TE emitter cathode was established along with some encouraging photoemission results from the first p-InGaP/p-InGaAs cathode.

Excellent progress has been achieved during this first year toward developing the necessary materials and vacuum processing technologies to reach the program goals. A continuing effort is clearly needed however to further improve the direct emitter and hybrid heterojunction TE cathodes. A more detailed analysis of the surface escape probability for a TE cathode is needed. More materials work is needed on the p-InGaP/p-InGaAs heterojunction cathode. Progress in this area should be rapid however since most of the initial growth system problems have been solved.

1. INTRODUCTION

It is the general purpose of this work to significantly improve the state-of-the-art in 1.06-micron photoemission devices for use in active laser imaging and communications systems. The overall goal of the program is to develop high sensitivity III-V semiconductor 1.06-micron photocathodes utilizing field-assisted, TE photoemission. The cathode structure should be capable of 20% quantum efficiency, large active area, and sealed-off tube operation.

In order to put the present field-assisted photocathode program in better perspective, it is worthwhile to briefly review some of the prior field-assisted work. The following section discusses three photocathode designs, based on the TE effect, which form the basis of the work described in this report.

As is well known, work function and surface barrier effects at the interface with the activating layer[1] make it necessary to consider biasing photocathodes in order to achieve useful photoemission beyond about 1.1-micron wavelength. In order to overcome the surface barrier effects, various externally-biased cathodes have been studied over the past 18 years beginning with the work of Simon and Spicer at RCA.[2,3] Historically, the bulk of the field-assisted photocathode work up to 1968 had been on reverse-biased p-n junction devices activated with Cs or Cs and oxygen to reduce the work function at the surface. The external quantum efficiencies achieved into vacuum however were limited to $\leq 10^{-4}$ (electrons/incident photon) in all cases.[4-6] With the advent of the negative electron affinity (NEA) cathode development in the late 1960's,[7] there was relatively little work done on externally-biased cathodes. However it soon became clear that the limit to high yield (> 0.10% quantum efficiency) NEA photoemission was around 1.1 micron.

A number of field-assisted projects were initiated under ARPA support in the early 1970's aimed at the 1-2 micron range. A passive night vision device taking advantage of the strong airglow radiation beyond 1 micron is the primary application of the 1-2 micron program, althougn other applications would certainly emerge if such a device could be demonstrated. Some of these approaches involved the reverse-biased p-n junction for either area or edge emission utilizing the improved device and vacuum technology of the day. Groups at RCA[8] and UCLA[9] pursued this approach most recently. Difficulties with junction breakdown during vacuum heat cleaning and fabrication of ultrathin plane parallel junctions were the most serious problems. Approximately 10^{-4} quantum efficiency at 1.06 microns into vacuum was achieved at UCLA from a silicon device. Another approach has been the reverse-biased Schottky-barrier device based on the work of White and Logan.[10] A thin metal film is evaporated onto a p-type semiconductor and reverse-biased. Experimental yields from these devices have been limited to less than 10^{-4} quantum efficiency.[11-13] A slight modification of the Schottky-barrier approach is an MOS structure reported by Foss at CBS Laboratories.[14] 10^{-3} quantum efficiency at 1.06 microns was achieved into vacuum from an Al-SiO_2-Si device activated with Cs and oxygen. The dark current from the MOS device under bias conditions was on the order of 10^{-5} A/cm^2 -- much too high for practical applications.

A similar approach to the MOS cathode is the tunnel emitter. This work, first carried out at the University of Minnesota, then at RCA Laboratories, and more recently at the Night Vision Laboratory, Ft. Belvoir, VA, is based on an ultrathin insulator sandwiched between either two semiconductors or a semiconductor and a thin metal film. Al_2O_3 grown by chemical vapor deposition was the major insulator studied. Field-assisted photoemission has been achieved from a Si-Al_2O_3-Ag structure activated with Cs and oxygen. High dark current and poor frequency response seem

to be the major difficulties with the Si tunnel emitter device. Similar structures fabricated from Ge have not shown photoemission into vacuum.

An entirely new approach to a field-assisted cathode was brought forward in the early 1970's by various groups employing the idea of a double heterojunction structure. The complete cathode consists of a low bandgap photon absorbing layer followed by a high bandgap hole barrier, necessary for external biasing, and an electron emitting layer capable of high efficiency NEA photoemission (e.g. GaAs). Ideally, under reverse-bias conditions, the conduction bands of the device should allow thermalized photoexcited electrons to diffuse and/or drift efficiently from the photon absorbing layer across the hole barrier layer into the electron emitting layer and finally into vacuum. Groups at Carnegie-Mellon University[15] and Rockwell International[16] have pursued this approach most recently. No vacuum photoemission results have come forward to date however. The Carnegie-Mellon cathode was a Ge-Zn-Se-GaAs:Cs-O device. Satisfactory fabrication of the complete structure was not achieved. Efficient electron transfer from the Ge into the ZnSe hole barrier could not be demonstrated. The cathode structure most extensively investigated by the Rockwell group for 1.06 microns was a GaAsSb-GaAlAs-GaAs structure grown on GaAs. This liquid phase epitaxial grown structure is not a completely lattice-matched system. The composition of the GaAlAs hole barrier was such that the entire lattice mismatch was accommodated at the GaAsSb-GaAlAs interface. Although no vacuum photoemission results have been obtained, on-the-bench internal photoemission results indicate poor electron transport across the GaAsSb-GaAlAs interface. It would also be expected that junction deterioration problems might be encountered with this or similar devices during the vacuum heat cleaning procedure commonly used to clean the semiconductor-vacuum surface.

Another interesting field-assisted cathode approach is the field emission photocathode based on earlier work on single field point emitters. Arrays of Si-based field emitters have been successfully fabricated by groups at Westinghouse Research Laboratories[17] and at SRI.[18] 7.5% quantum efficiency into vacuum has been achieved at 300°K. The major problems are a room temperature dark current on the order of 10^{-6} A/cm^2 under bias conditions and a limited MTF. Arrays of Ge-based field emitters, for > 1 micron response, have not been successfully fabricated to date.

The work at Hughes on thin Ag films on Si[19] is particularly relevant to the present program. The initial idea of their "Studies of Silver Interlayer Photocathodes at 1.06 Microns" was to demonstrate improved 1.06-micron semitransparent yield from a thinned Si:Cs-O photocathode through the introduction of a thin Ag interlayer at the Si:Cs-O interface. An enhancement in 1.06-micron semitransparent quantum efficiency of approximately 50% would arise simply from the increased optical reflection of near bandgap radiation back into the Si. Furthermore, it was felt that since the work function of Cs-O activated Ag could be processed to $\leq$ 1.0 eV[20] and that electron losses through a thin Ag film should not be a serious loss for low energy electrons[21] the transport of photogenerated electrons into vacuum should be good. The feeling was that the work function on the Ag film could be made lower than the interface Cs-O barrier height ($\sim$ 1.1 to 1.2 eV) found on semiconductor:Cs-O interfaces.[22] In principle the device could operate with an applied reverse bias to the Ag film to give an additional "effective" negative electron affinity between the conduction band in the bulk and the vacuum potential. In practice, the Si:Ag:Cs-O yields were low. Sputter-Auger depth chemical profiling and Rutherford backscattering of 280 keV He^{++} analysis indicated a significant region of mixed semiconductor-metal. The depth of the intermixing

was difficult to measure directly since it was felt that the thinnest films (100-200 Å) may well have microscopic thickness variations on the same order as the film thickness. SEM micrographs at 120,000x supported the thickness variation or surface roughness contention. The net effect of the intermixing was to reduce the surface escape probability either through (1) Ag acting as a compensating impurity leading to a relatively deep band-bending region or (2) increased photoelectron scattering in the mixed region. A final experimental observation made by the Hughes group was that the photoelectric threshold on Si:Ag:Cs-O surfaces was found to be thickness-dependent for films less than about 300 Å thick. The thinnest Ag films were found to have a photoelectric threshold 0.10 to 0.15 eV higher than the thickest films.

Several conclusions can be drawn from the above brief history of field-assisted photocathode work (which has excluded recent work here at Varian). First, significant difficulties have been encountered with junction deterioration during vacuum heat-cleaning procedures. Junctions which are exposed should be passivated such that they can be cycled to around 600°C in vacuum. Second, all heterojunctions that photoexcited electrons cross must be nearly "ideal" heterojunctions--i.e. low recombination interfaces. In practice this means the heterojunction pair must be very closely lattice-matched. The GaAs-GaAlAs combination is the most well-known pair but InGaAsP alloys lattice-matched to InP are another example. Third, another major difficulty with reverse-biased p-n junction devices, apart from junction breakdown, is the fact that part of the transport is by hot electron transport across an ultrathin n-type region. Efficient electron transfer across such a region (without going to avalanching) is extremely difficult because of the short mean-free path for hot electrons. Internal p-n junctions therefore should not be considered as strong candidates for high efficiency field-assisted cathodes. Finally, the ability to fabricate reasonably large-area devices with good MTF and operate with stability at or near room temperature must be considered.

2. THE TRANSFERRED-ELECTRON PHOTOCATHODE

2.1 Previous Work on the TE Cathode

The work at Varian on field-assisted devices began in 1974 with the successful demonstration of TE photoemission from p-type InP.[23] Figure 1 shows an energy band diagram for bias and no bias conditions for a p-InP TE cathode. Since the active (photon absorbing and electron generating) layer should contain few free electrons in the absence of illumination, it should be a p-type semiconductor. In order to apply a bias voltage, a "hole barrier" is needed. A simple metal/semiconductor Schottky barrier is used. The Schottky barrier to hole flow for metallic contacts on p-InP ($\approx$ 0.75 eV) are sufficiently high for a satisfactorily low value of hole current, easily sustained by the biasing contact. A $\approx$ 150 Å thick Ag film is evaporated, in situ, for this biasing contact. Transmission of energetic electrons through a thin Ag film can be reasonably efficient. Hot electrons in transit lose energy to phonons, impurities, and electron-electron collisions. In addition, they suffer phonon back-scattering (in our case from the Cs-O layer) and quantum mechanical reflections at the layer interfaces. These losses can be substantial unless the electrons arrive at the surface with more than 0.1 eV excess energy. A single scattering by any of the mechanisms listed can result in loss of the electron. The ballistic mean-free path is therefore of interest. Experimental values for 1-eV electrons are reported to be 265 Å in Ag.[21] Typical overall experimental transmissions for $\approx$ 100 Å Au films are in the region of 15 to 35% depending on the exact values of the excess kinetic energy at the surface. Similar values for Ag would be expected. The surface of the Schottky barrier is treated with Cs and oxygen in a manner similar to NEA activations[7] in order to reduce the work function and maximize the photoemission process.

In operation, a positive (reverse) bias on the metallic contact depletes the p-InP emitter and establishes an electric field

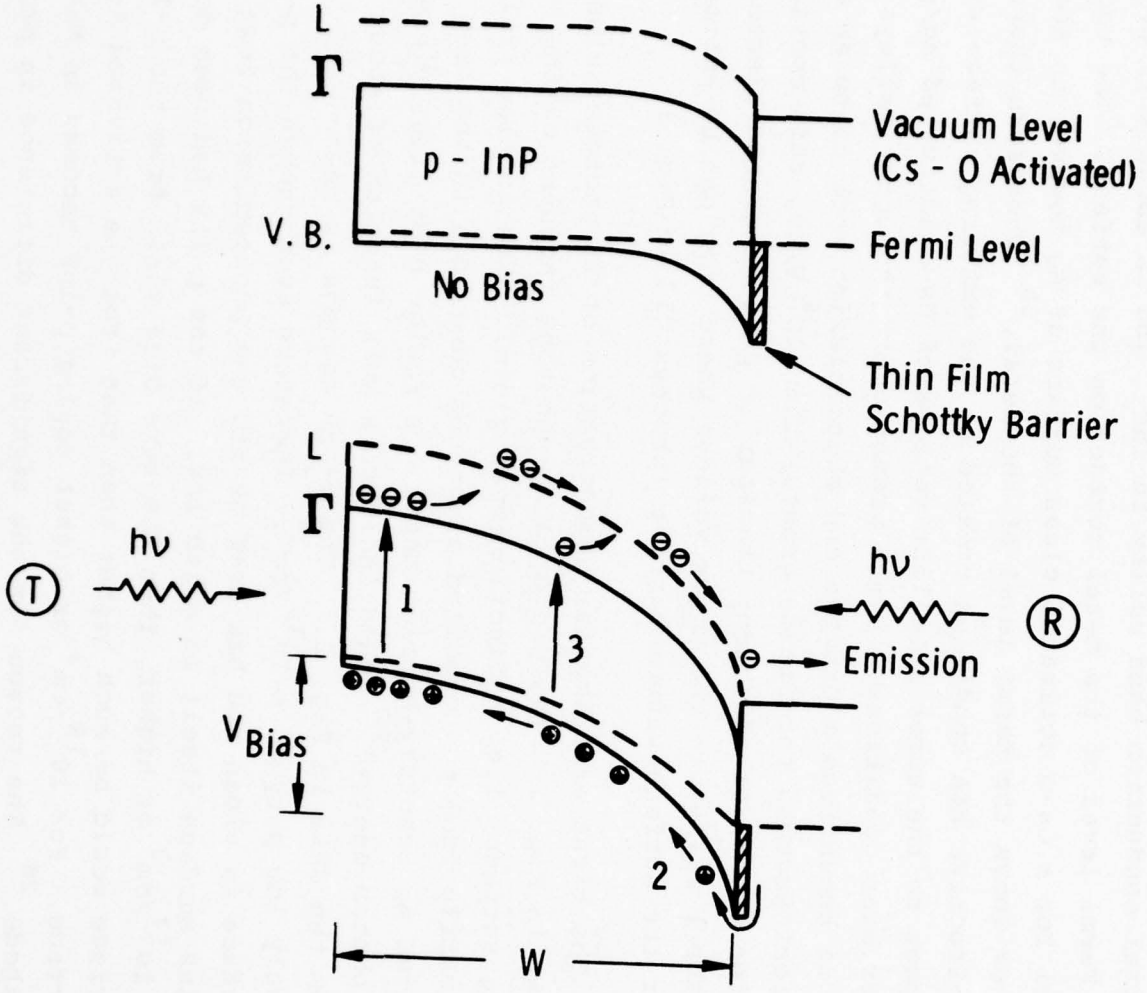

Fig. 1. Energy band diagram of a p-InP TE emitter cathode.

region which is a maximum at the surface and extends back into the bulk of the cathode. For fields on the order of 10^4 V/cm, it is known that conduction electrons in InP are promoted (transferred) into upper satellite valleys (e.g. from the Γ into the L in Fig. 1). The L valley lies about 0.5 eV above the lowest central conduction band valley in InP[24] and is about 1.15 eV above the Fermi level of the metal contact on the surface. The vacuum level for a Cs-O activated clean surface of Ag however is about 1.0 eV above the Fermi level of the metal.[20] Therefore there is an effective NEA condition created at the emitting surface with respect to the upper satellite valleys of Cs-O activated Ag/p-InP under bias conditions. Since promotion to the upper valleys in InP is known from microwave and photoemission work to be an efficient process for fields greater than 10^4 V/cm, this configuration makes for efficient transfer of photogenerated electrons in the Γ valley to the upper valleys where they can be emitted over the surface vacuum barrier (process "1" in Fig. 1).

The first experimental demonstration of TE photoemission is shown in Fig. 2. The yield is for photons incident on the emitting surface (i.e. reflection-mode yield). The no-bias yield is primarily from photoexcited electrons generated in the Cs-O coated Ag Schottky-barrier metal. A Fowler plot (i.e. yield$^{1/2}$ vs photon energy)[25] would indicate a work function of about 1.0 eV from the data in Fig. 2. The p-InP cathode is relatively low p-type, $\sim 10^{15}/cm^3$. Therefore even though the p-InP surface is clean and has Cs+O on it, the photoemission from the p-InP surface itself is quite low. If the p-InP had been doped to $10^{17}/cm^3$ or higher, then the zero bias yield from the p-InP surface would be much higher than that from the activated Ag surface. For $10^{18}/cm^3$ or higher doping p-InP becomes an NEA cathode.[26] The reason for the significant difference in photoemission (at zero bias) for p^--InP vs p^+-InP is the difference in depth of the surface space charge region. For effective NEA photoemission, high p-type doping is necessary in order to

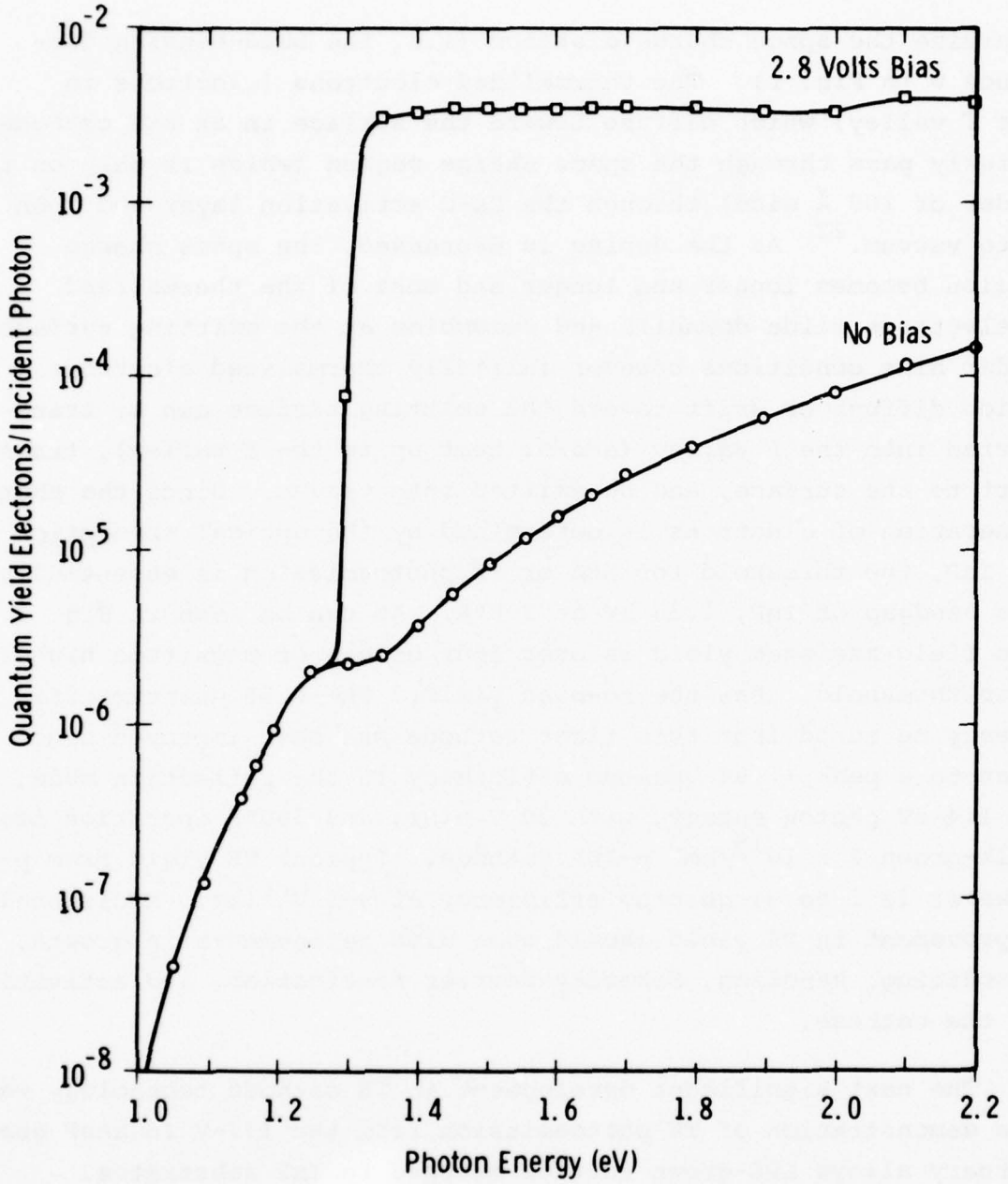

Fig. 2. Reflection-mode quantum yield from the first successful p-InP TE cathode.

minimize the space charge distance (i.e. the band-bending distance W in Fig. 1). The thermalized electrons (electrons in the Γ valley) which diffuse toward the surface in an NEA cathode quickly pass through the space charge region (which is only on the order of 100 Å wide) through the Cs-O activation layer and then into vacuum.[22] As the doping is decreased, the space charge region becomes longer and longer and most of the thermalized Γ electrons slide downhill and recombine at the emitting surface. Under bias conditions however initially thermalized electrons which diffuse or drift toward the emitting surface can be transferred into the L valley (and/or heat up in the Γ valley), transport to the surface, and be emitted into vacuum. Since the photogeneration of electrons is determined by the optical absorption of InP, the threshold for NEA or TE photoemission is essentially the bandgap of InP, 1.35 eV at 300°K. As can be seen in Fig. 2, the field-assisted yield is over four orders of magnitude higher, near threshold, than the no-bias yield. The 0.5% quantum efficiency measured from this first cathode has been improved since then to a peak 11.9% quantum efficiency in the reflection mode, at 1.4-eV photon energy, with 20 V bias, and 300°K operation from a bulk-grown 2 x $10^{15}/cm^3$ p-InP cathode. Typical TE yield from p-InP however is 1 to 3% quantum efficiency at 3-5 V bias. Additional improvement in TE yield should come with refinements in growth, processing, handling, Schottky-barrier fabrication, and activation of the cathode.

The next significant development in TE cathode technology was the demonstration of TE photoemission from the III-V InGaAsP quaternary alloys LPE-grown lattice-matched to InP substrates. Development of the InGaAsP alloys for NEA 1.06-micron cathodes began in early 1972.[27] The InGaAsP quaternary system with the InP lattice constant can generate bandgaps spanning the region from 1.35 eV (InP) to 0.75 eV (InGaAs)--see Fig. 3. References 28 and 29 provide the most recent materials developments and additional references on earlier work.

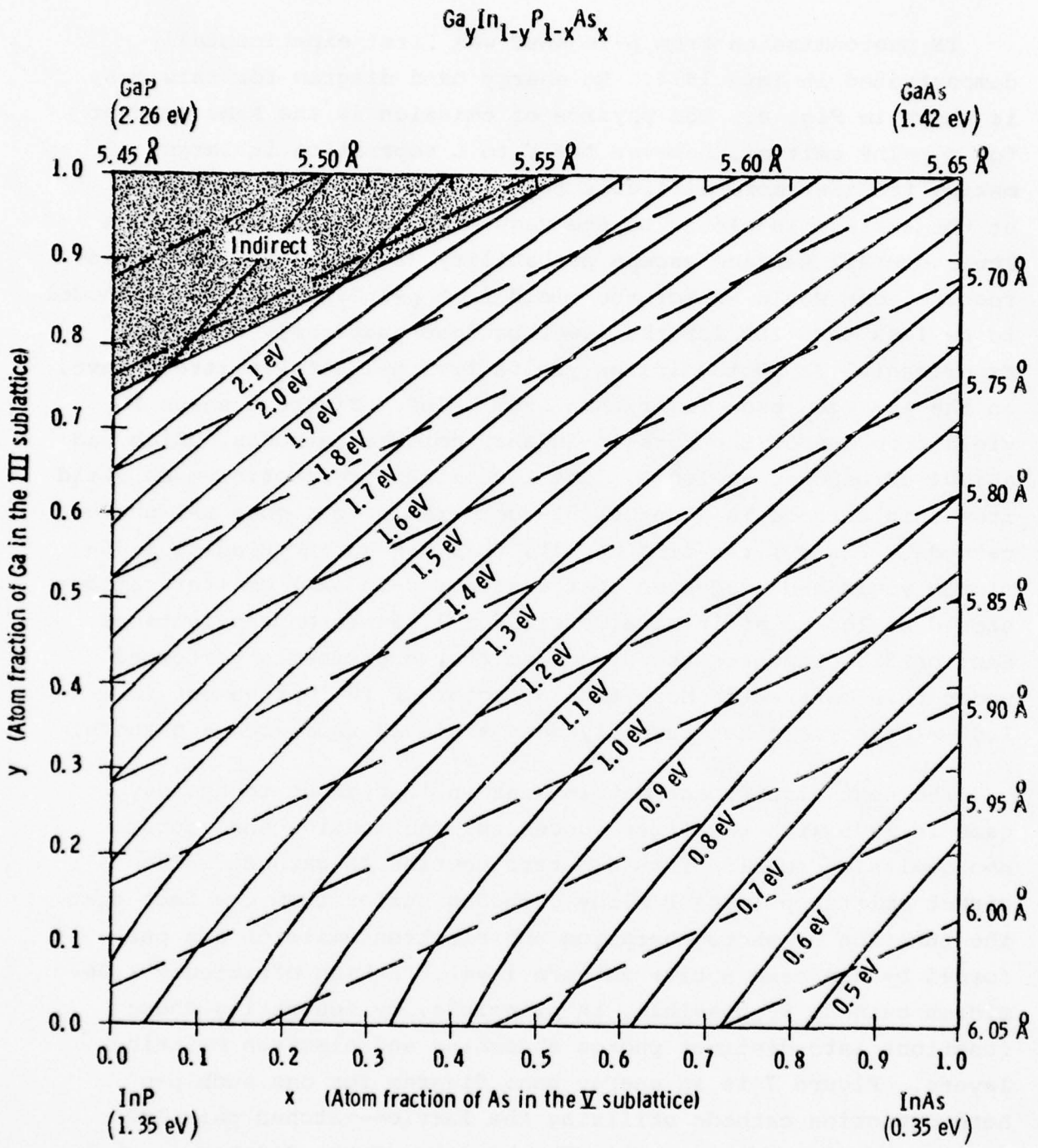

Fig. 3. Calculated bandgap and lattice constant for the InGaAsP quaternary system.

TE photoemission from p-InGaAsP was first experimentally demonstrated in late 1974. An energy band diagram for this case is shown in Fig. 4. The physics of emission is the same as that for a p-InP emitter, however the Γ to L separation is larger making transfer more difficult than in InP and the L band edge at the surface is closer to the vacuum level which results in a lower overall surface escape probability (see Fig. 5). For these reasons, one would expect the yield from p-InGaAsP emitter cathodes to be less than InP for the lower bandgap quaternary cathodes. Experimental TE photoemission yields from p-InGaAsP emitters have, on the average, been lower than from p-InP. Figure 6 shows TE yield from one of the first p-InGaAsP emitter cathodes, which had a 1.04-eV bandgap at 300°K. The 1.06-micron reflection-mode yield from this cathode is about 0.15%--comparable to a good S-1 photocathode. For a first-time result, this was an encouraging 1.06-micron yield and suggested that a direct p-InGaAsP emitter cathode should be looked at in more detail for 1.06-micron applications. Section 3.5 discusses the direct emitter experiments performed under this contract. More than a factor of 10 improvement in 1.06-micron yield has recently been achieved from such a cathode.

The next significant development in TE cathode technology came in 1975 with the first successful fabrication and vacuum photoemission results from a heterojunction TE cathode. The direct emitter p-InGaAsP alloy cathodes suffer from the fact that the function of photogeneration and electron emission are performed by the same active cathode layer. A high efficiency 1.06-micron cathode is possible, in principle, by separating these functions into distinct photon absorbing and electron emitting layers. Figure 7 is an energy band diagram for one such p-p heterojunction cathode utilizing the lattice-matched pair InP (emitter)/InGaAsP(absorber). The bandgap of the InGaAsP is such as to be optimal for 1.06-micron detection, $\approx$ 1.15 eV at 300°K. Under zero bias conditions there is therefore a $\approx$ 0.20-eV conduction band barrier to thermalized electron transport between

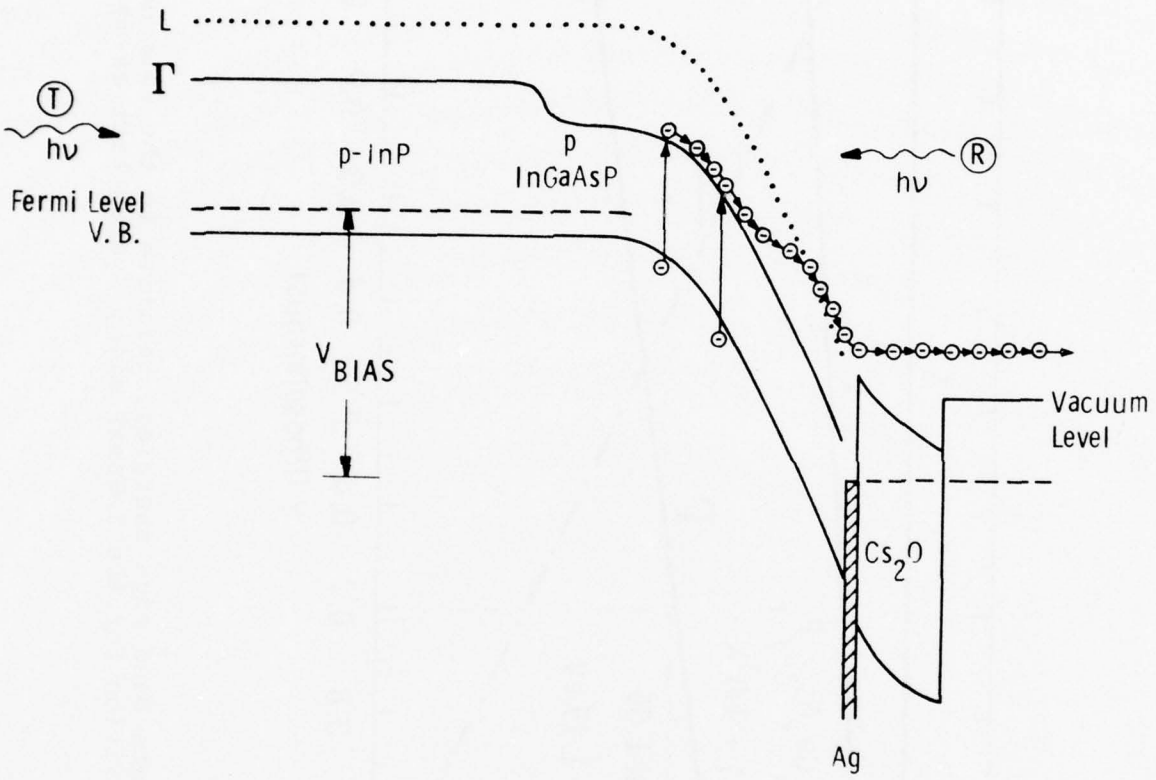

Fig. 4. Energy band diagram of the quaternary emitter TE photocathode under bias conditions.

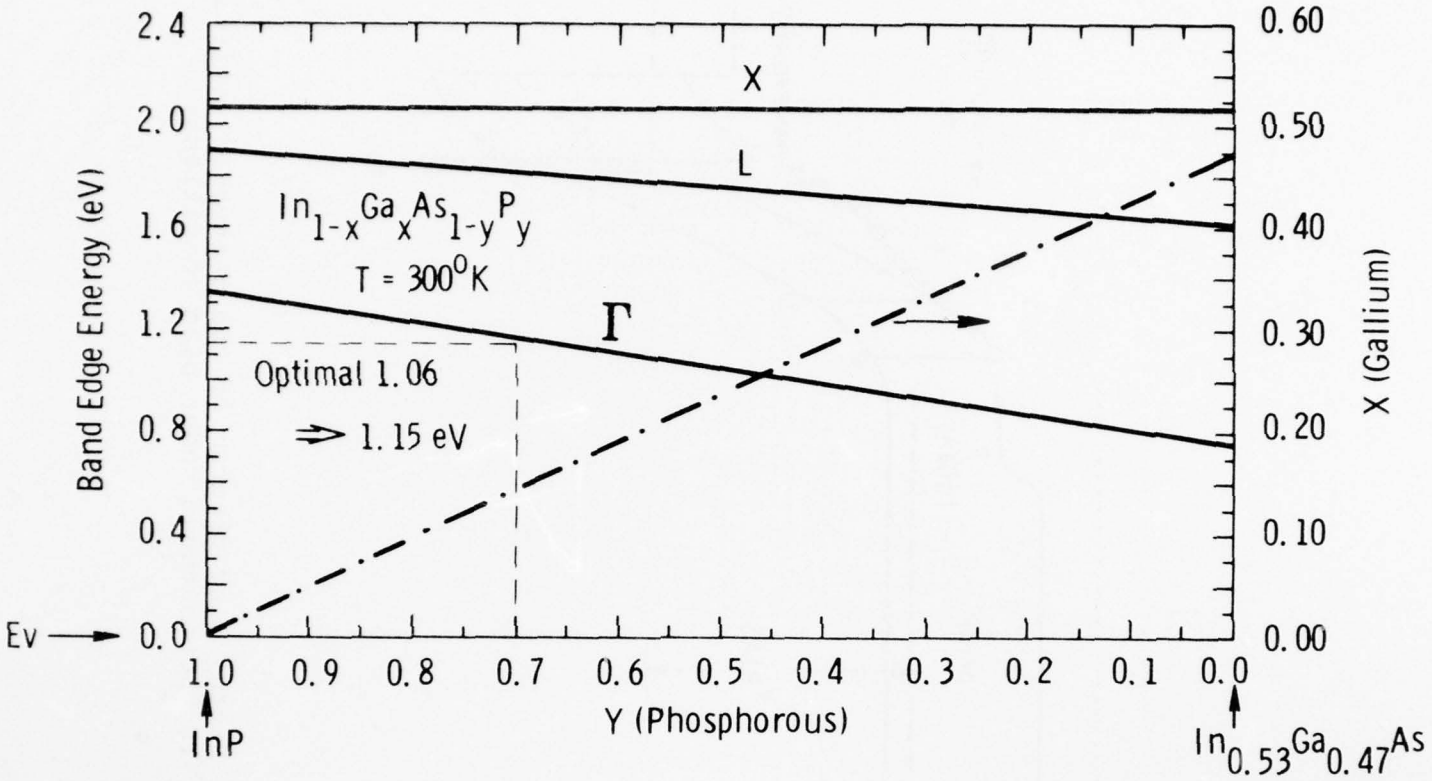

Fig. 5. Approximate band edge energies, relative to the valence band maximum, vs composition for the InGaAsP alloy system lattice-matched to InP.

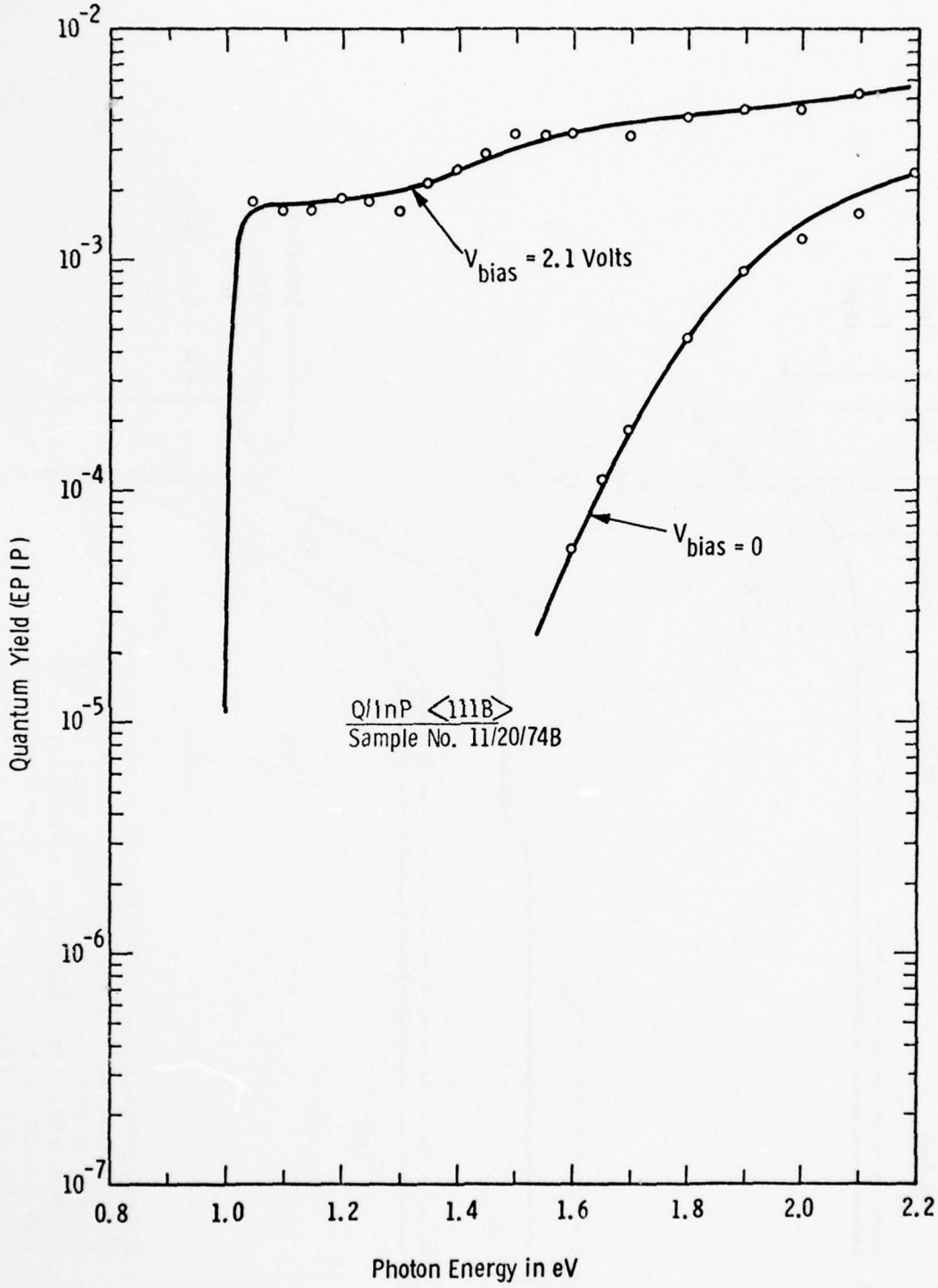

Fig. 6. Reflection-mode quantum yield from one of the first InGaAsP direct emitter TE cathodes.

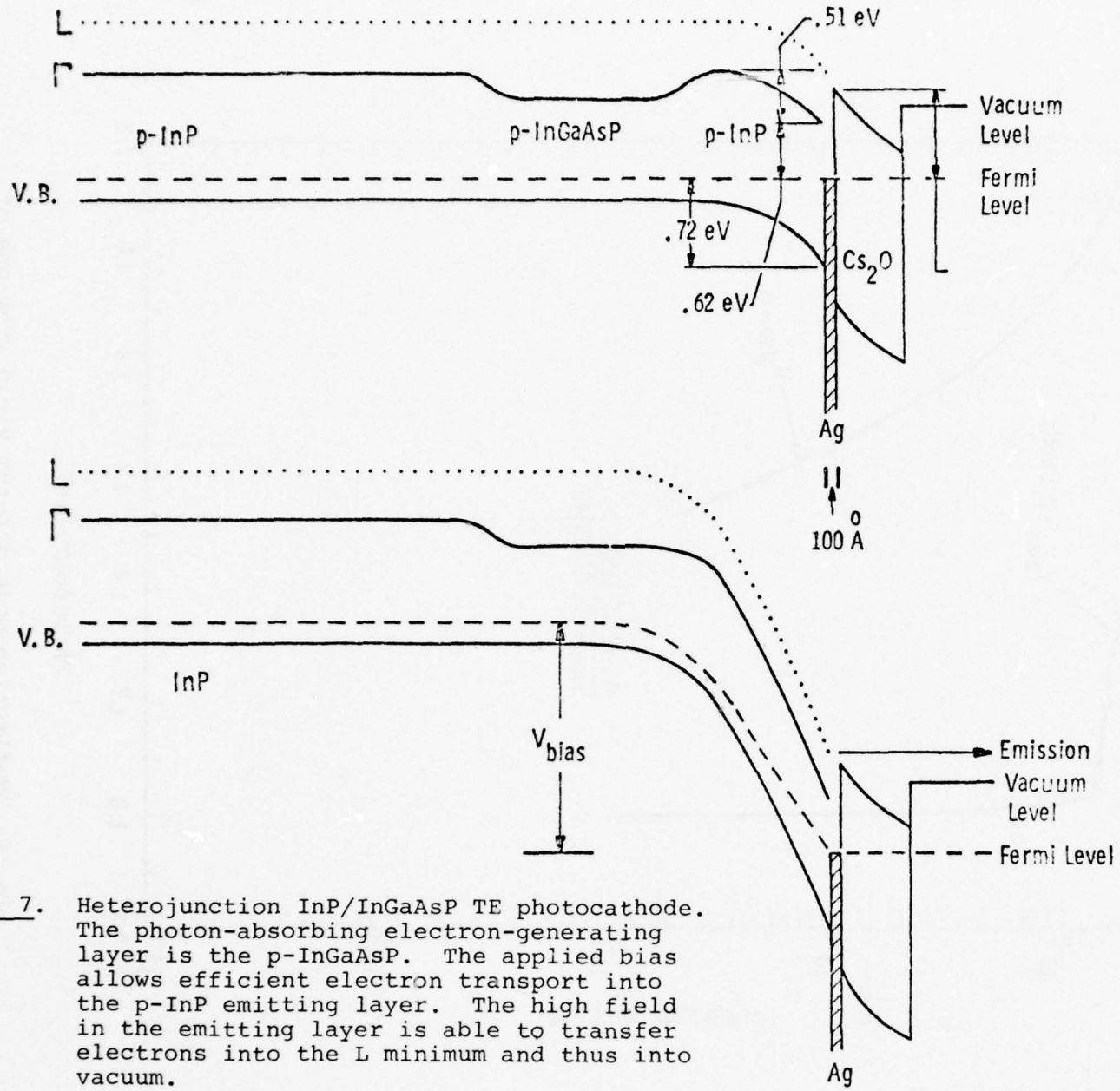

Fig. 7. Heterojunction InP/InGaAsP TE photocathode. The photon-absorbing electron-generating layer is the p-InGaAsP. The applied bias allows efficient electron transport into the p-InP emitting layer. The high field in the emitting layer is able to transfer electrons into the L minimum and thus into vacuum.

the absorber and emitter. Under bias conditions, the depletion field from the reverse-biased Schottky barrier can essentially eliminate the conduction band barrier. At least three conditions must be satisfied for there to be efficient photoelectron transfer from the absorber into the emitter. First, the emitter doping level and thickness must be such that the depletion field can reach the interface at modest applied biases. Second, the interface must be compositionally graded and third, the interface must have no significant recombination centers. Section 2.2 discusses the first two points in some detail.

Figure 8 shows the first experimental demonstration of a heterojunction TE cathode.[30] The zero bias yield is again primarily from the Cs-O activated Ag/InP surface. For biases of about 1 V or more, the InP emitter becomes a TE photocathode. Bandgap-limited photoemission from the InP is clearly seen in Fig. 8 for the 3.5-V bias yield. For photon energies less than 1.35 eV the InP becomes optically transparent and photoelectrons are generated in the $\approx$ 1.23-eV bandgap InGaAsP absorber. A small fraction of these are able to transfer into the InP and are emitted into vacuum at 3.5-V bias. As the bias is increased, the InP yield increases somewhat but the transfer of electrons from the InGaAsP into the InP increases significantly. Under full bias conditions the yield into vacuum from the InGaAsP is quite high-- about 2.0% at 1.00 micron, 300°K operation.

The ratio of the yield from the InGaAsP to that from the InP is an approximate measure of the heterojunction transfer efficiency for electron transport from the absorber into the emitter. Figure 9 shows these data vs applied bias for the cathode shown in Fig. 8. Again these results were extremely encouraging and provided a basis for further work on the heterojunction TE cathode for 1-2 micron detection which is continuing at this time.[31] The absorber bandgap of the cathode shown in Figs. 8 and 9 was not low enough for 1.06-micron detection. However, optimization of the cathode for 1.06-micron detection is relatively straightforward. Section 3.6 describes the most recent

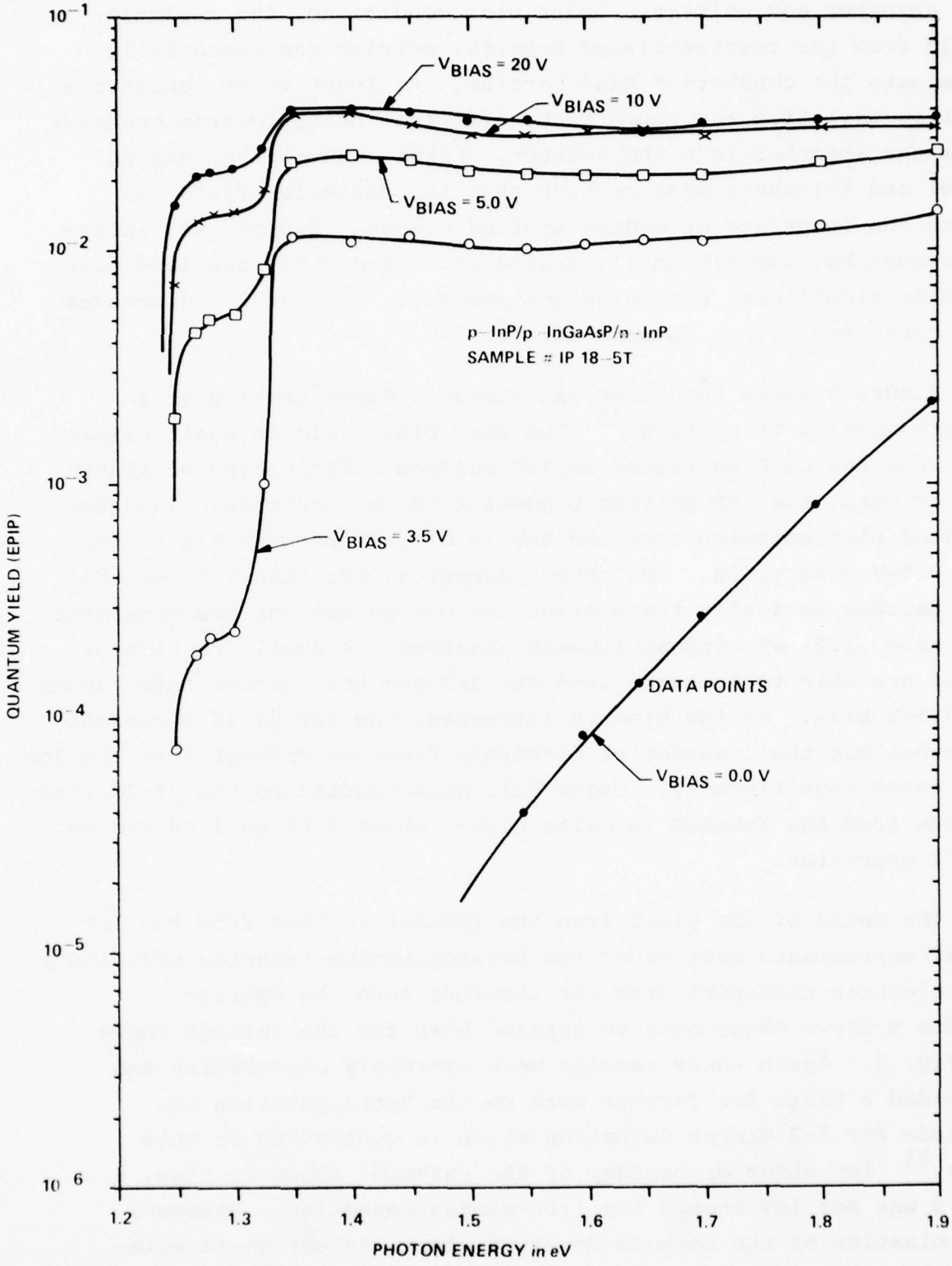

Fig. 8. Experimental reflection-mode quantum yield from the first successful hybrid heterojunction photocathode.

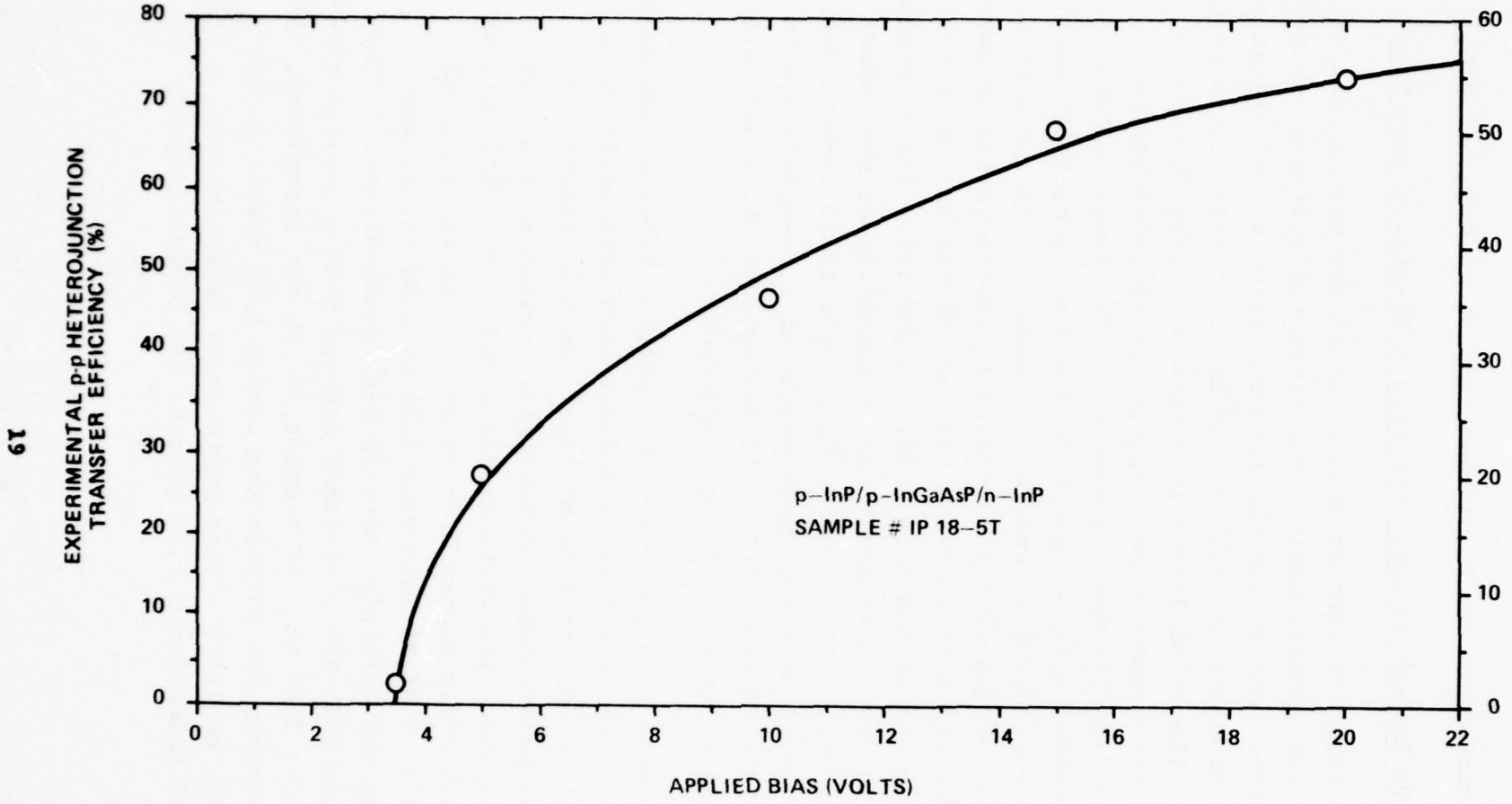

Fig. 9. Experimental heterojunction transfer efficiency vs applied bias from a hybrid heterojunction cathode.

InP/InGaAsP heterojunction TE cathode results at 1.06 microns.

2.2 Proposed TE Cathode Designs for High 1.06-Micron Detection

There are three TE cathode designs which are viable candidates for achieving the program goals. The first two designs, the direct p-InGaAsP emitter cathode and the heterojunction p-InP/p-InGaAsP cathode, have demonstrated 1.06-micron detector feasibility as discussed above. The third design is a heterojunction TE cathode employing a wide bandgap p-InGaP emitter lattice-matched to a narrow bandgap p-InGaAs optical absorber. The direct emitter cathode and the InP/InGaAsP cathode have been developed especially for 1.06-micron detection under this program. A number of cathodes of each type have been fabricated and successfully vacuum-tested to date. Current photoemission results and further details on the operation of each cathode can be found in Secs. 3.5 and 3.6. The remainder of this section is devoted to a detailed description of the InGaP/InGaAs heterojunction TE cathode. It is this third cathode design which is felt to offer the highest potential 1.06-micron sensitivity and is the cathode (InGaP, in particular) which has received the most attention from a materials standpoint.

Of the several requirements of the present photocathode development program, the principal difficulty lies with achieving a 20% quantum efficiency at 1.06 microns. At the present time there are two photocathodes commercially available with 1.06-micron sensitivity. The first is the standard S-1 photoemitter. Typical quantum efficiencies from an S-1 are in the range of 0.05 to 0.20% at 1.06 microns with 1.2% at 1.06 having been achieved using the multiple internal reflection effect.[32] The second is a (cooled) NEA p^+-InGaAsP cathode with a quantum efficiency of 0.5 to 3.0% at 1.06 microns.[33] In the laboratory, the highest performance NEA cathode has been a 9.0% result in the reflection mode at 300°K. This represents, approximately, a 90% probability of absorbing a 1.06 photon, 50% probability of

successful electron diffusion to the emitting surface, and a 20% probability of escape into vacuum over the interfacial barrier between the semiconductor and the Cs-O activator layer. The basic processes of optical absorption of the incoming photon and generation of an electron-hole pair are very efficient processes. The main losses occur in the transport of the photogenerated electron to the surface, and in the emission of this electron into vacuum. For the semitransparent mode of operation (light incident on the opposite side of the cathode from that which electrons are emitted), the probability that a photogenerated electron will reach the surface can be even greater than the 50% figure for a reflection-mode cathode. The net conclusion is that the problem of achieving very high quantum efficiency from a III-V photoemitter is largely a question of electron escape probability.

The highest TE escape probability observed to date from a p-InP cathode is 18% with 3-10% being more typical. Therefore one might expect a heterojunction p-InP/p-InGaAsP TE cathode to be capable of approximately 1-10% quantum efficiency at 1.06 microns. A direct p-InGaAsP emitter cathode would be expected to perform below that of an ideal InP/InGaAsP heterojunction cathode--primarily because of the lower surface escape probability from a p-InGaAsP emitter (1.15 eV) relative to a p-InP emitter (1.35 eV). A higher TE escape probability than that from p-InP would be anticipated if a larger bandgap emitter, such as p-InGaP, were used, thereby promoting the photoelectrons higher in energy at the surface relative to the vacuum level. A similar idea has recently been experimentally demonstrated in the case of NEA GaAsP alloy cathodes.[35] The third TE cathode design for achieving high 1.06-micron yield is based on a p-InGaP/p-InGaAs heterojunction cathode. The effectiveness of the TE emitter layer is increased by substituting InGaP of a specific composition for an InP emitter previously discussed. InGaP has a

greater bandgap at the gamma point and the upper band edges are higher in InGaP than in InP, thereby increasing the electron escape probability into vacuum.

Figure 10 is an energy band diagram for a possible InGaP/InGaAs cathode for no bias and biased operation. The InGaAs is the optical absorbing layer which dictates that it have a 1.15-eV or lower bandgap at 300°K. Figure 11 indicates that the InGaAs composition should be approximately 16% In--i.e. $In_{.16}Ga_{.84}As$. InGaAs layers are grown routinely in this and other laboratories by vapor phase epitaxy on GaAs substrates.[36,37] The InGaAs-GaAs (substrate) interface is lattice mismatched; however this is not an active part of the photocathode and careful compositional grading procedures have been worked out for this system. The InGaP/InGaAs (emitter-absorber) interface is lattice matched to reduce the number of potential recombination centers. Figures 12 and 13 show that the proper InGaP composition to lattice match to $In_{.16}Ga_{.84}As$ (a_o = 5.71 Å) is approximately 63% In, i.e. $In_{.63}Ga_{.37}P$. An $In_{.49}Ga_{.51}P$ composition is approximately correct for growing on GaAs substrates. (Most of the initial InGaP growth experiments described in Sec. 3.3 were made on GaAs substrates.) Figure 14 shows the approximate band edge energies (relative to the valence band maximum) vs InGaP composition. Note that for the $In_{.63}Ga_{.37}P$ emitter proposed, that the gamma minimum is at approximately 1.7 eV and the L and X minima at approximately 2.15 eV. Two important points can be made. First, the height of the L,X minima are approximately 0.25 eV higher than that in InP. Therefore photoexcited electrons which are able to transfer into these valleys should have a higher probability of escape into vacuum than from InP. Second, the E_L-E_Γ separation is about 0.15 eV less for $In_{.63}Ga_{.37}P$ than it is for InP. This would suggest that InGaP should have a higher population of electrons in the upper valleys than InP under the same internal field conditions. (This assumes that InP and InGaP would have similar phonon scattering processes, etc.) A deliberately grown InGaAsP

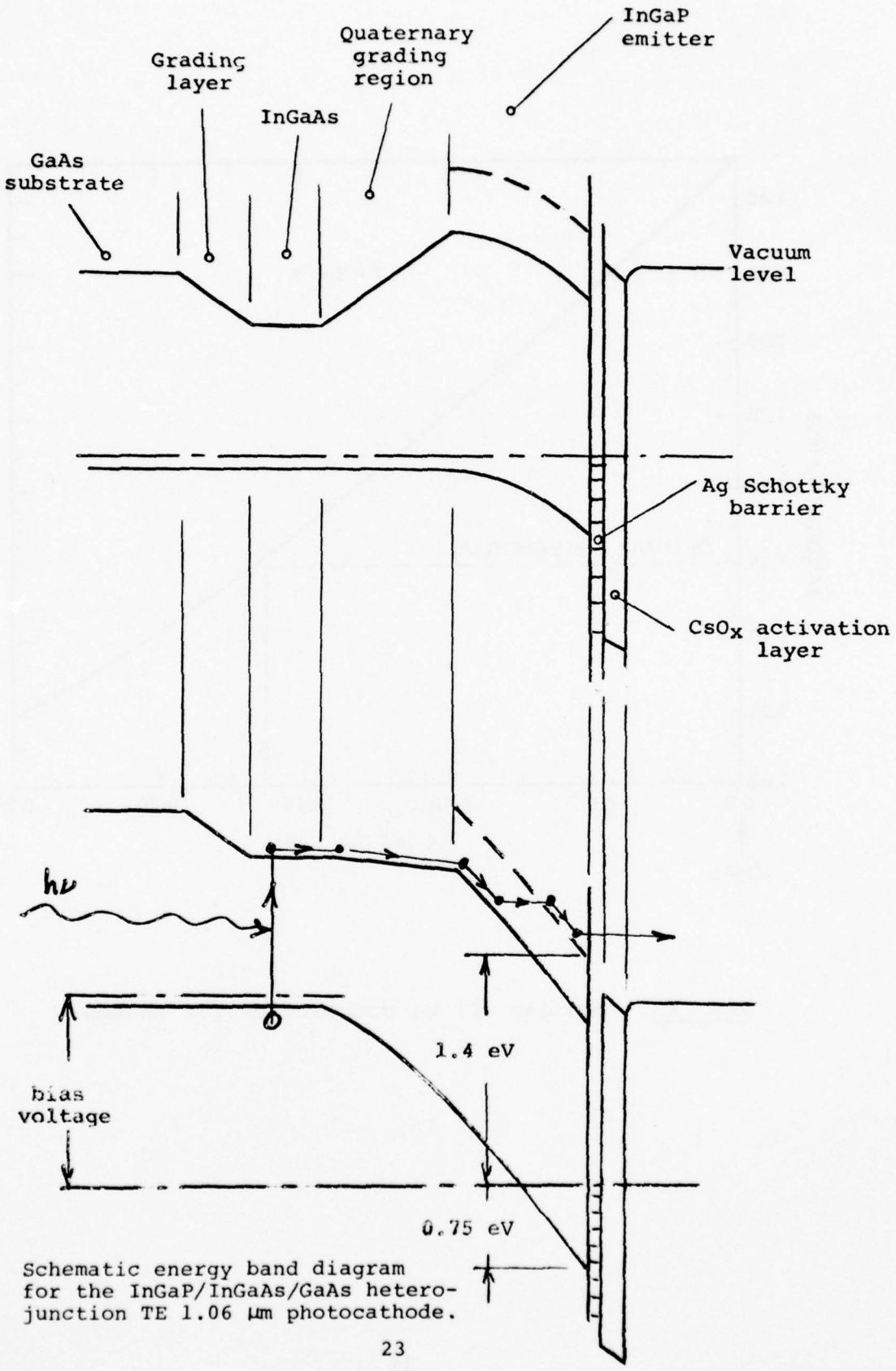

Fig. 10. Schematic energy band diagram for the InGaP/InGaAs/GaAs heterojunction TE 1.06 μm photocathode.

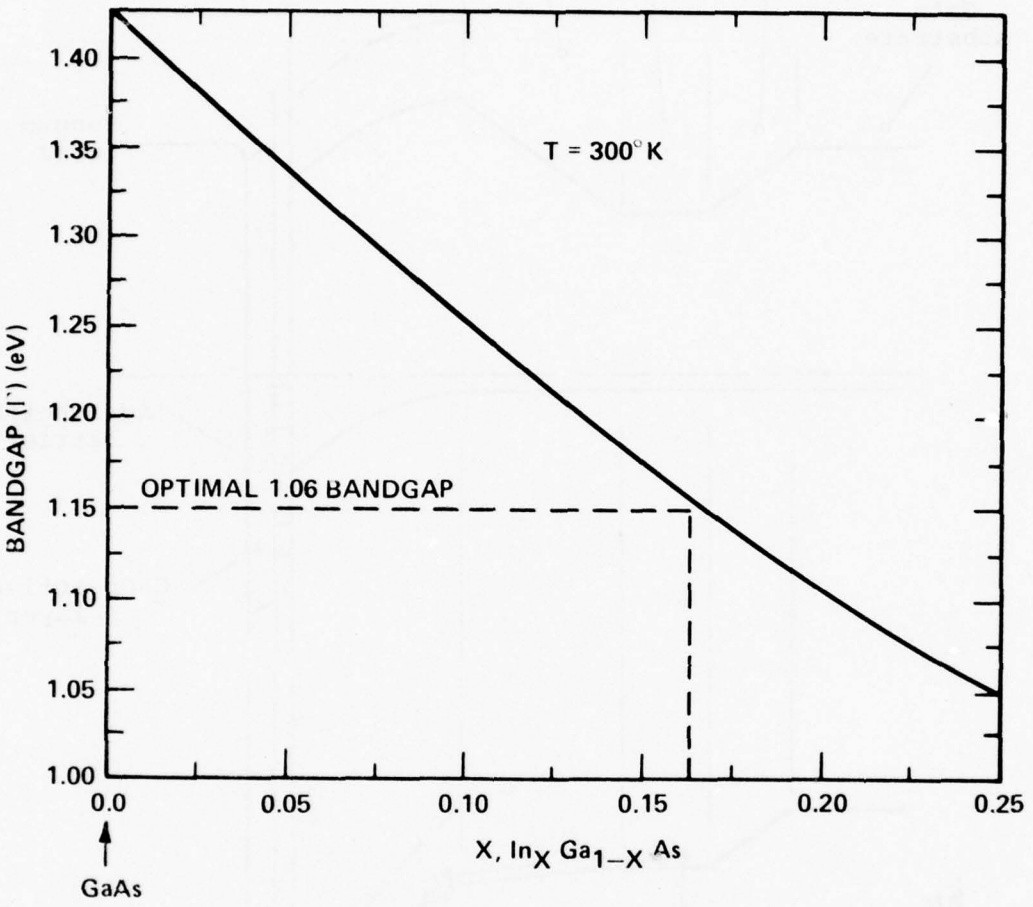

Fig. 11. Bandgap (Γ) vs composition for InGaAs.

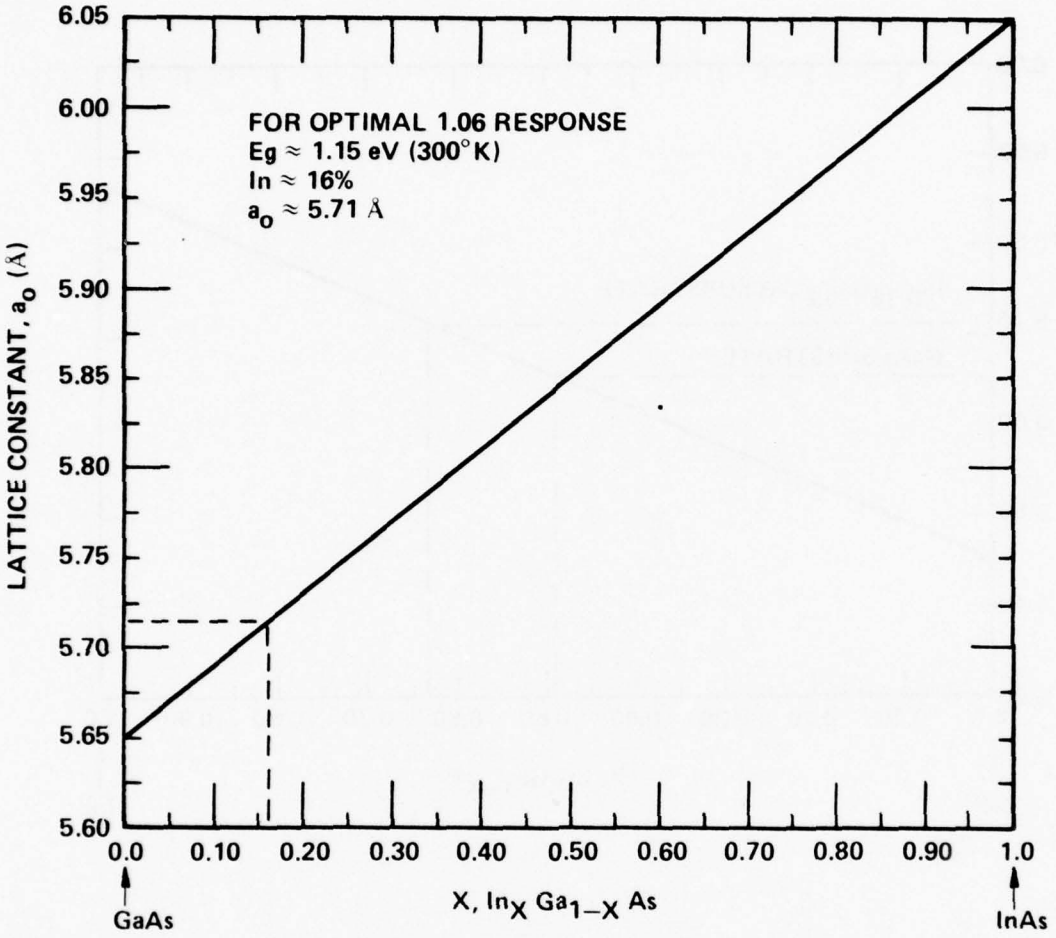

Fig. 12. Lattice constant vs composition for InGaAs.

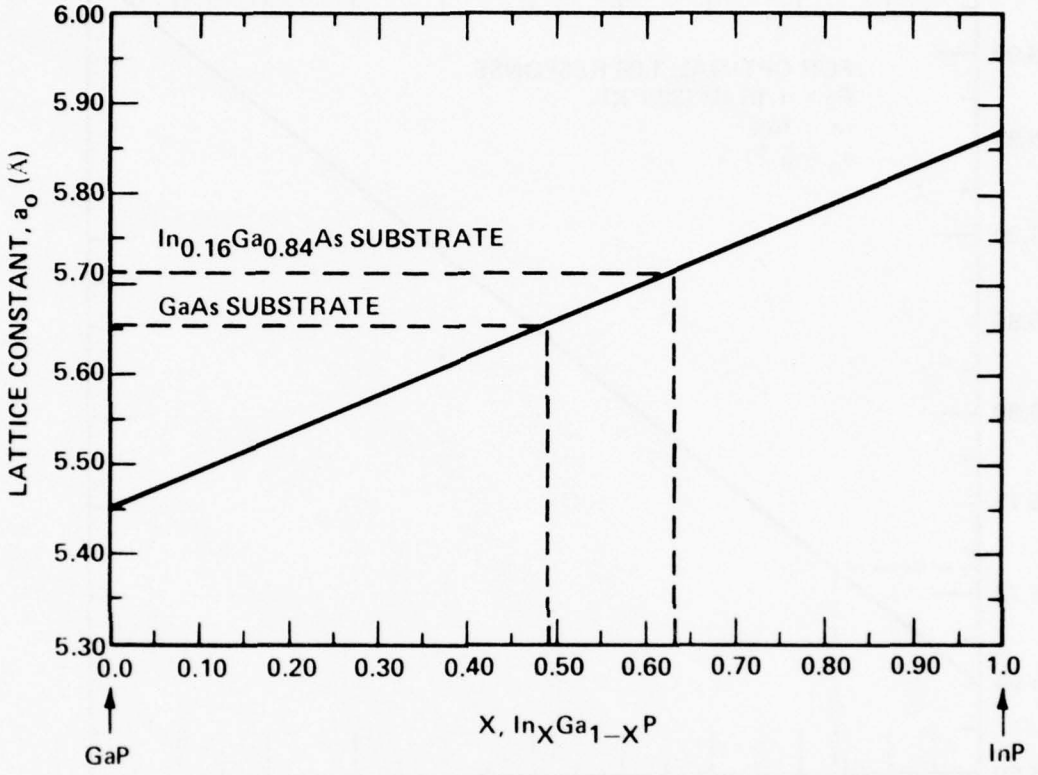

Fig. 13. Lattice constant vs composition for InGaP.

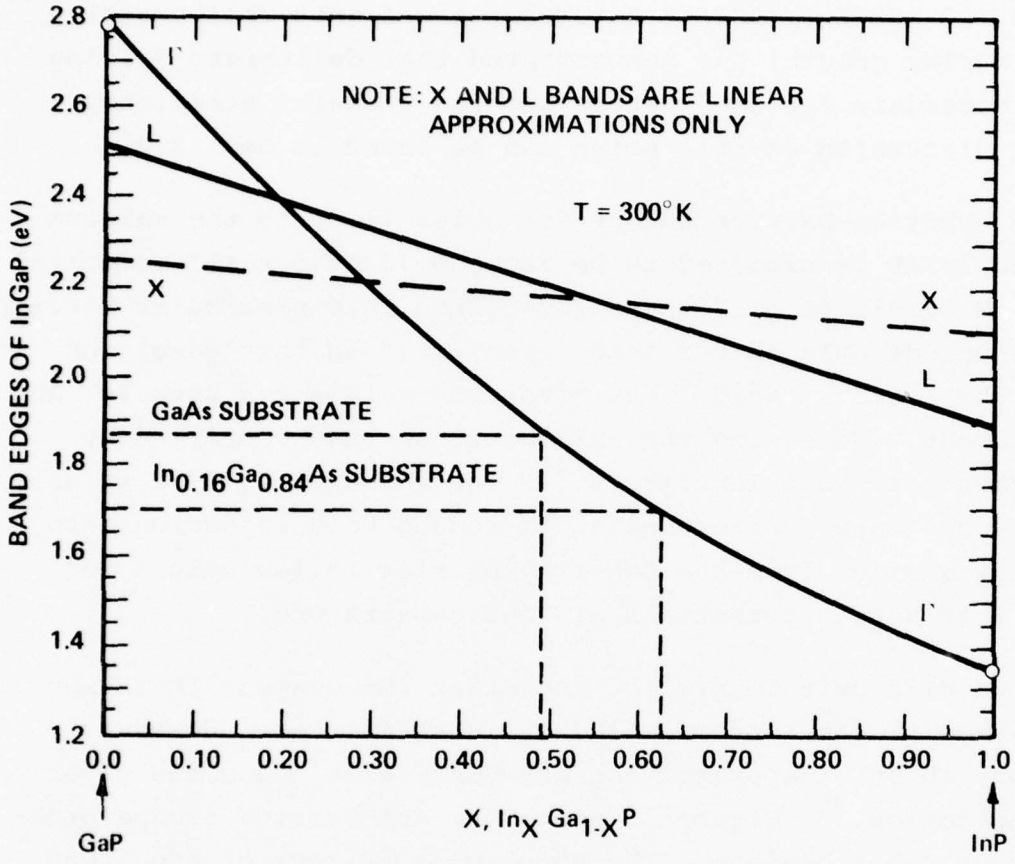

Fig. 14. Approximate band edge energies vs composition for InGaP.

quaternary grading region shown in Fig. 10 between the InGaAs and the InGaP may not be necessary. Recent experience with both VPE-LPE and LPE-LPE InP/InGaAsP heterojunctions (not deliberately graded during growth) has demonstrated that deliberate grading is not necessary for good heterojunction transfer efficiency. Further discussion of this point can be found in Sec. 3.4.

The Schottky-barrier height for holes (i.e. to the valence band) on InGaP is expected to be about 0.75 eV for all compositions. McCaldin et al.[38] have shown that this particular barrier height depends only on the anion species (P in this case) and not on the cation. Mead[39] has given the values for both InP and GaP as about 0.75 eV and the InP value has been confirmed by measurements in this laboratory.[40] The value of 0.75 eV is an entirely adequate barrier height to reduce hole injection into the InGaP emitter from the Schottky barrier to low values for modest 3-10 V bias potentials at room temperature.

It is difficult to predict the exact improvement in TE surface escape probability of a 1.7-eV InGaP emitter. However, work done in this laboratory on NEA GaAsP alloy cathodes gives some indication.[35] Figure 15 shows the NEA surface escape probability vs GaAsP bandgap. The upper mass valleys of the InGaP emitter are estimated to be approximately 0.25 eV higher than thos of InP. Therefore if the behavior of escape probability vs bandgap shown in Fig. 15 is approximately valid, one would expect a factor of two improvement in escape probability. The actual improvement could be even better however because of a potentially higher population of photoexcited electrons in the upper mass valleys of InGaP relative to InP. Therefore the InGaP/InGaAs design offers the highest potential 1.06-micron yield of the three cathode designs proposed. It seems reasonable to postulate a TE surface escape probability from an InGaP emitter of 30-50% with development. The photon absorption process in the InGaAs and transfer of the photoelectrons into the InGaP emitter can,

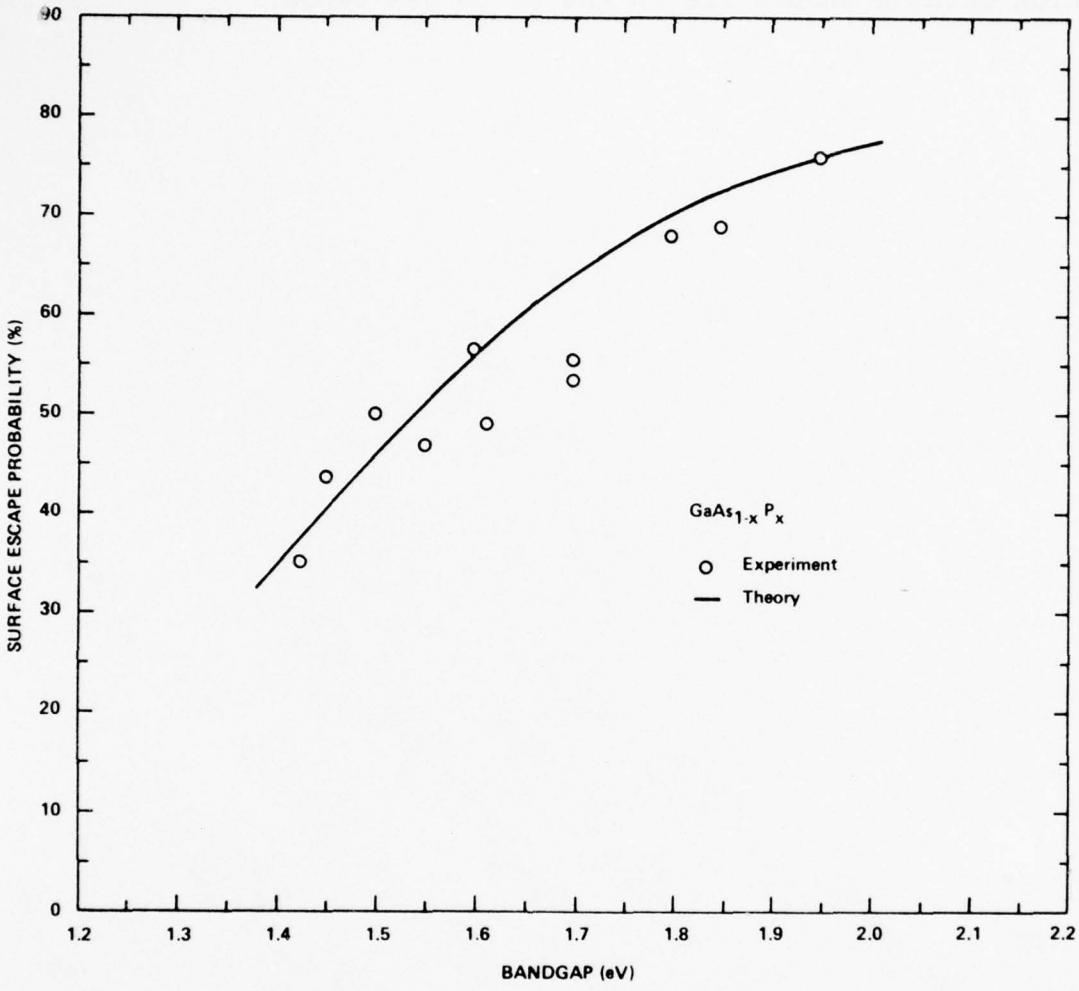

Fig. 15. Surface escape probability vs bandgap for GaAsP alloy NEA photocathodes.

in principle, be very efficient with a 75% probability feasible. Thus the final quantum efficiency for the InGaP/InGaAs heterojunction cathode should lie in the 20 to 30% range.

3. INVESTIGATION

3.1 LPE Growth of InGaAsP Direct Emitter TE Cathodes

The direct emitter TE cathode is the simplest of the three cathode designs in that it involves only a single epitaxial growth. The processes of photogeneration (optical absorption) and electron emission are carried out in the single grown layer. For direct bandgap III-V alloys, optimal 1.06-micron detection is achieved for a 1.15 eV $\pm$ 0.02 eV bandgap (300°K). A slightly higher bandgap alloy would not have sufficient optical absorption at 1.06 microns and a lower bandgap would have a lower surface escape probability and Schottky-barrier height. Early TE photoemission results from p-InGaAsP cathodes, e.g. Fig. 6, indicated that a direct emitter cathode may be capable of > 1% quantum efficiency at 1.06 microns with only modest development.

Details on the LPE growth of InGaAsP alloys lattice-matched to InP substrates can be found in the literature and will not be repeated here. See Refs. 28 and 29, for example. Initially, growth of InGaAsP alloys was restricted to (111)-oriented InP substrates. However, more recent work has established the melt compositions and growth temperatures for high quality quaternary growth on (100)-InP substrates. There are some differences in the distribution coefficient of Ga for example, depending on (111) or (100) growth. The distribution coefficients of Ga, As, and P during growth have been measured and their temperature dependence fit to a simple model.[41]

The growth of InGaAsP for a direct emitter TE cathode is similar to that previously developed in this laboratory for NEA InGaAsP cathodes. The biggest difference is that lightly p-type InGaAsP layers are required instead of high p-type. The reason for this doping requirement is two-fold. First, the Schottky-barrier leakage on p^+-InGaAsP would be very high due to tunneling and little external bias could be applied to the cathode. Second,

the depletion width or space charge region is extremely narrow (on the order of 100 Å) for p^+-InGaAsP. Even if an external bias of several volts could be applied, the depth of the high field region would not be sufficient for there to be efficient TE photoemission. 1000 Å or more of the high field region are needed for efficient electron transfer. This imples that a p-type doping of 10^{15}- $10^{16}/cm^3$ is needed. With proper care and melt preparation, LPE InGaAsP can be grown with a background level of N_D-N_A = $1 \times 10^{15}/cm^3$ at 300°K. Therefore p-type layers in the proper range of doping can be achieved.

Figure 16 shows a typical photoluminescence (PL) spectra from a lightly doped p-InGaAsP direct emitter TE cathode. P-type doping is achieved with Zn added to the melt. The primary peak at 1.21 eV is near bandgap radiation[42] and the smaller intensity side peak at lower photon energy is associated with the Zn acceptor level. Van der Pauw measurements on the sample shown in Fig. 16 showed N_A-N_D = $4 \times 10^{15}/cm^3$ and a mobility of 360 cm^2/Vsec at 300°K and a mobility of 630 cm^2/Vsec at 77°K. Photoemission results from direct emitter cathodes are presented in Sec. 3.5.

3.2 LPE-VPE Growth of the Hybrid Heterojunction p-InP/p-InGaAsP Cathode

Growth of InP/InGaAsP heterojunction TE photocathodes was accomplished using a hybrid LPE and VPE technique. This hybrid growth procedure was adopted because of the need to grow low-doped active InP emitter layers, which is possible by VPE growth on (100)-oriented InP substrates. The 1.15 eV InGaAsP absorber layer doped p-type to $\simeq 10^{16}$ cm^{-3} was grown by LPE on (100)-InP substrates. The InP emitter layer was then grown on the InGaAsP by VPE and Zn-doped to low 10^{15} cm^{-3}. The PCl_3-In-H_2 system used for VPE growth of InP is shown schematically in Fig. 17. A high purity Spectrosil boat with 6-9's pure In was placed in a Spectrosil reactor which was heated by a two-zone furnace lined

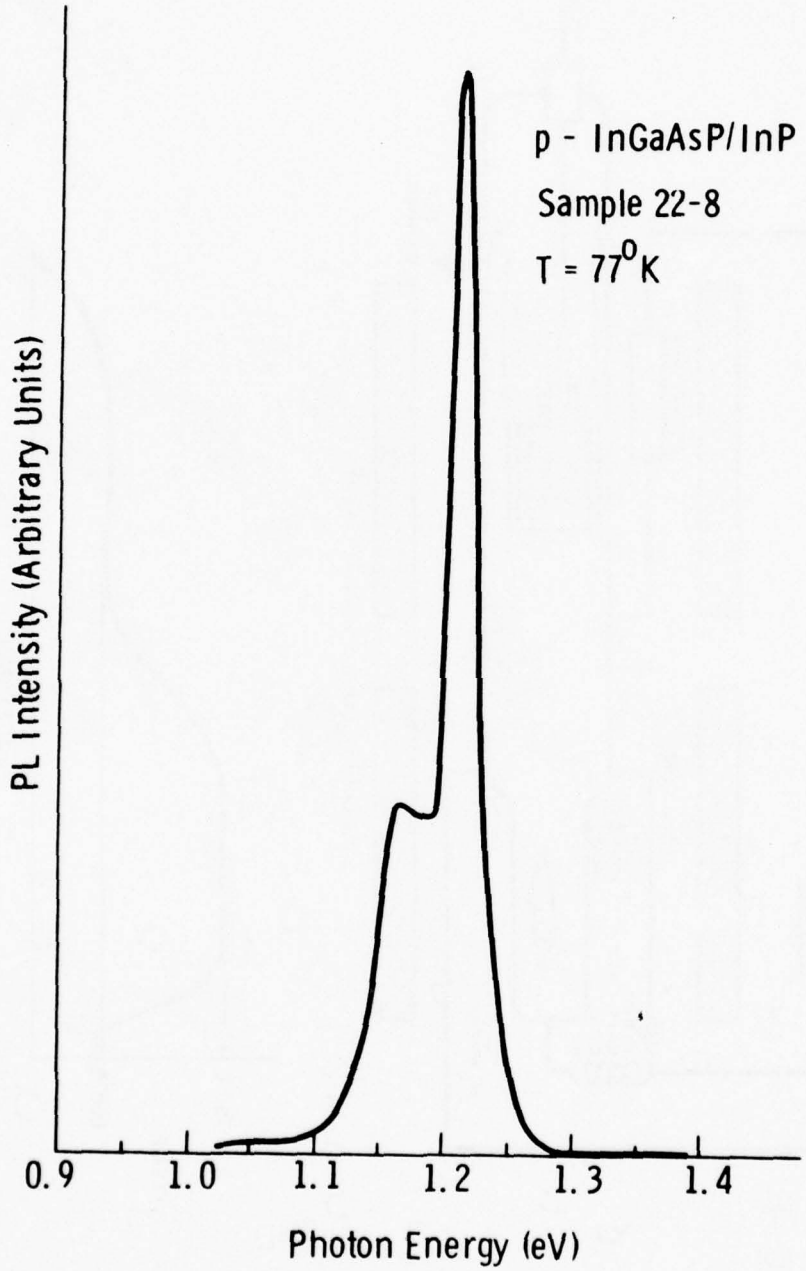

Fig. 16. Photoluminescence spectra from a p-InGaAsP direct emitter cathode at 77°K.

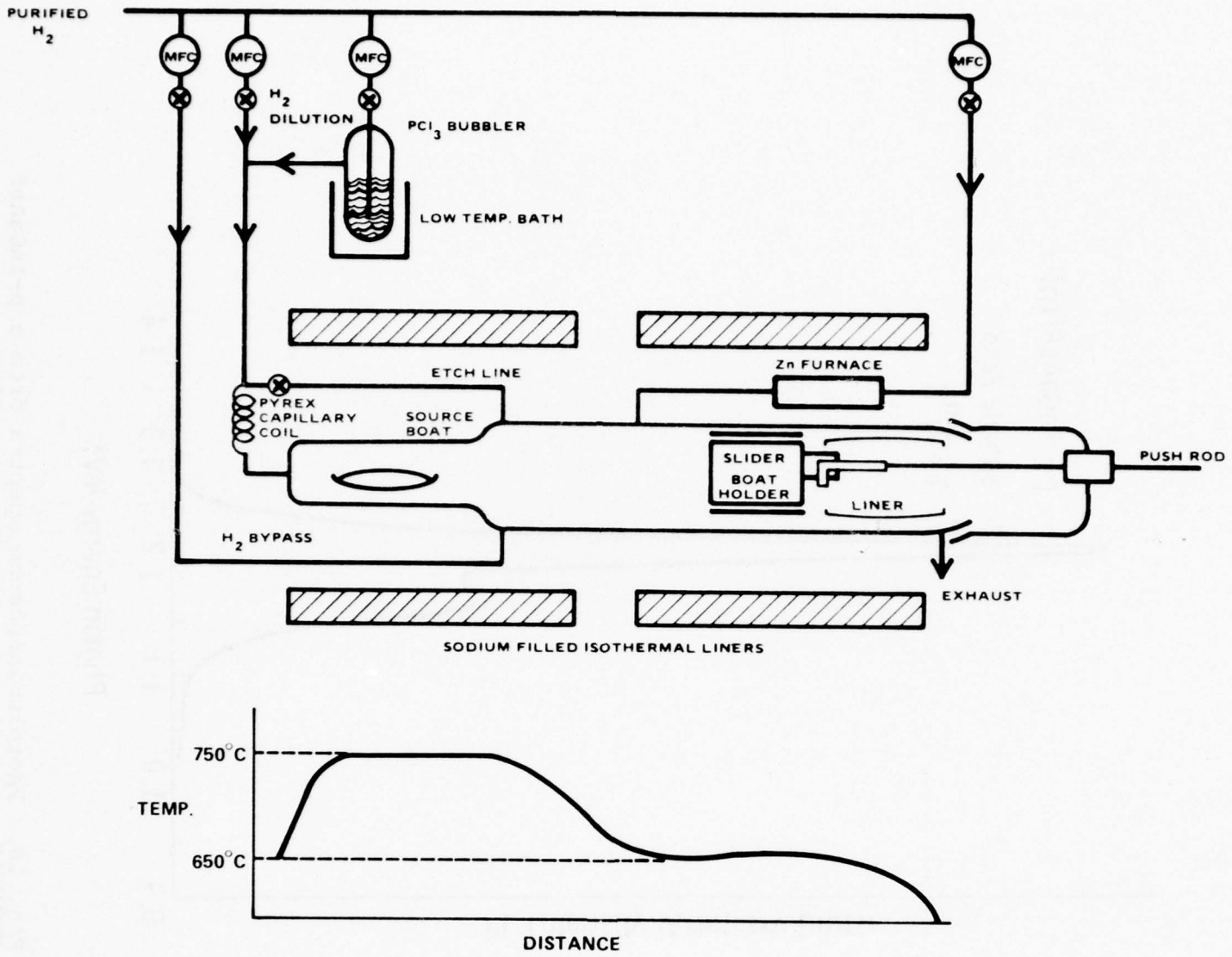

Fig. 17. Schematic diagram of the PCl_3-H_2-In VPE system and approximate temperature profile.

with sodium-filled heat pipes. The indium source was initially saturated with P by passing PCl_3 over the source at 750°C with purified hydrogen as a carrier gas. A H_2 dilution line and a H_2 bypass line also enters the reactor allowing adjustments to the PCl_3 mole fraction over the source and over the substrate respectively. Substrate etch conditions were obtained by diverting the PCl_3/HCl flow ahead of the source through the etch line. A zinc furnace attached to the reactor provided the p-type doping. InP was deposited on the InGaAsP/InP wafer kept at 650°C in the region of the temperature profile where the temperature variation was less than 0.5°C per inch. The temperature profile at the In source was essentially flat, which eliminated source instability and yielded low background doping levels.

To avoid excessive etching of the InGaAsP absorber layer (which was typically 2-4 microns thick) during source resaturation, the substrates were enclosed in the recess of a specially designed Spectrosil slider boat holder shown in Fig. 18. The polished, flat, slider plate covering the substrates could be actuated by a push rod allowing controlled etch and subsequent growth while the substrates are held at 650°C throughout the growth process. A PCl_3 flow of 2070 moles/min was used over the source yielding growth rates of the order of 0.2 micron/min.

3.3 Growth of p-InGaP Emitter Cathodes

Growth of epitaxial InGaP layers has been achieved by both LPE[43] and VPE[44] techniques in this and other laboratories. A new VPE InGaP-InGaAs reactor was constructed, debugged, and generally made operational during this reporting period. VPE homoepitaxy of InP/InP was first achieved, then VPE InGaP/GaAs, and finally at the end of the period VPE InGaP/VPE InGaAs was achieved. During the initial construction phase of the VPE reactor a modest effort was made to grow LPE InGaP for the purpose of quickly demonstrating TE photoemission from InGaP. The LPE experiments are described first, followed by the VPE InGaP experiments.

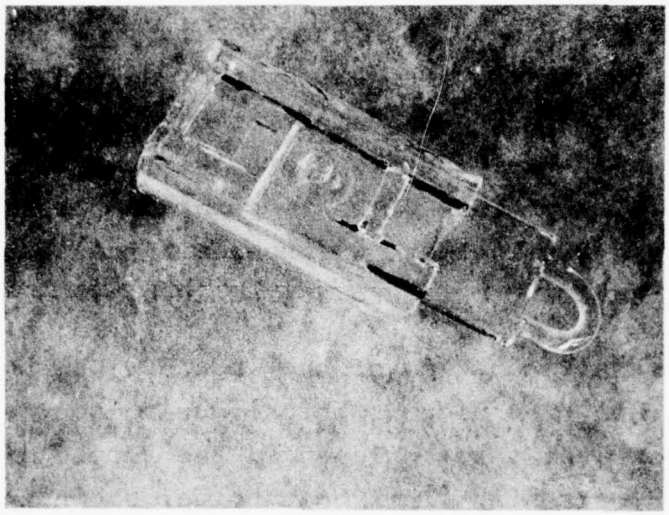

Fig. 18. Spectrosil slider boat holder and plate used to cover the substrate prior to growth.

3.3.1 LPE Growth of InGaP

InGaP was grown at 800°C by LPE from an In-rich melt. A Ga/In ratio of 0.014 in the melt was found to give specularly reflective, near lattice-matched growth surfaces on (111)B GaAs substrates. The In-Ga melt was saturated about 10°C above growth temperature with PH_3. After homogenizing, the melt was cooled down to 800°C at a cooling rate of 0.4°C/min. The melt was then pushed over the substrate and cooled further. Melt wipe-off was invariably good. Although the melt was resaturated before each growth to compensate for the loss of P, good growths were difficult to reproduce. The surface quality was found to deteriorate and the density of growth hillocks increased sharply within two to three growths from the same melt. Low doping levels and better surface quality were observed when the epilayers were less than 0.5 micron thick. Thicker layers showed high doping levels and deterioration in surface quality. Use of graphite boats lined with pyrolitic boron nitride did not significantly improve the background doping level. Figure 19(a) shows the surface micrography of a 0.4 micron thick InGaP epilayer grown on (111)B GaAs that showed a background doping level of 1.4×10^{16} cm^{-3}, whereas Fig. 19(b) is the micrograph of a 4-micron thick layer grown from the same melt which showed a doping level of 2.5×10^{17} cm^{-3}. This indicates a change in the melt composition during the growth which leads to lattice mismatch and strain with a consequent increase in carrier concentration. Several LPE InGaP/GaAs samples were vacuum tested for TE photoemission with negative results. In all cases the effective acceptor density was quite high, resulting in extremely leaky Schottky barriers and relatively high zero bias yields from the p-InGaP surface.

From this point of view, VPE--although more complicated--has the advantage of yielding fixed compositions, the capability of varying the composition at which to lattice-match a substrate,

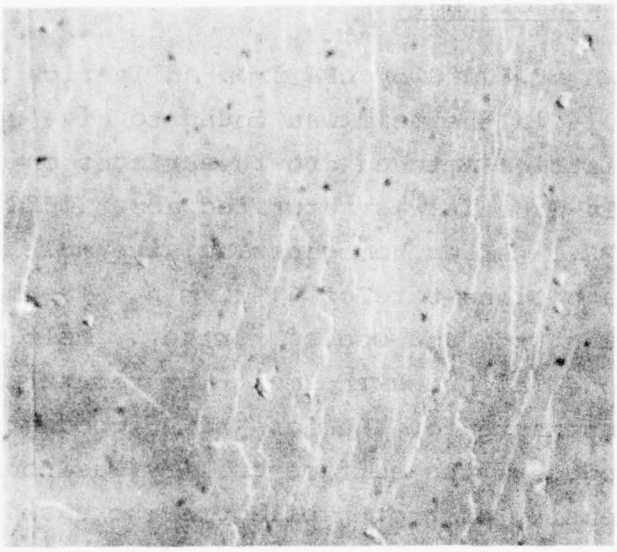

Fig. 19(a). Surface micrograph of a 0.4 micron thick InGaP layer grown by LPE.

Fig. 19(b). Surface micrograph of a 4.0 micron thick InGaP layer grown from the same melt as that used in Fig. 19(a).

and the ability to grade for composition. Background doping levels in VPE material are dictated, in principle, by the purity of the sources of the gases used.

3.3.2 VPE Growth of $In_xGa_{1-x}P$

A schematic diagram of the reactor used for vapor phase epitaxial (VPE) growth of InGaP is shown in Fig. 20 and a picture of the system itself in Fig. 21. (This includes all the modifications to the initial setup to date.) The growth system can be divided into three zones. In the first zone, In and Ga metal sources are placed in two separate chambers and a mixture of HCl and H_2 is passed over each. The HCl reacts with the metal sources to form volatile metal chlorides which are swept downstream. The system has a provision for using either electronic grade HCl/H_2 gas mixture or higher purity HCl from cracking $AsCl_3$ at high temperatures. Since under typical growth conditions the HCl flow over the Ga source is much smaller than that over the In source, a H_2 mixer is added to the HCl(Ga) so that equal total flow of gases over both the sources can be maintained. This ensures equal residence time of gases on the sources. A baffle is placed in each of the source chambers to enhance mixing and residence time and to avoid back-diffusion of gases toward the sources.

In the central zone various gases are introduced. Bypass H_2 and HCl for etching the deposits on the reactor walls and the substrate are also brought in. For p-type doping, a H_2 stream passing over a heated Zn pellet is used. Electronic grade gas mixtures are used for PH_3 and AsH_3. Although the experiments during this period have concentrated primarily on InGaP growth lattice-matched to GaAs, an AsH_3 system has been incorporated for InGaAs growth. Two baffles in tandem are used in this zone to ensure proper mixing of gases.

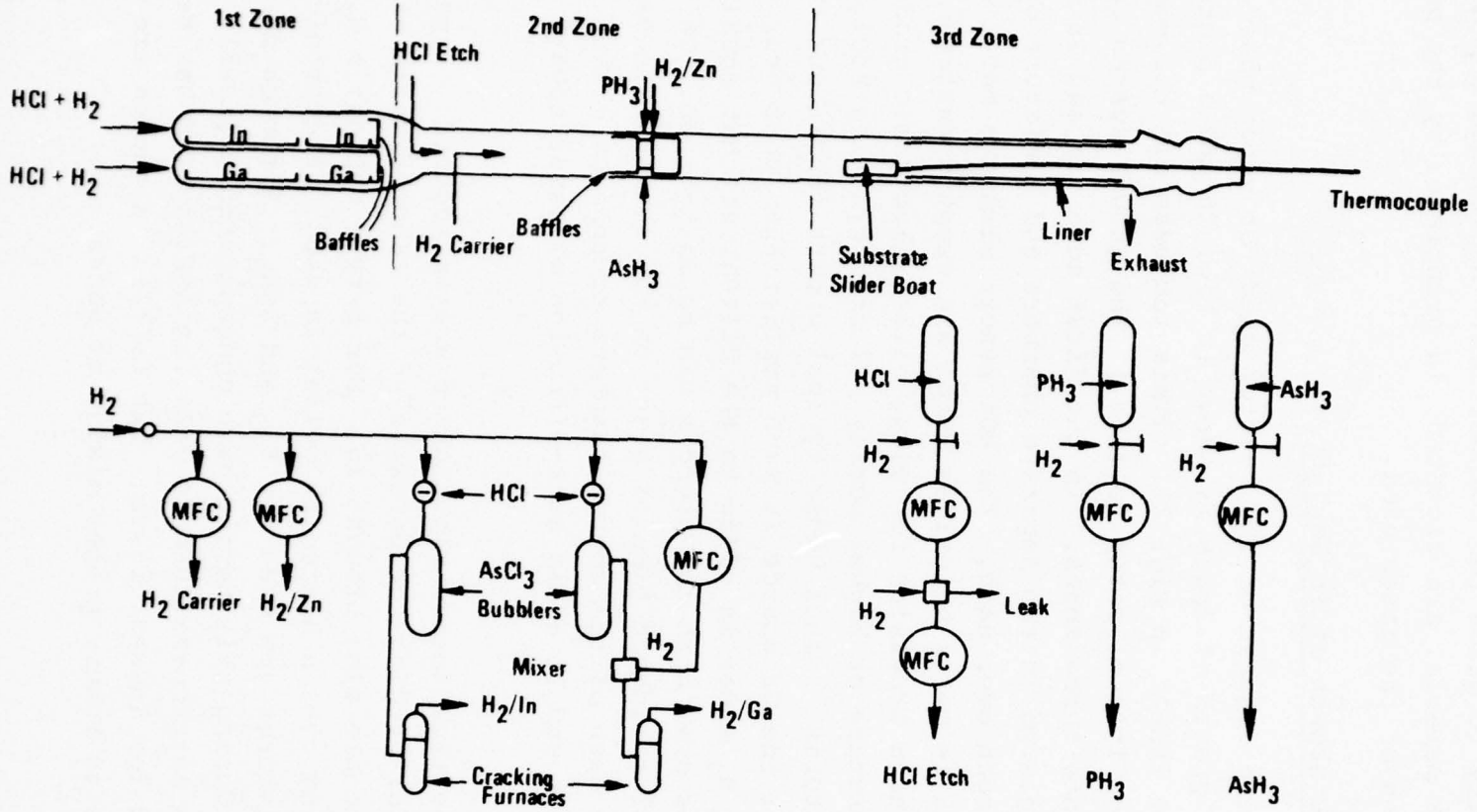

Fig. 20. Schematic diagram of the VPE InGaP-InGaAs system.

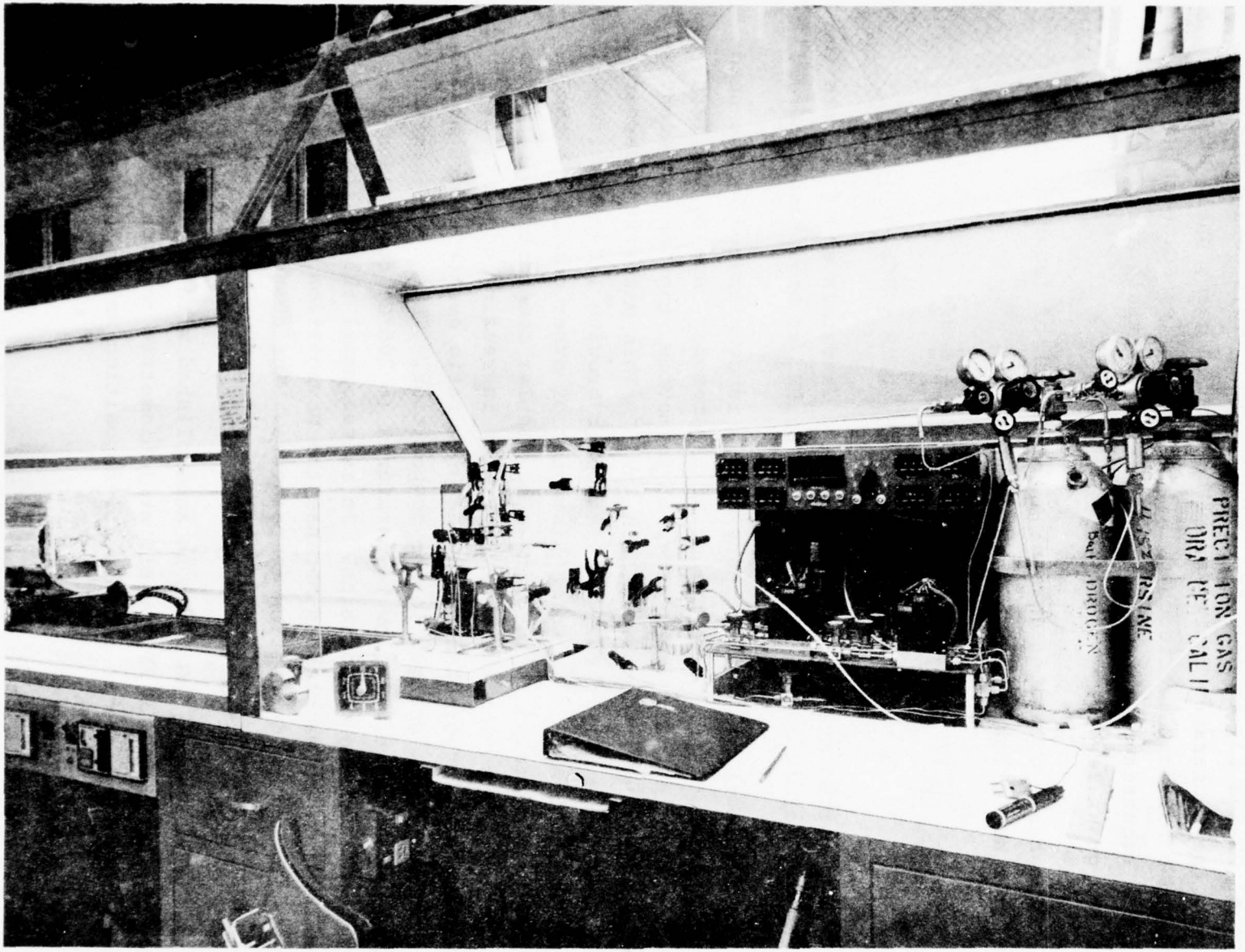

Fig. 21. Photograph of the VPE InGaP-InGaAs reactor system.

In the third zone deposition takes place. A slider boat (Figs. 22 and 23) is used for InGaP growth. This design protects the substrates during equilibration of gases until stable growth conditions are reached, allows controlled HCl etching of the substrates, and makes it possible to attain abrupt changes in the grown layers.

The basic equations governing the growth of InGaP can be written as follows:

$$yM + HCl \rightarrow yMCl + (1-y)HCl + \frac{y}{2} H_2$$

$$MCl + \frac{1}{3} PH_3 + \frac{1}{6} P_2 + \frac{1}{12} P_4 \rightleftharpoons MP + HCl$$

where M represents either of the In and Ga metals and P_2,P_4 are the products formed by the decomposition of PH_3 at high temperatures.[45]

The growth of InGaP ternary alloys is complicated by the need for precise control of a number of parameters. Due to the large difference in their free energy of formation, the GaP component is much more readily deposited than InP.[45] This makes it necessary to have large HCl(In)/HCl(Ga) ratio for growing InGaP lattice-matched to GaAs.[44-46] For a fixed set of other conditions the In/Ga ratio needed for growing a particular composition increases with the deposition temperature. With increasing deposition temperature larger changes in the In/Ga ratio are therefore needed to affect small changes in the composition. Thus it is preferable to grow at relatively low temperatures ($\approx$ 700°C) for reasonable control over the composition. It is essential that a steady temperature be maintained because the composition is a strong function of the deposition temperature. The change in the composition is of the order of 0.3 mole % per degree centigrade.[47]

The growth of InGaP can be accomplished with either stoichiometric (i.e. $\Sigma MCl = \Sigma P$) or off stoichiometric conditions. A surplus of P tends to promote InP deposition while a surplus

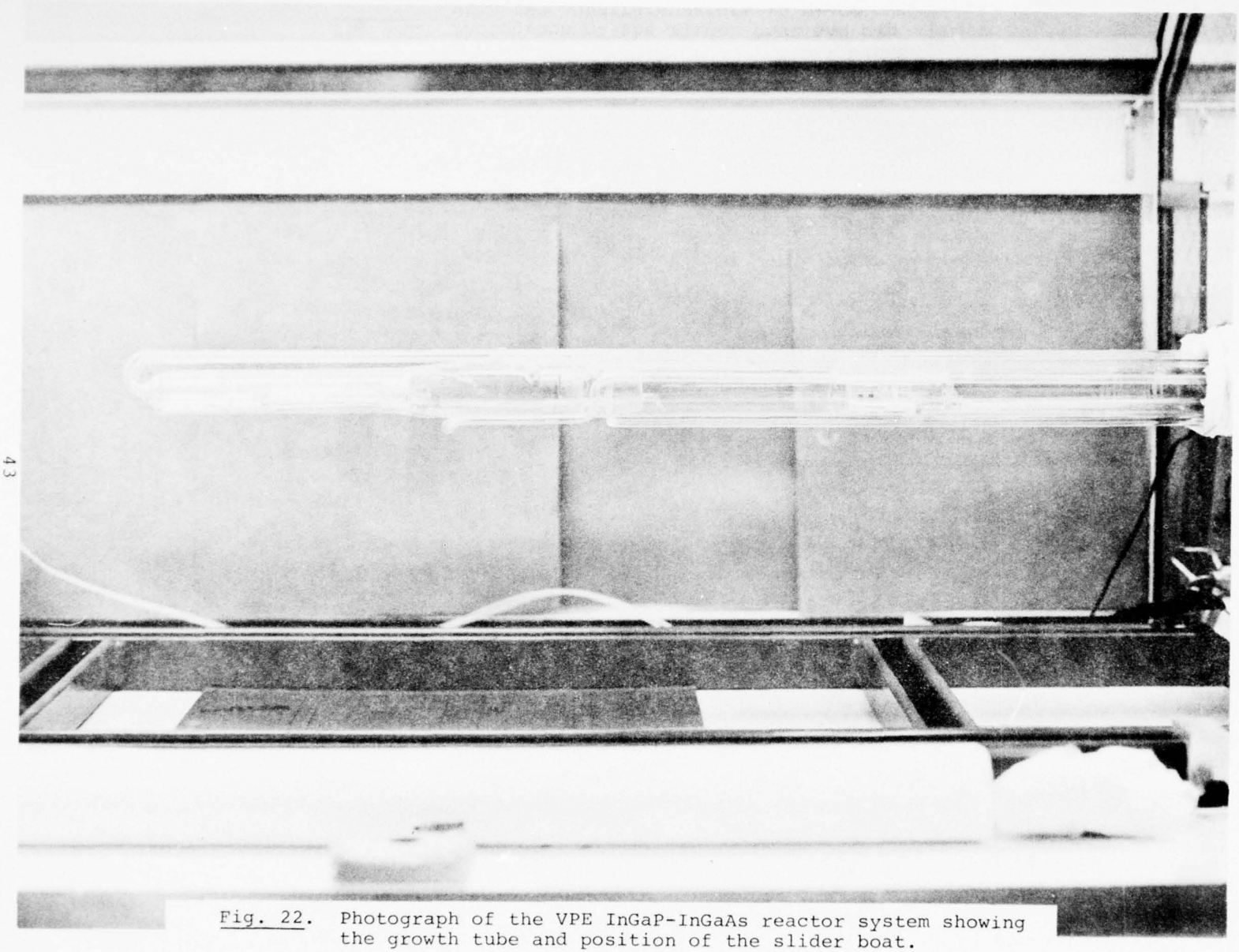

Fig. 22. Photograph of the VPE InGaP-InGaAs reactor system showing the growth tube and position of the slider boat.

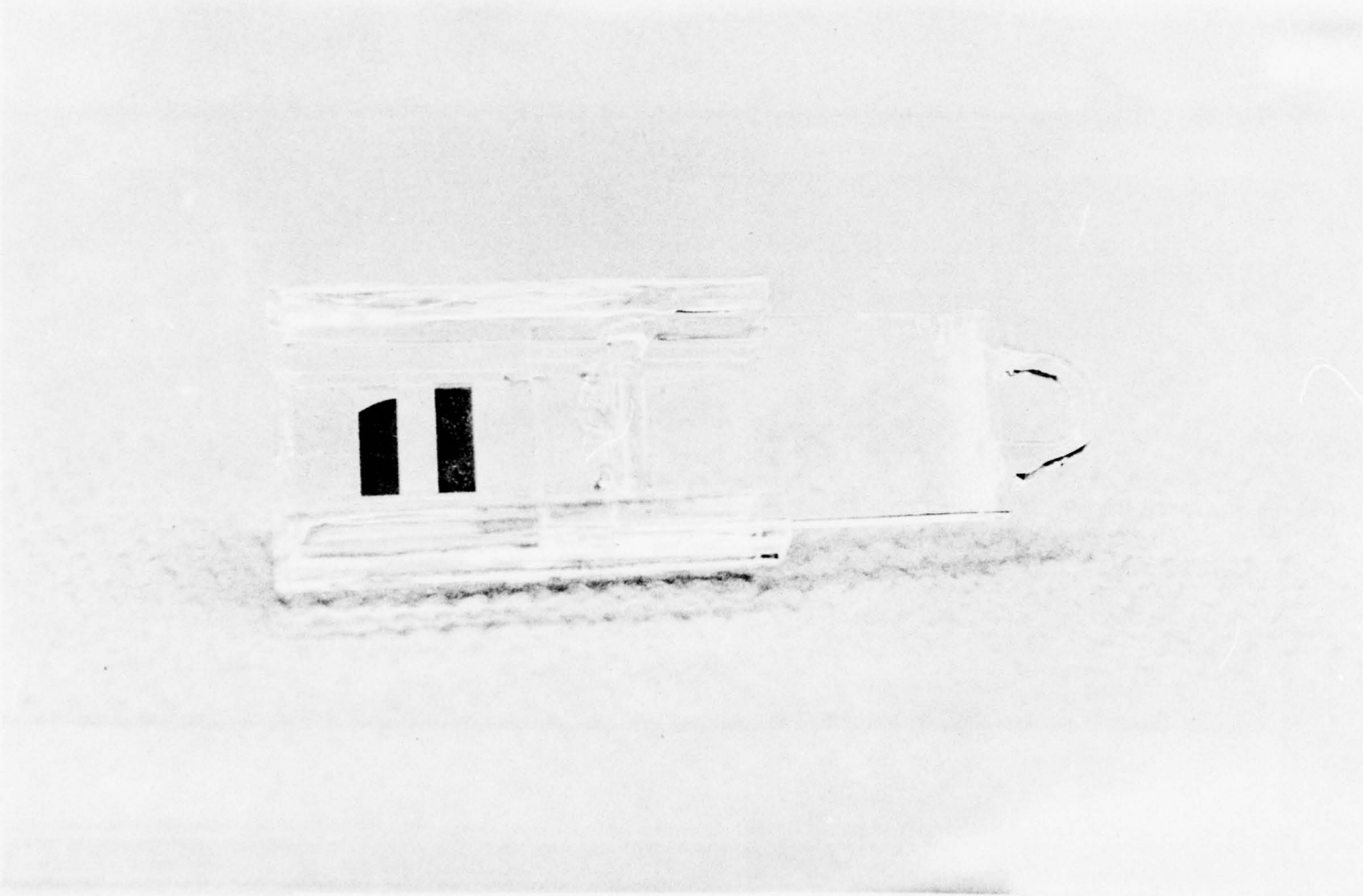

Fig. 23. Photograph of the slider boat and cap with two substrate wafers in place.

of HCl lowers the InP content.[48] At higher source temperatures the conversion of HCl to MCl is more efficient, and this affects the composition as the total HCl present in the deposition zone changes. The decomposition of PH_3 also increases with temperature. The extent of PH_3 dissociation is important since InP deposition is more favorable through a reaction of InCl with PH_3 rather than with P_2 or P_4.[48] It is also important to ensure adequate mixing of gases for good homogeneity of composition. Finally, it is imperative that a clean, leak-free system be maintained to avoid excessive wall deposits that reduce the growth rate and indirectly affect the composition by nonuniform depletion of the gas stream.

Although thermodynamic calculations for InGaP growth have been performed,[45,46] the results cannot be directly used for growing desired compositions since it has been found that the experimental conditions deviate from equilibrium. Also, the growth parameters used in other studies usually are not directly applicable because of the differences in reactor design, furnace profile, etc. Hence for each new reactor system it is necessary to go through an initial stage of experimentation to determine the optimum conditions for the desired growth.

The reactor assembly was complete and ready for operation by the end of June 1977. The single-zone furnace was profiled to obtain a flat source zone at ~ 800°C and a flat deposition zone at 720-730°C. Even after numerous attempts, a flat zone at 700°C could not be obtained with this furnace. Since a primary requirement was low background doping material, HCl from cracked $AsCl_3$ was used in the beginning. From the measurement of As deposited in the cracking furnace it was determined that the $AsCl_3$ cracking efficiency was almost 100%. However, the cracking furnace for $AsCl_3$ would get clogged with too much As and had to be changed after about five hours of run time. Also, because of the large HCl flow, the In source would deplete quite rapidly and had to be replenished to ensure complete conversion of HCl to MCl and maintain reproducible growth. Hence the initial experiments

were necessarily slow and were further slowed down due to temperature drifts in the furnace. As mentioned earlier, the composition is strongly influenced by the deposition temperature. Any drift during a run leads to compositional grading of the growth layer. The furnace problems also caused the temperature to vary from one run to another.

Most of the effort initially concentrated upon making design changes to incorporate desired features into the system. The position of the dilution H_2 line was changed to prevent back-diffusion of PH_3 to the sources. The In source could be easily baked out and most dissolved gases removed, however the Ga source, once contaminated, had to be changed because of P saturation. The baffle system was also modified to achieve the same end result. A Ga/H_2 mixer was installed to ensure equal residence time of gases on the sources.

The first objective was to establish conditions for growth of InGaP lattice-matched to GaAs (which occurs for about 50% InP[49]) and then go on to VPE growth of InGaAs/GaAs and InGaP/InGaAs/GaAs. The initial experiments confirmed the ease with which GaP deposits compared to InP. In spite of judicious choice of parameters based upon a careful literature survey,[44-48] the first layers grown were too high in GaP content. The surface appearance was also poor, the growth nonuniform, and a slight orange appearance indicated a high GaP content. After incorporating the changes mentioned above both the visual appearance and photoluminescence of the InGaP growth improved. Apart from continuing furnace problems it was now possible to effect changes in the grown layer by changing parameters. To establish appropriate conditions for growing InGaP lattice-matched to GaAs, two experimental approaches were used. First, the ratio of In(HCl)/Ga(HCl) was changed and, second, the PH_3 flow compared to MCl was changed. Excess PH_3 compared to MCl tended to produce a poor quality surface. Although the growth rate did increase with PH_3 flow as expected,[48] the composition was

still too high in GaP content. For good surface quality (e.g. fewer hillocks, specularly reflective, uniform area coverage, etc.) it was decided to grow InGaP under conditions of $PH_3 \leq MCl$. By changing the In(HCl)/Ga(HCl) ratio with fixed Ga(HCl) and PH_3 flows modest success was achieved toward this end. Since the use of HCl from cracking $AsCl_3$ was limiting the total number of growth runs before having to clean the system, commercial electronic grade HCl is now used until the growth conditions are well established and very high purity HCl becomes necessary.

It was found beneficial to have a gentle temperature gradient from the PH_3 entry point to the substrate position to reduce excessive wall deposits. Too high a gradient slows down the growth rate and affects the composition by nonuniform depletion of the gas stream. The total bypass H_2 flow was also increased to reduce wall deposits and obtain maximum deposits at the substrate position.

With these charges to optimize conditions for InGaP growth lattice-matched to GaAs, reasonably good growth of nearly lattice-matched InGaP to GaAs has been achieved. InGaP growths were characterized using x-ray diffraction for lattice constant determination, 77°K photoluminescence (PL) measurements, and vacuum photoemission studies. The composition values determined from these techniques are in reasonable agreement with each other. Although hillocks are often present, a cross-hatch pattern characteristic of close lattice-matching[50] can be clearly seen in Figs. 24 and 25.

To more quickly establish the feasibility of the proposed InGaP/InGaAs heterojunction photocathode, InGaP growth on already available InGaAs (grown in another VPE reactor) was successfully pursued. The PL spectrum and surface micrograph for InGaP/InGaAs sample #2-18 are shown in Figs. 26 and 27, respectively. The PL spectrum is sharp with clearly resolved side bands[49,51] and the surface shows the characteristic cross-hatch pattern.

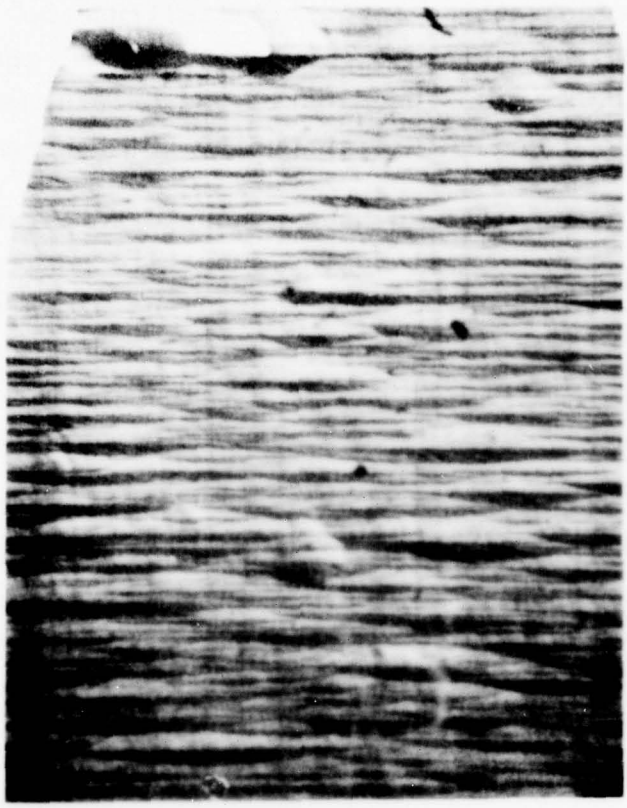

Fig. 24. Photomicrograph of the surface of InGaP/GaAs sample #2-16, 212x.

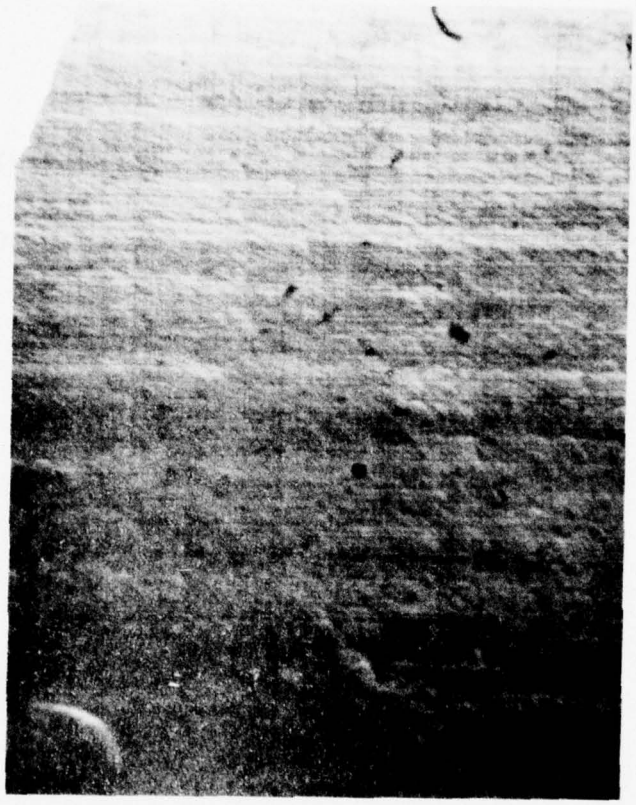

Fig. 25. Photomicrograph of the surface of InGaP/GaAs sample #2-16, 212x.

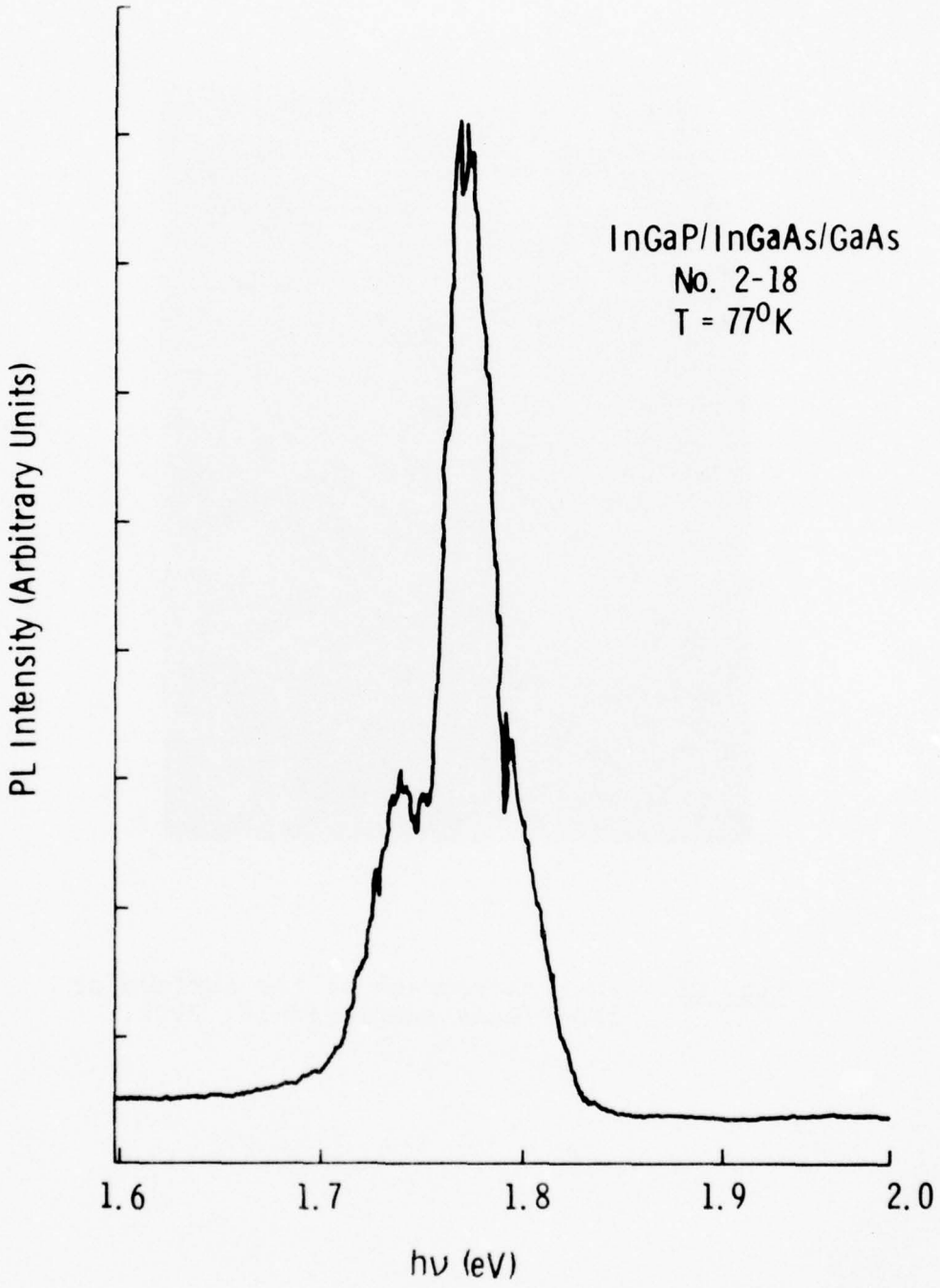

Fig. 26. Photoluminescence spectrum from InGaP/InGaAs/GaAs sample #2-18 taken at 77°K.

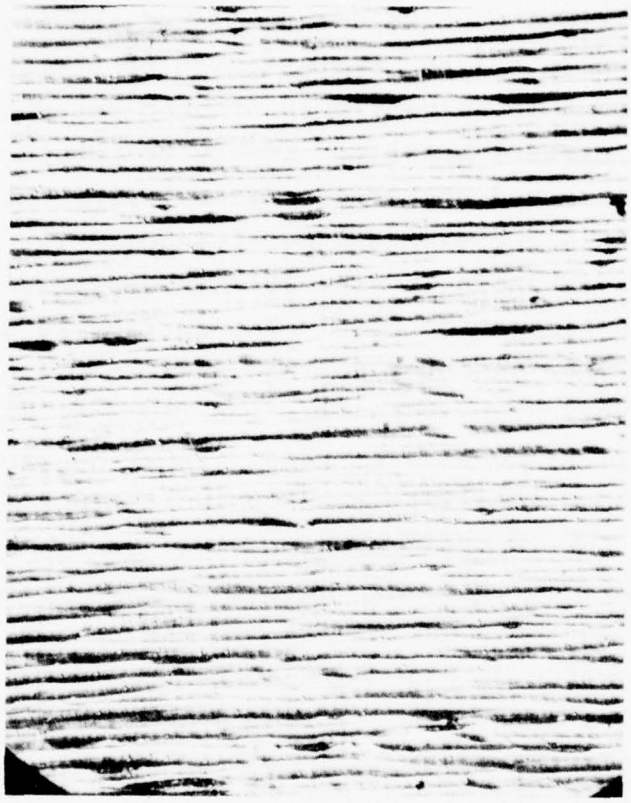

Fig. 27. Photomicrograph of the surface of InGaP/InGaAs/GaAs sample #2-18, 212x.

The furnace instabilities were found to be due to a manufacturing defect in the furnace itself. An improved three-zone furnace was then purchased for the InGaP system. 5-9's pure cylinder HCl was also included for quick experimentation until the growth conditions were well established and higher purity HCl became necessary. After installation of the new furnace, some time was spent in adjusting shunts and set-points to obtain the desired temperature profile. Steady temperatures and reproducible growths are now possible. InGaP layers lattice-matched to GaAs have been grown with the new furnace. The PL spectrum from sample #3-2 is shown in Fig. 28. The spectrum has two clearly resolved side bands.[49,51] The surface is shiny but with a few hillocks. The acceptor doping level in the grown layer has been relatively high ($> 10^{16}/cm^3$) because of Zn incorporation from the p^+-GaAs(Zn) substrates used. InGaP growth on semi-insulating Cr-doped GaAs substrates is suitable for Van der Pauw studies but not for TE photoemission work because of the difficulties in making electrical contact to the substrate. Undoped GaAs substrates (n-type) would not have the Zn diffusion problem but may be the source of high dark current emission for the TE cathode under bias conditions. Lighter doped p-type GaAs substrate material in the 10^{16}- $10^{17}/cm^3$ range would be ideal, and material of this type is being acquired.

Outside of the substrate problem and some improvements needed in reducing hillocks, etc., the current status of the VPE InGaP reactor is good. Sufficient growth experience has been achieved so that it is reasonable to go ahead on growth of the complete InGaP/InGaAs heterostructure. TE photoemission results from the p-InGaP emitters grown during this period are encouraging. These experiments are discussed in Sec. 3.7.

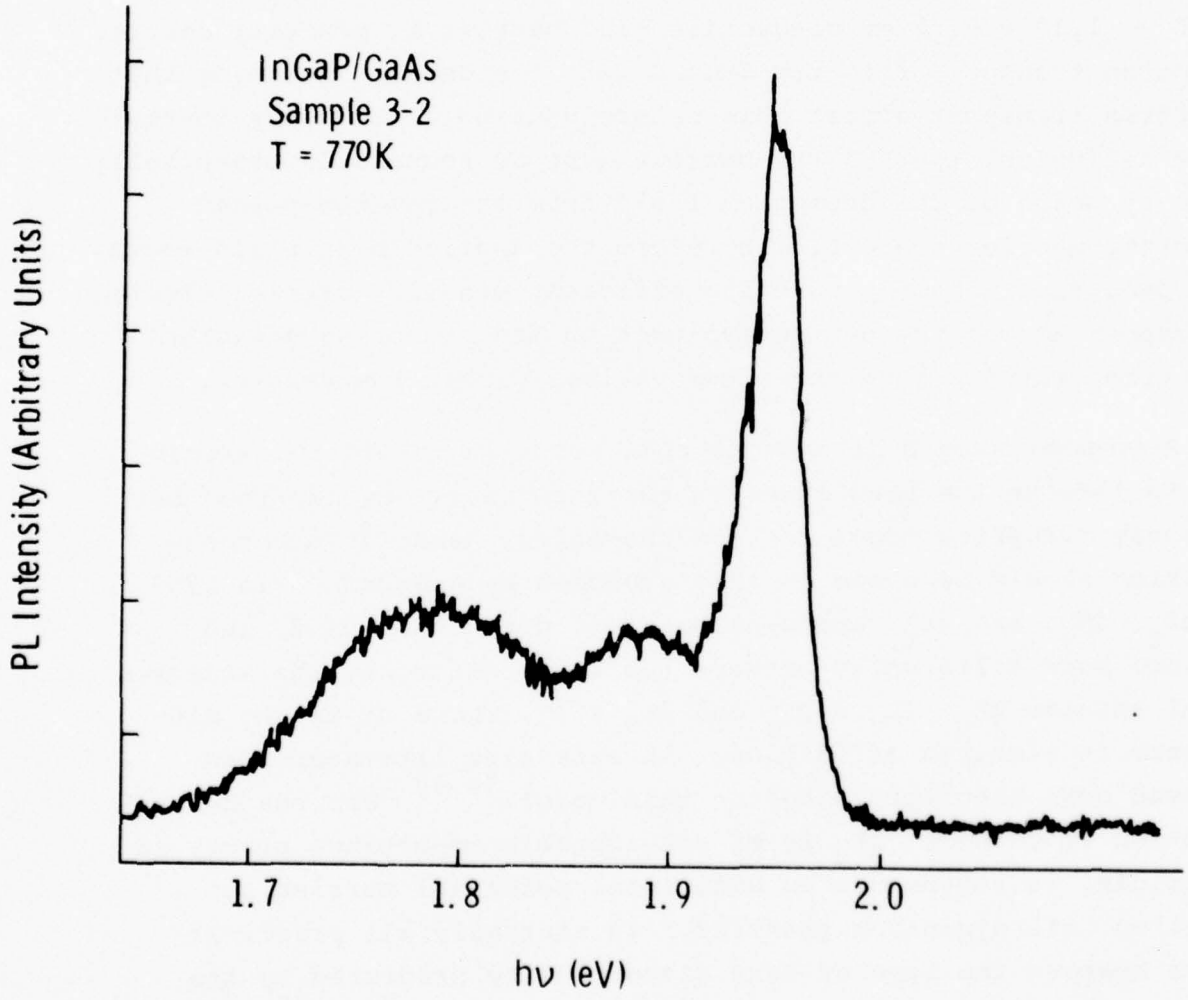

Fig. 28. Photoluminescence spectrum from InGaP/GaAs sample #3-2 taken at 77°K.

3.4 Model Calculations of the p-InGaP/p-InGaAs Heterojunction Cathode

In this section a relatively simple model calculation for the conduction band profile of a p-InGaP/p-InGaAs heterojunction cathode is presented. The main purpose of the model is to give a feeling for what emitter thickness, doping, compositional grading distance, and applied bias are necessary in order to achieve a good heterojunction transfer efficiency for photoelectrons crossing the absorber-emitter interface.

Under zero applied bias conditions, there is an approximately 1.70 - 1.15 = 0.55 eV conduction band barrier to minority carrier electron transport from the InGaAs into the InGaP. Assuming that electron transport across this heterojunction is to be by thermalized diffusion, the 0.55-eV barrier must be reduced to essentially zero by means of the depletion field from the reverse-biased Schottky-barrier contact. Therefore the applied bias field serves the dual function of permitting efficient minority carrier electron transport across the p-p heterojunction and promoting efficient electron transfer into the upper valleys within the emitter.

A comment should be made at this point in regard to exactly how to line up the band edges at the interface. By far the most commonly discussed model for how the energy bands at a heterojunction should be drawn is that proposed by Anderson[52] in 1962. If ΔE_g, ΔE_c, and ΔE_v represent bandgap, conduction band, and valence band differences between two semiconductors, the Anderson model assumes $\Delta E_c + \Delta E_v = \Delta E_g$ and $\Delta E_c = \Delta\chi$, where $\Delta\chi$ is the difference in electron affinities. An extensive literature has evolved over the years based on this model.[53,54] For the heterojunction TE cathode, ΔE_c is of considerable importance since, in principle, it represents an additional potential barrier to electron heterojunction transfer. In virtually all practical cases however the type of band discontinuity predicted by the Anderson model or any of the other more current models[55] can be ignored. The reason for this is that under typical VPE or

LPE growth conditions, there is a finite region over which the composition is graded. The interface is not an abrupt transition step but rather a compositionally graded region on the order of 1000 Å or more. The net effect of this grading region is to essentially smooth out the predicted ΔE_c discontinuity at the heterojunction interface. The work of Oldham and Milnes[56] and Cheung et al.[57] discusses this point in more detail. The predicted heterojunction discontinuity barriers may only be observable experimentally in extremely abrupt heterojunctions such as those produced by molecular beam epitaxy[58] or by special LPE or VPE growth techniques.[59]

The first part of the model to be discussed is the grading function, G(X). The grading function is taken to be a simple mathematical function describing the bandgap variation over the heterojunction transition region. The simplest function would be linear grading function of the form $G(X) \sim E_g(L-x)/L$. However, a physically more attractive function is the hyperbolic tangent which has been employed by others for this purpose.[56,57] The grading function is then given by[60]

$$G(X) = E_g(\text{InGaAs}) + \left(\frac{\Delta E_g}{2}\right)\left[1-\tanh\left(\frac{X-T(\text{InGaP})-L/2}{L}\right)\right]$$

where T(InGaP) is the p-InGaP emitter thickness, L is an effective bandgap grading distance, and X the distance from the emitter-vacuum interface. Note that L in this case is approximately half the distance over which the bands vary from 10-12% to 90-88% of maximum change, ΔE_g.

To complete the model, a Schottky-barrier surface contact is assumed on the p-InGaP surface, i.e. X = 0. The spatial potential variation, V(X), due to an applied bias, V_{bias}, is given by

$$V(X) = \frac{qN_a}{\epsilon}\left(W(V_{bias})\cdot X - \frac{1}{2}X^2\right) - Q_B + V_{bias}$$

where q is the electronic charge, ϵ the relative dielectric constant of the emitter, Q_b the p-Schottky-barrier height, and N_a the acceptor doping concentration. $W(V_{bias})$ is the depletion width which is given by

$$W(V_{bias}) = \left(\frac{2\epsilon}{qN_a} \left(V_{bi} - V_{bias} - \frac{K_B T}{q} \right) \right)^{1/2}$$

where K_B is the Boltzmann constant, T the absolute temperature, and V_{bi} is the amount of band bending at the surface. V_{bi} is Q_B minus the Fermi level height, F, above the valence band maximum in the bulk. As the depletion field sweeps back from the emitting surface into the absorber, the initial 0.55 eV conduction band barrier is pulled down. The bands in the InGaAs also begin to be pulled down. The model calculates V(X) in the InGaAs using the same formula as that shown above but using materials parameters appropriate for InGaAs and an effective Schottky-barrier height based on how much the InGaAs bands are pulled down at the InGaP/InGaAs interface due to the depletion field from the surface Schottky-barrier contact.

The complete model for the conduction band variation (relative to the bulk Fermi level) vs X is simply G(X) + V(X). Several sample calculations for the p-InGaP/p-InGaAs heterojunction cathode have been performed and are shown in Figs. 29-34. It is clear in Figs. 29, 30, and even 31 that thermalized electron transport from the InGaAs into the InGaP would be poor. As the heterojunction grading distance, L, becomes longer and longer the initially rather sharp band discontinuity begins to smooth out and essentially vanishes for the case of Fig. 28 and $V_{bias} \geq$ 3 volts. Note that the emitter thickness and doping level are kept constant in this series. Figure 33 indicates that increasing the doping in the InGaAs absorber to $1 \times 10^{16}/cm^3$ would not cause heterojunction problems, however Fig. 30 shows that $1 \times 10^{17}/cm^3$ would be a problem. Additional calculations indicate that the emitter should be 0.5 to 1.0 micron thick for an

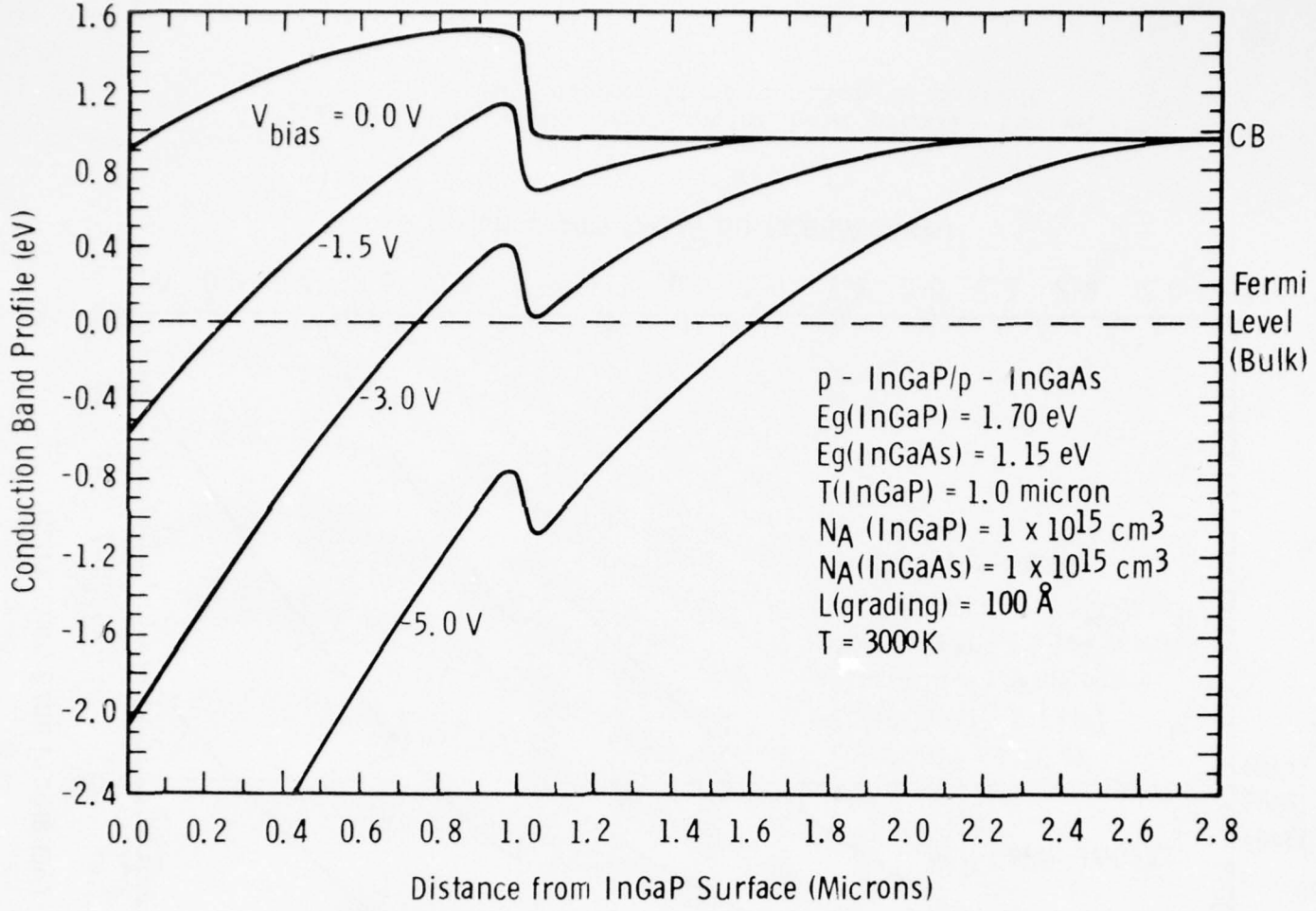

Fig. 29. Calculated conduction band profile for an InGaP/InGaAs heterojunction TE cathode.

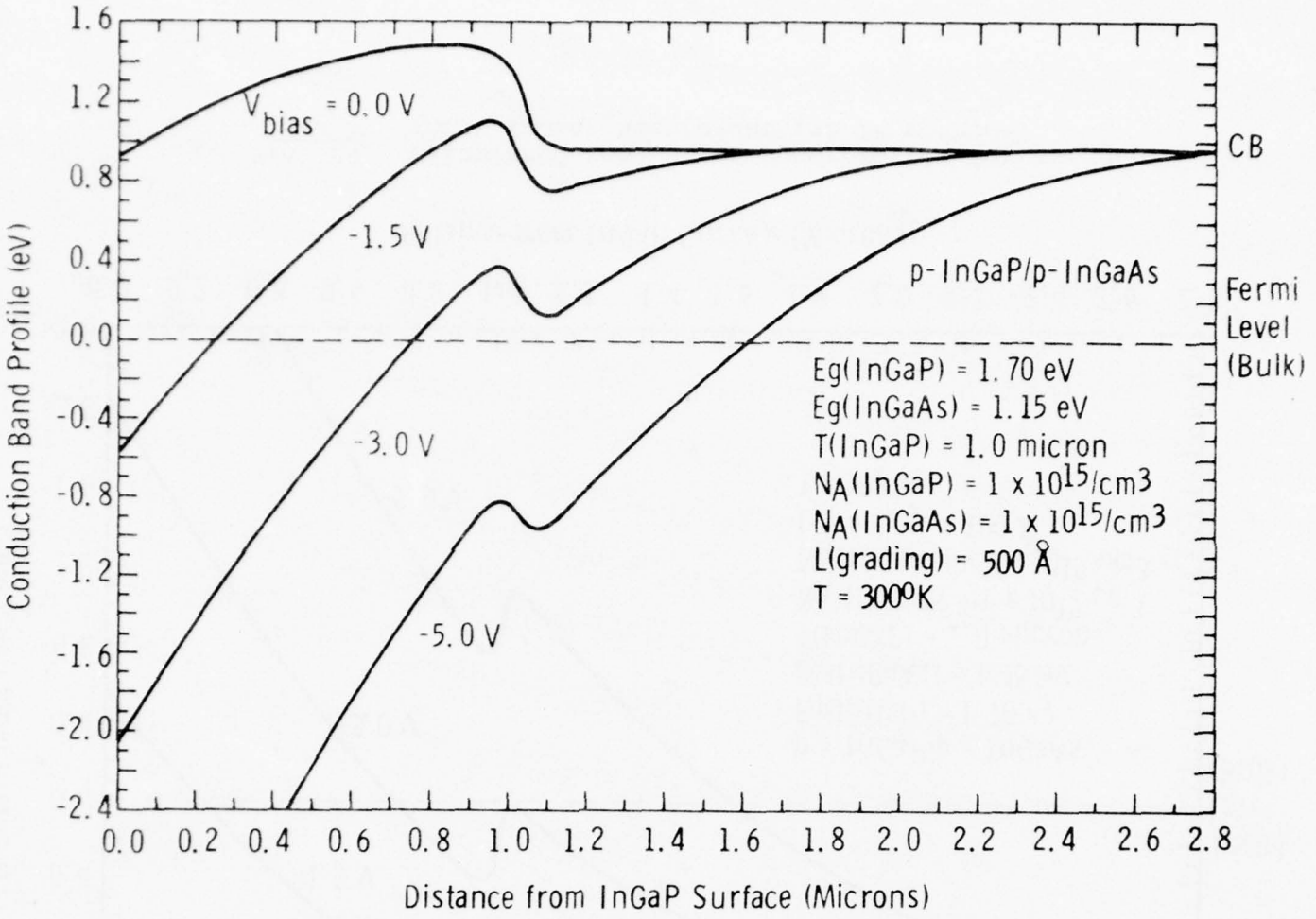

Fig. 30. Calculated conduction band profile for an InGaP/InGaAs heterojunction TE cathode.

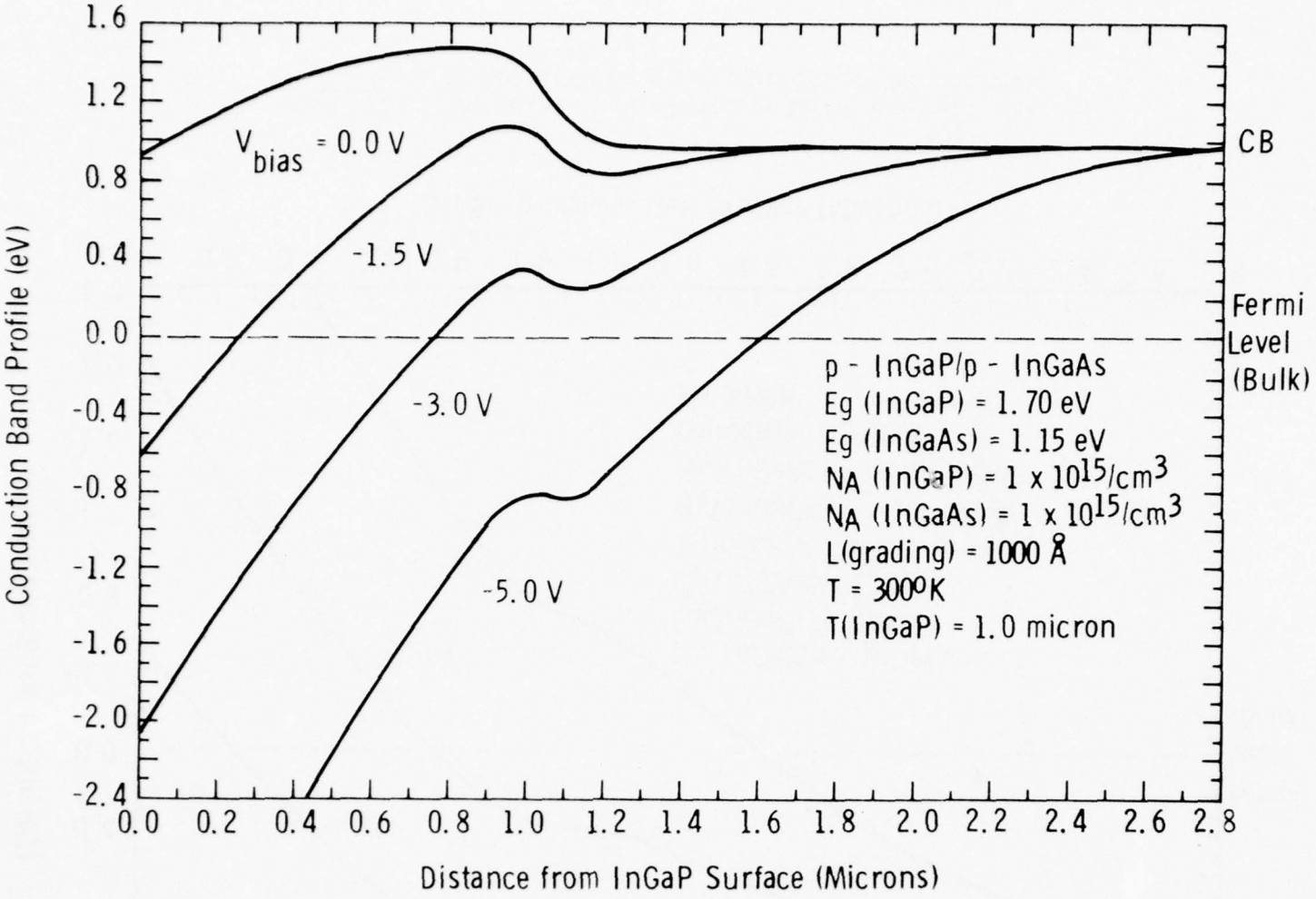

Fig. 31. Calculated conduction band profile for an InGaP/InGaAs heterojunction TE cathode.

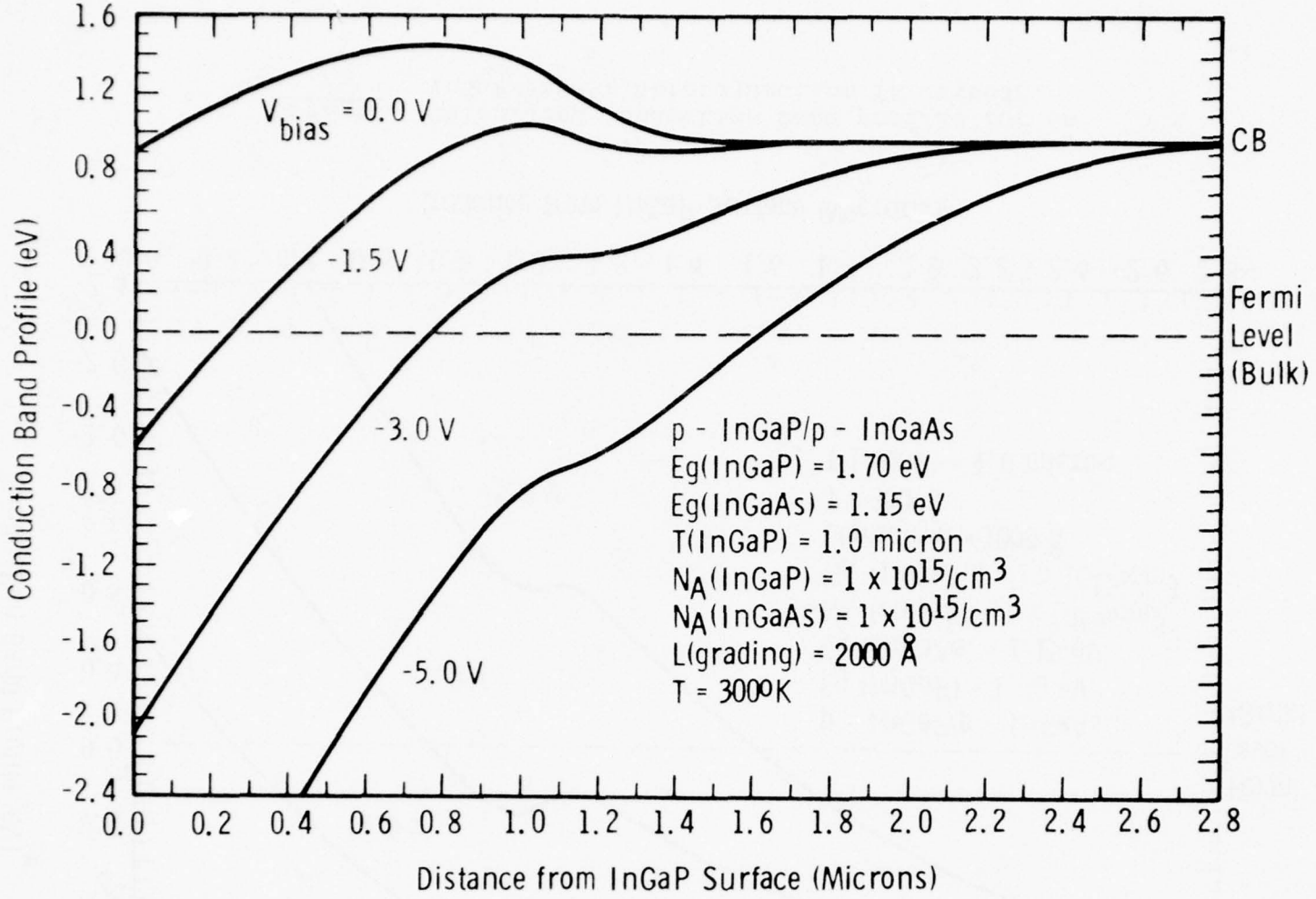

Fig. 32. Calculated conduction band profile for an InGaP/InGaAs heterojunction TE cathode.

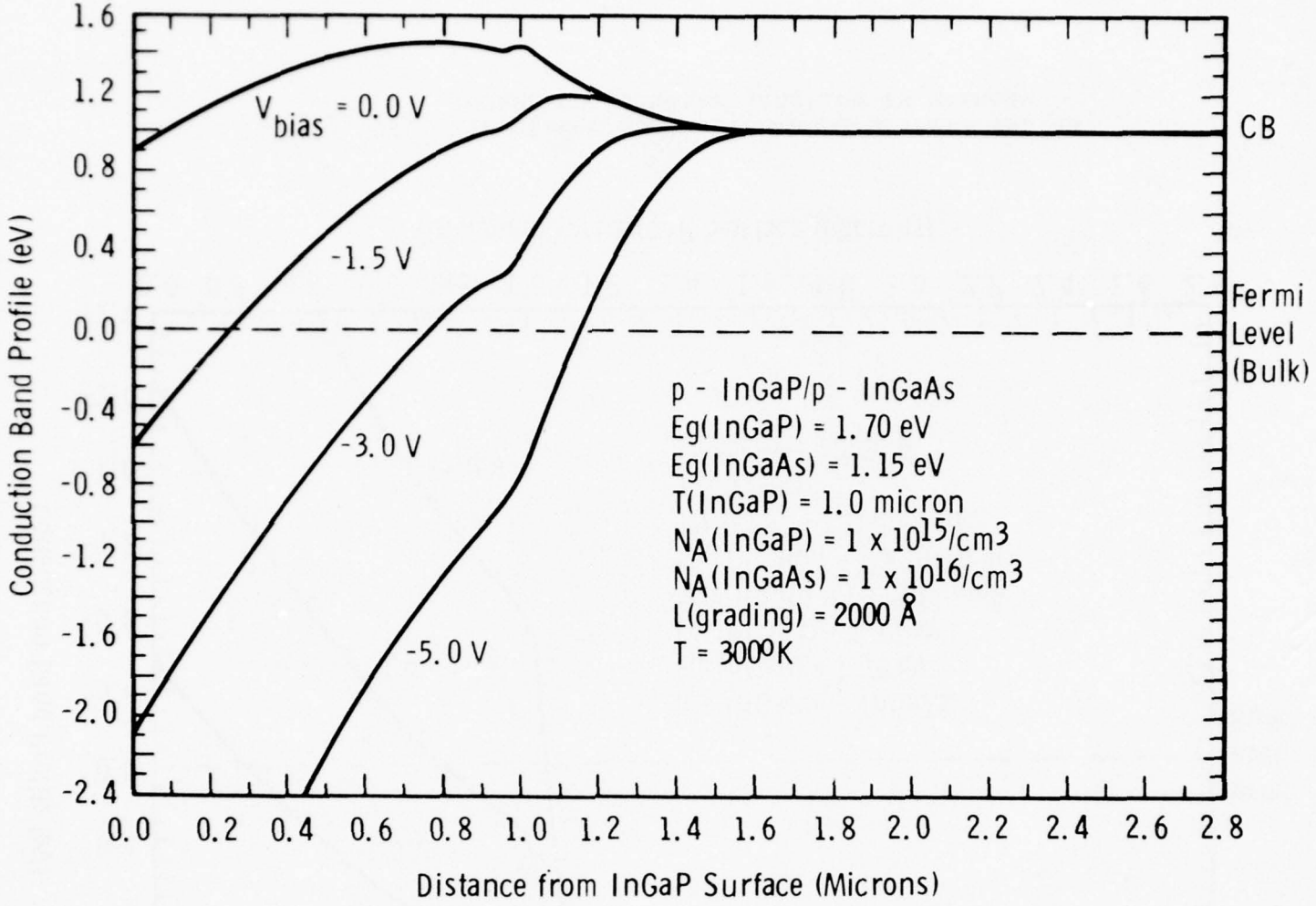

Fig. 33. Calculated conduction band profile for an InGaP/InGaAs heterojunction TE cathode.

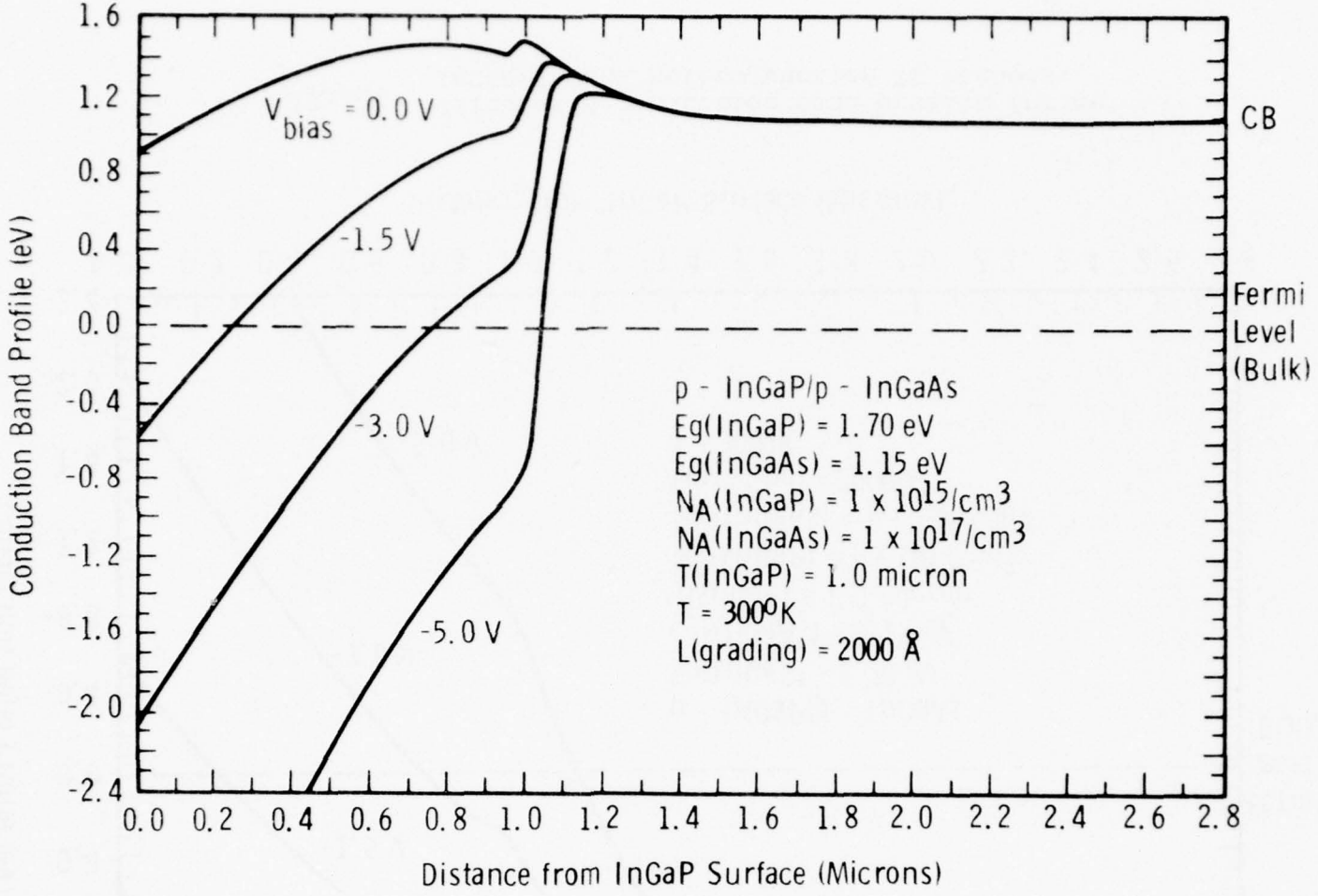

Fig. 34. Calculated conduction band profile for an InGaP/InGaAs heterojunction TE cathode.

emitter doping of 1-5 x $10^{15}/cm^3$. A much thinner emitter is needed if the emitter doping rises much above 1 x $10^{16}/cm^3$. A compositional grading distance on the order of 1000 Å or more is essential for thermalized electron transport across the p-p heterojunction.

Another feature of the model is that it takes the derivative of the potential, V(X), thereby generating the local electric field, E(X). These results show that even in the cases where there is rather abrupt bandgap grading, e.g. Figs. 29 and 30, that there can be a moderately high electric field ($\sim 10^4$ V/cm) extending well into the absorber layer. Therefore there exists the possibility that even if there is less compositional grading at the heterojunction interface than is ideal, there may be enough field to cause partial or complete electron transfer across the heterojunction via the TE effect. At the moment this is only conjecture, and experimental confirmation of this point has not been established.[61]

3.5 Direct Emitter Photoemission Results from p-InGaAsP

Before discussing the vacuum photoemission results a few comments should be made in regard to cathode preparation, vacuum processing, Schottky-barrier evaporation, and Cs-O activation procedure. It is well known that surface carbon contamination is a serious obstacle to achieving high performance NEA (and presumably TE) cathodes. Once the cathode is removed from the growth system the emitting surface is exposed to various atmospheric gases and pollutants until the time comes for it to be vacuum processed. The ideal situation is for the cathode to be grown and immediately transferred into the vacuum system without delay. The hybrid cathode discussed in detail in Sec. 3.6 was handled in this fashion. The next best interim procedure would probably be storage in UHV. For longer-term storage, a week or more, a nitrogen dry box is used. Just prior to transfer into vacuum the cathode is given a chemical cleaning procedure

consisting of hot solvent baths, and 4:1:1 (sulfuric acid, hydrogen peroxide, and water), and dilute bromine methanol etches. The chemical cleaning procedure helps remove the surface contaminants built up during storage in the dry box. The above cleaning procedure is certainly not unique and many others would probably be just as satisfactory. The direct emitter cathodes discussed in this section and several of the InGaP emitter cathodes were stored in a N_2 dry box from a few days to several weeks prior to chemical cleaning and vacuum testing.

After chemical cleaning and immediate transfer into the vacuum system the cathode surface is further cleaned. The procedure used for all the cathodes discussed in this report consisted of heat cleaning in vacuum to near the cathode surface decomposition temperature and then cooling to room temperature. No sputtering techniques were used. Ion sputtering is a common technique for surface cleaning, especially for carbon contaminated surfaces. However it has not been demonstrated to be a superior technique to simple vacuum heat cleaning for the NEA III-V photocathodes, provided that the cathode was not badly contaminated prior to the vacuum cleaning procedure. An Auger electron spectrometer was found to be essential in setting up and monitoring from time to time the entire cathode surface cleaning procedure.

So far the procedure discussed above is identical to that for handling and surface cleaning a NEA photocathode. At this point, after vacuum heat cleaning, the TE cathode requires a Schottky-barrier contact to be evaporated onto the active emitter surface. A simple tungsten filament source with 5-9's pure Ag wire wrapped about the filament is used for this purpose. A Sloan digital film thickness monitor is employed to monitor the evaporation process. The Sloan monitor is calibrated by evaporating a relatively thick Ag film and measuring its thickness using a Varian model 980-4000-Å scope interferometer.

An evaporation rate of approximately 1 to 3 Å/sec is used and the Ag film thickness is on the order of 100 to 300 Å. The Cs-O activation procedure is essentially that used for NEA cathodes, i.e. Cs-only and then Cs+O to a photoemission peak. Sometimes TE photoemission can be detected at the Cs-only point in which case the Cs+O activation procedure is monitored with a bias potential on the cathode. However whether the activation is monitored with no bias on the cathode (i.e. just a white-light monitor) or with a bias seems to give about equally good TE photoemission results. The bias is physically applied in the vacuum system by means of a point contact probe that is allowed to just touch the evaporated Ag film. The cathode holder, which is electrically isolated from the vacuum system walls, provides the other side of the biasing circuit contact. A battery-operated, regulated voltage supply is used for the external biasing source. The electron current leaving the cathode or the collector current is used for photoemission and dark current measurements. A mirror at the back of the vacuum system is positioned such that light from a monochromator source can be focussed onto the back of the cathode for semi-transparent (i.e. transmission-mode) photoemission measurements. Photoemission results from three direct emitter cathodes are presented below.

Since feasibility of the general approach had already been demonstrated (e.g. Fig. 6), the primary new task was one of optimizing the direct emitter cathode for 1.06-micron detection. From a materials standpoint this implies growing high quality p-InGaAsP on InP of the correct composition ($\approx$ 1.15 eV bandgap) and doping concentration ($\sim 10^{15}/cm^3$). From a device processing standpoint this implies careful cathode surface cleaning procedures, Schottky-barrier evaporation, and Cs-O activation. Figure 35 shows reflection-mode yield from a direct emitter cathode (#PQ22-2) which has nearly an optimal bandgap and achieved approximately 1.0% yield at 1.06 microns. Figure 36

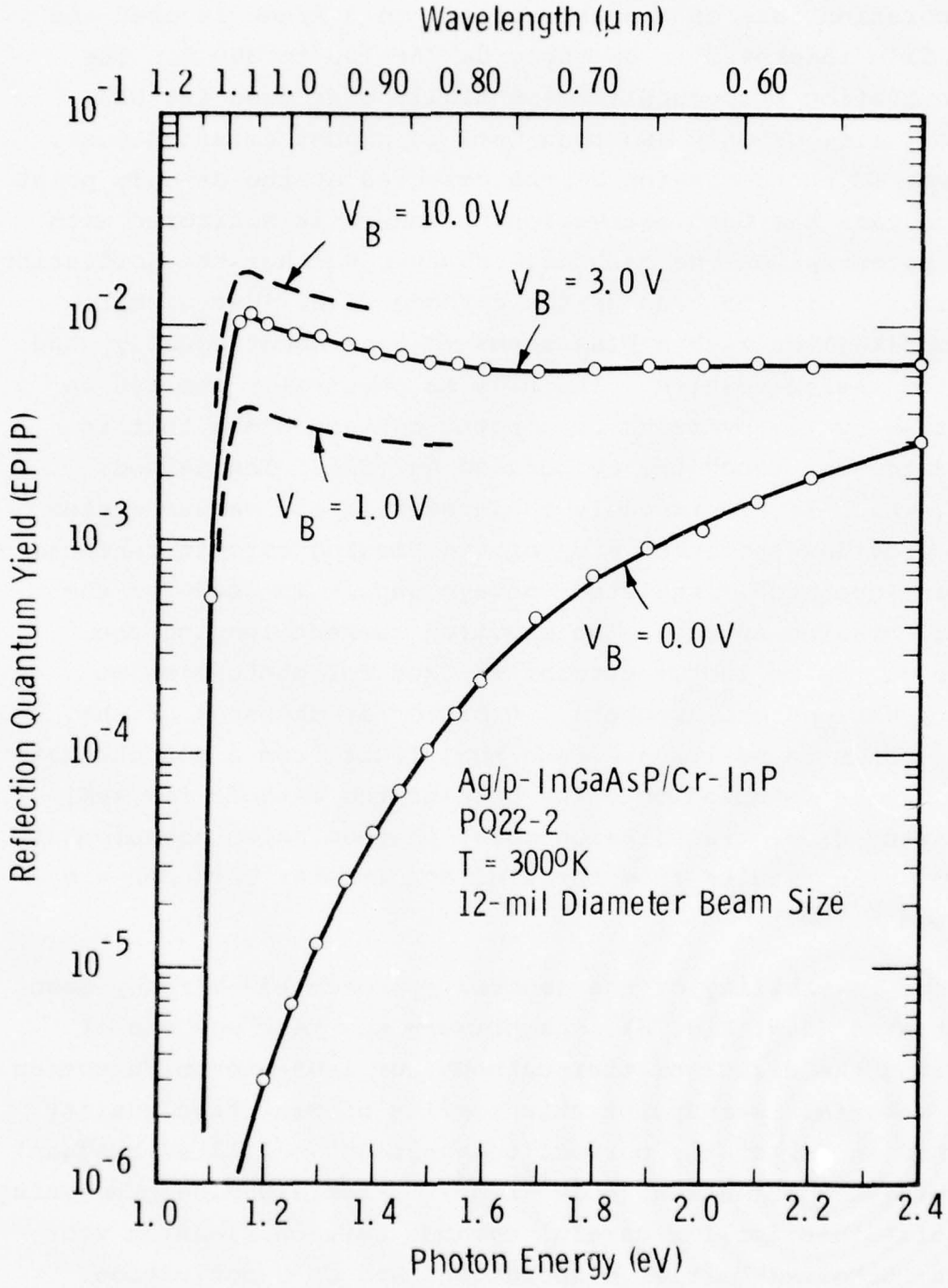

Fig. 35. Reflection-mode quantum yield from a direct emitter p-InGaAsP/InP TE cathode.

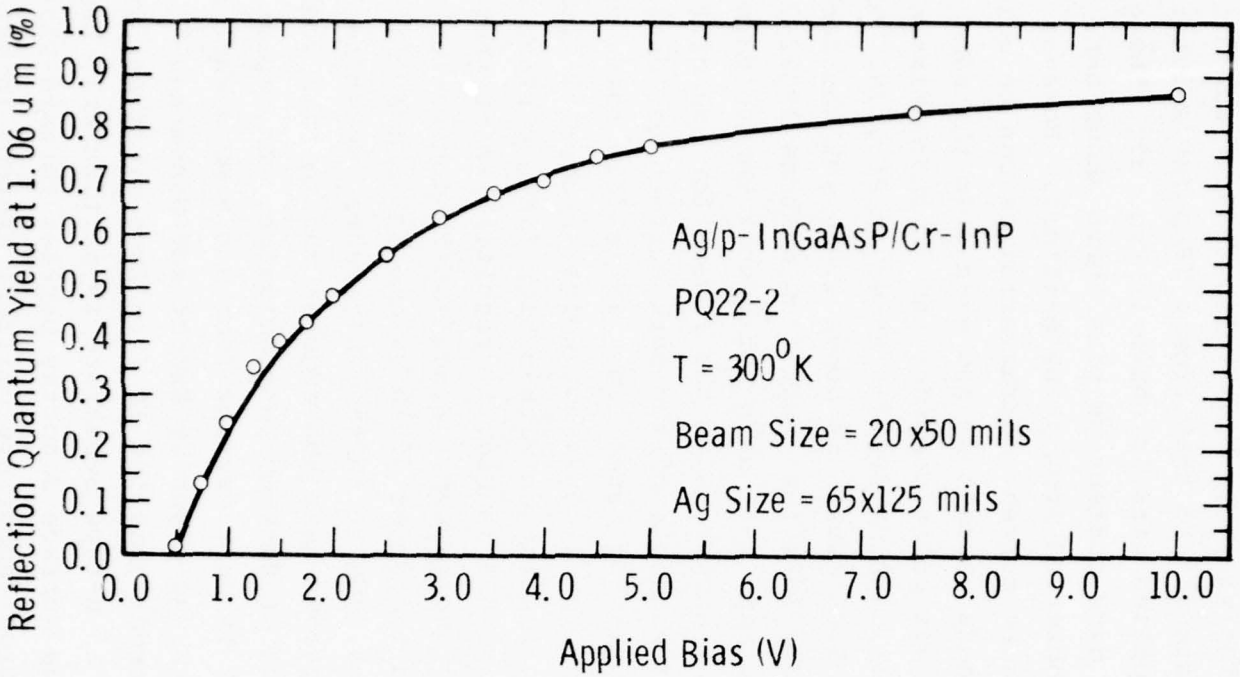

Fig. 36. Reflection-mode quantum yield at 1.06 microns vs applied bias from a p-InGaAsP direct emitter cathode.

shows the field-assisted 1.06-micron yield vs applied bias. Note the Ag film and optical beam sizes. The cathode itself is 150 x 400 mils. The yield vs bias voltage curve shown in Fig. 36 is quite similar to that from a TE p-InP emitter. Dark current vs applied bias is shown in Fig. 37. The general shape of the dark current vs bias curve shown here is typical of those observed from p-InP emitters. However the magnitude of the dark current characteristics can be quite variable from cathode to cathode and even from the same cathode. As an example of this point consider the TE photoemission results from direct emitter cathode #PQ22-5 shown in Fig. 38. The field-assisted yield at 1.06 micron is above 1.0%, yet the dark current is considerably less than that from cathode #PQ22-2. Sufficient dark current data have not been taken to date to give a satisfactory answer as to the reason for the difference. The general bias dependence of the dark current is consistent with an impact ionization mechanism. It is felt that, under strong reverse bias conditions, hot holes (process "2" in Fig. 1) could cause impact ionization within high field surface depletion region (process "3" in Fig. 1) resulting in further TE electron emission into vacuum. Since impact ionization phenomena requires fields on the order of 10^5 V/cm, it is most likely that localized hot spots, due to surface blemishes, scratches, hillocks, etc., or regions near the edge of the Ag film would be the primary sources of dark current emission. An impact ionization analysis of TE dark current from a 0.9 eV direct emitter cathode is given in the paper by Escher and Sankaran.[62] Another source of dark current emission is from free electrons in the substrate. Using an n-type substrate is particularly bad in that reverse biasing the surface Schottky-barrier forward-biases the internal p-n junction (substrate-emitter) thereby injecting electrons from the substrate into the emitter and hence into vacuum.[23] The role of semi-insulating or p-type InP substrates in terms of dark current has not been experimentally established.

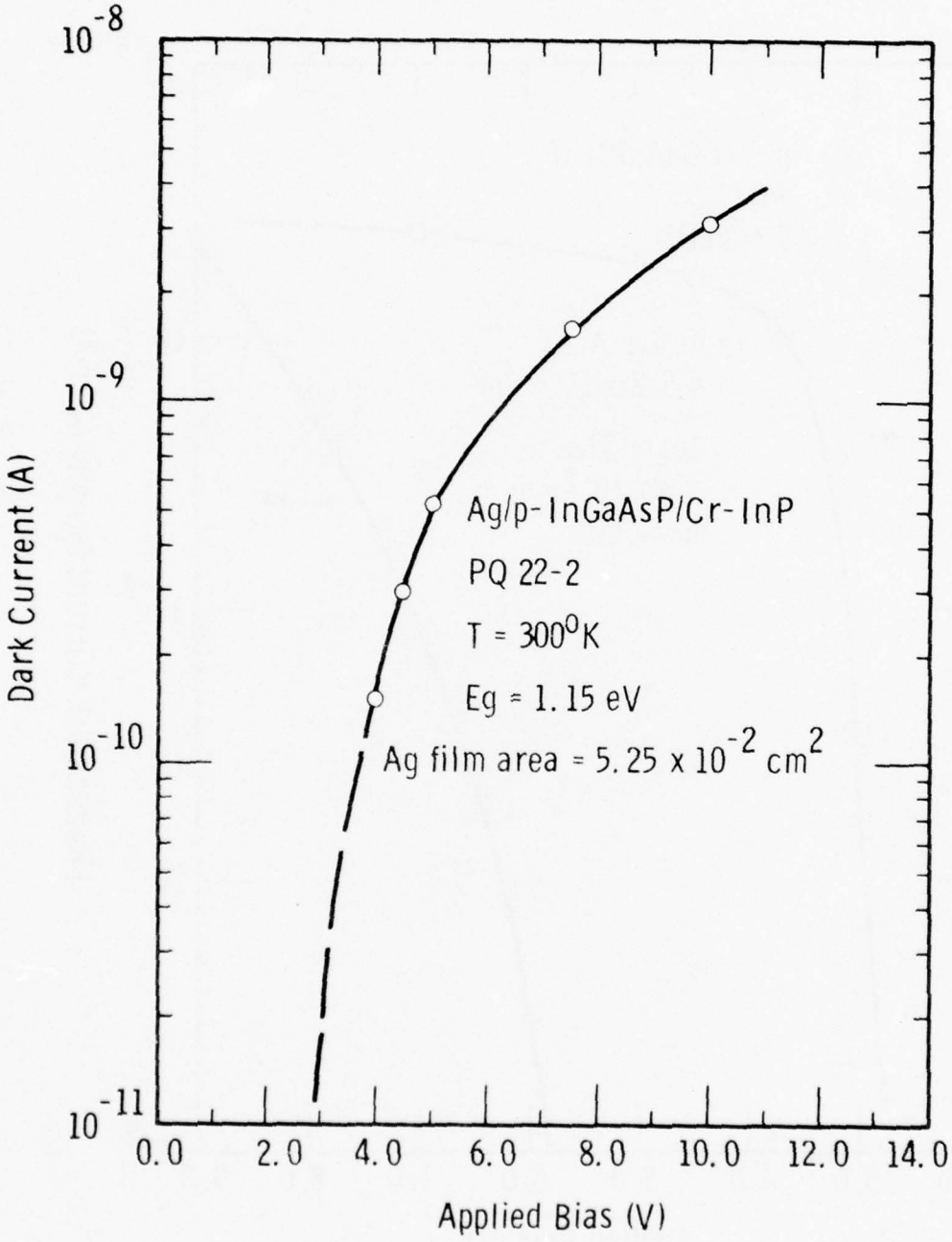

Fig. 37. Dark current emission vs applied bias from a p-InGaAsP direct emitter cathode at 300°K.

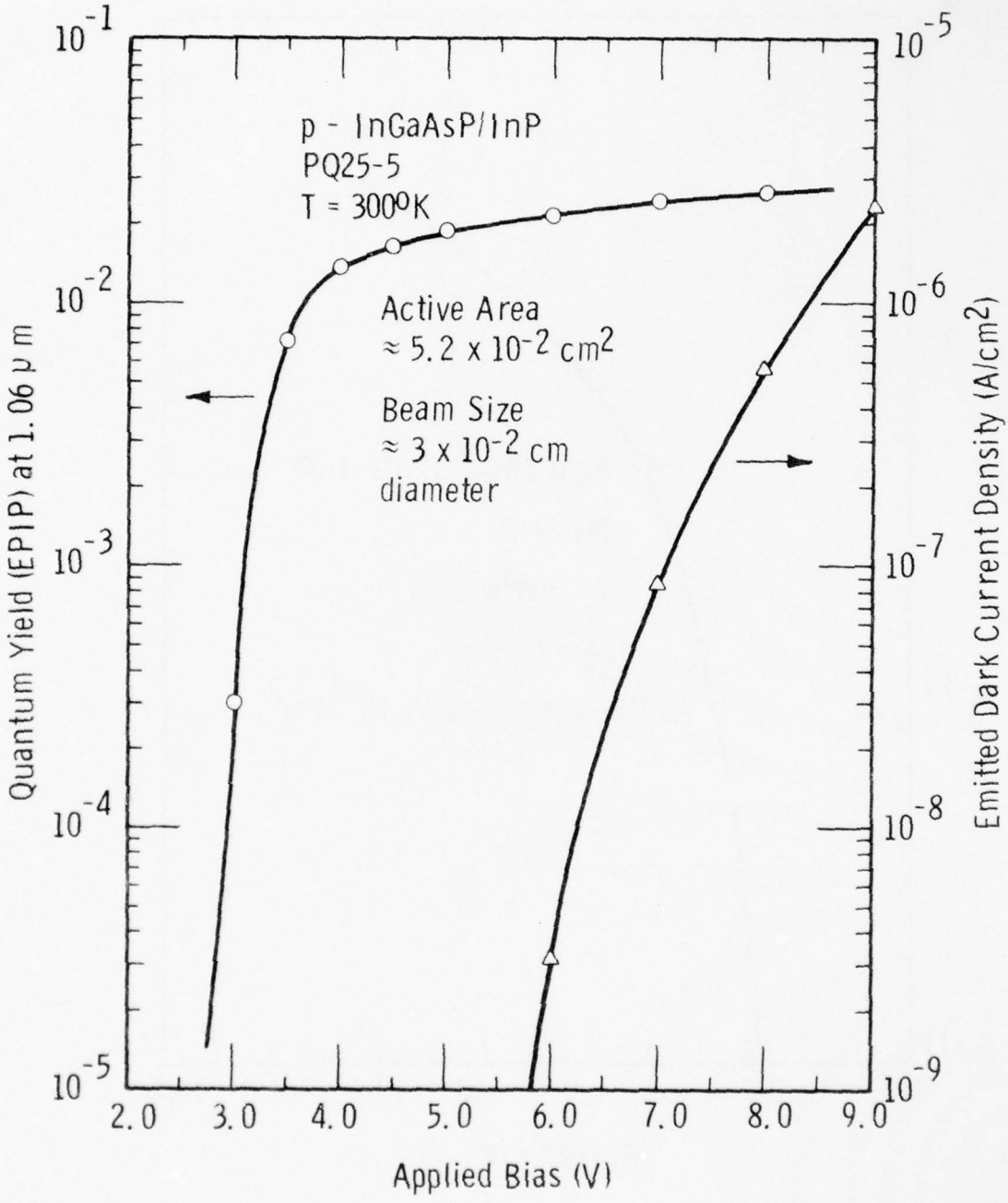

Fig. 38. Reflection-mode quantum yield at 1.06 microns and dark current density vs applied bias from a p-InGaAsP direct emitter.

A high quality, low p-type substrate would most likely be the substrate of choice.

Feasibility of semitransparent operation from a direct emitter cathode is shown in Fig. 39. The transmission-mode response is lower than the reflection yield due to the fact the back of the cathode was neither polished nor had an antireflection coating. If the cathode had been optimized for transmission response, the semitransparent yield at 1.06 microns could well have been 20% or so higher than the front-surface yield. The short wavelength cut-off at approximately 9300 Å is due to the optical absorption edge of the InP substrate (1.35 eV bandgap = 9185 Å). Bias dependence of the reflection and transmission yield at 1.06 microns is shown in Fig. 40.

Figures 41 and 42 show Cs-only and Cs+O activation reflection-mode yield curves from the best direct emitter cathode tested to date (#PQ22-8). The bias dependence of the 1.06-micron yield is shown in Fig. 43. Note that under full bias conditions the Cs+O yield is 2.7% at 1.06 microns. This is an excellent yield representing a factor of 20 to 30 improvement over a conventional S-1 cathode. Dark current emission vs bias is shown in Fig. 44. For a dark current density of $\leq 10^{-9}$ A/cm^2, the operating bias potential would be about 5-6 V which corresponds to a 1.06-micron photoemission yield of about 75% of maximum, i.e. approximately 2.0%. There exists therefore a bias potential at which the dark current emission is satisfactory and the 1.06-micron photoemission sensitivity is a good fraction of the peak (full bias) yield.

Figure 45 is a rather crude spatial photoemission curve derived from scanning a small diameter spot vertically across the face of the sample. The peak yield is seen to occur through the Ag film with a modest yield apparently coming from off the Ag film--i.e. from the p-InGaAsP surface itself. This is not

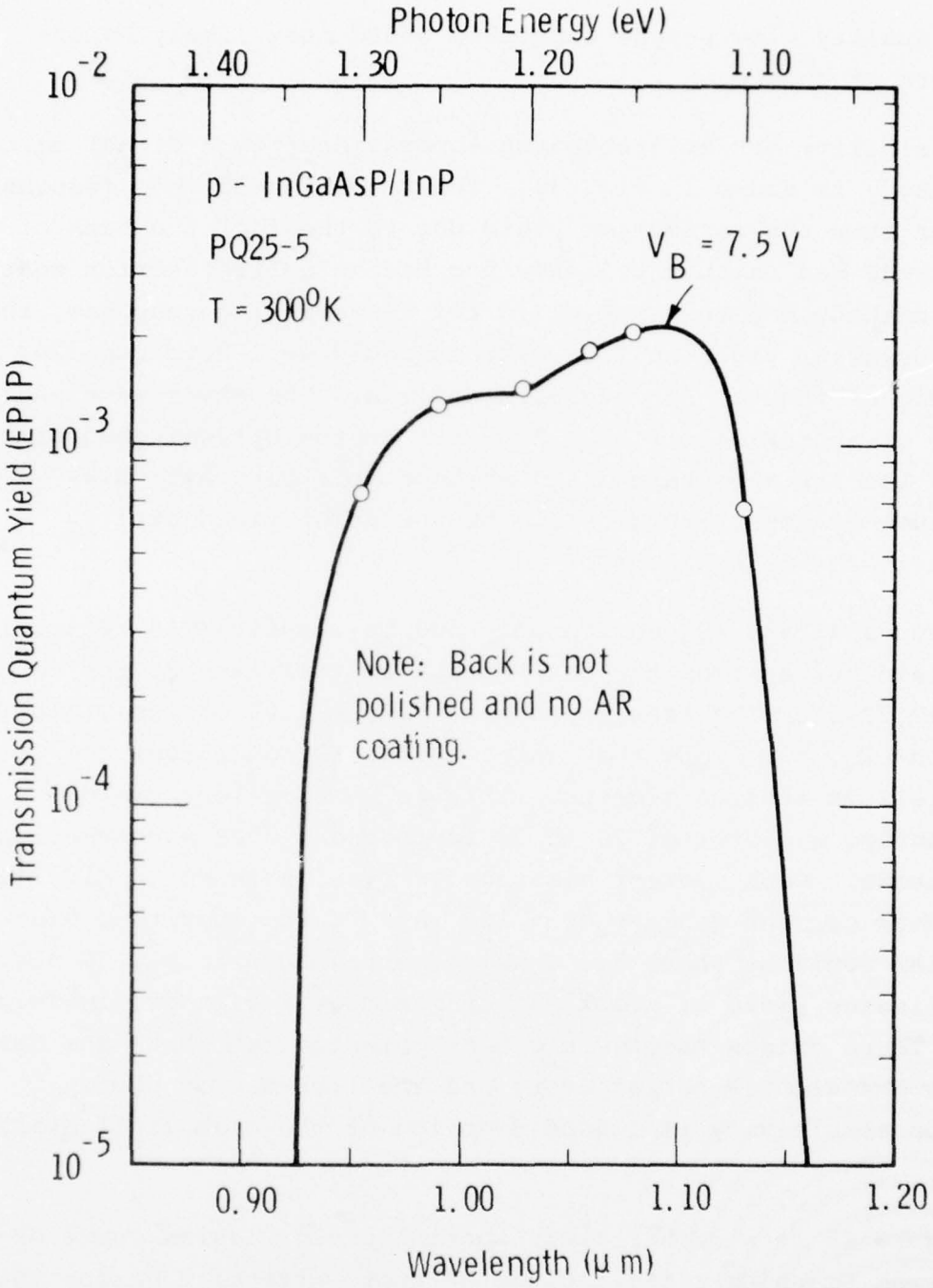

Fig. 39. Transmission-mode quantum yield from a p-InGaAsP direct emitter cathode.

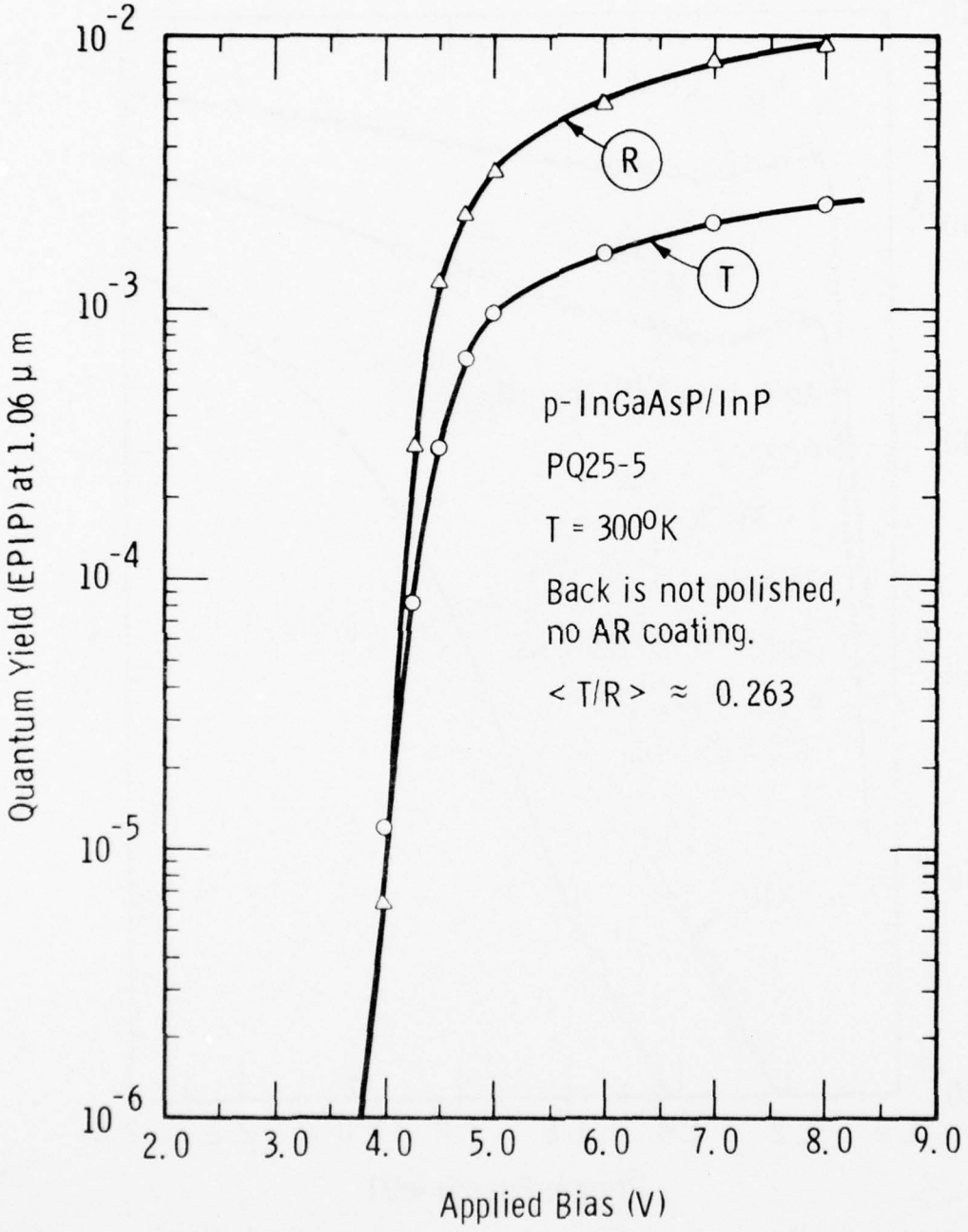

Fig. 40. Reflection-mode (R) and transmission-mode (T) yield at 1.06 microns vs applied bias from a p-InGaAsP direct emitter cathode.

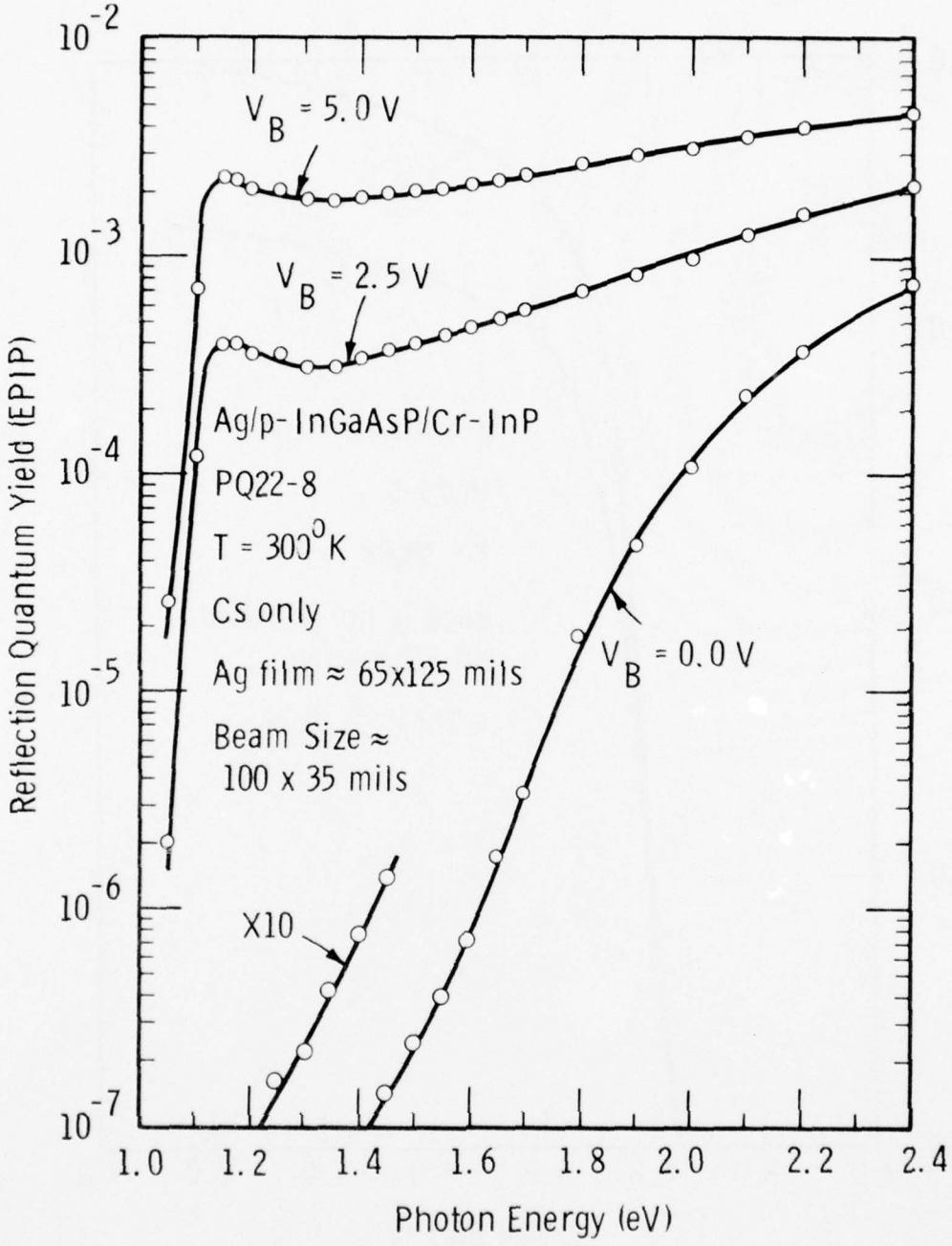

Fig. 41. Reflection-mode quantum yield, Cs-only, from a p-InGaAsP direct emitter cathode.

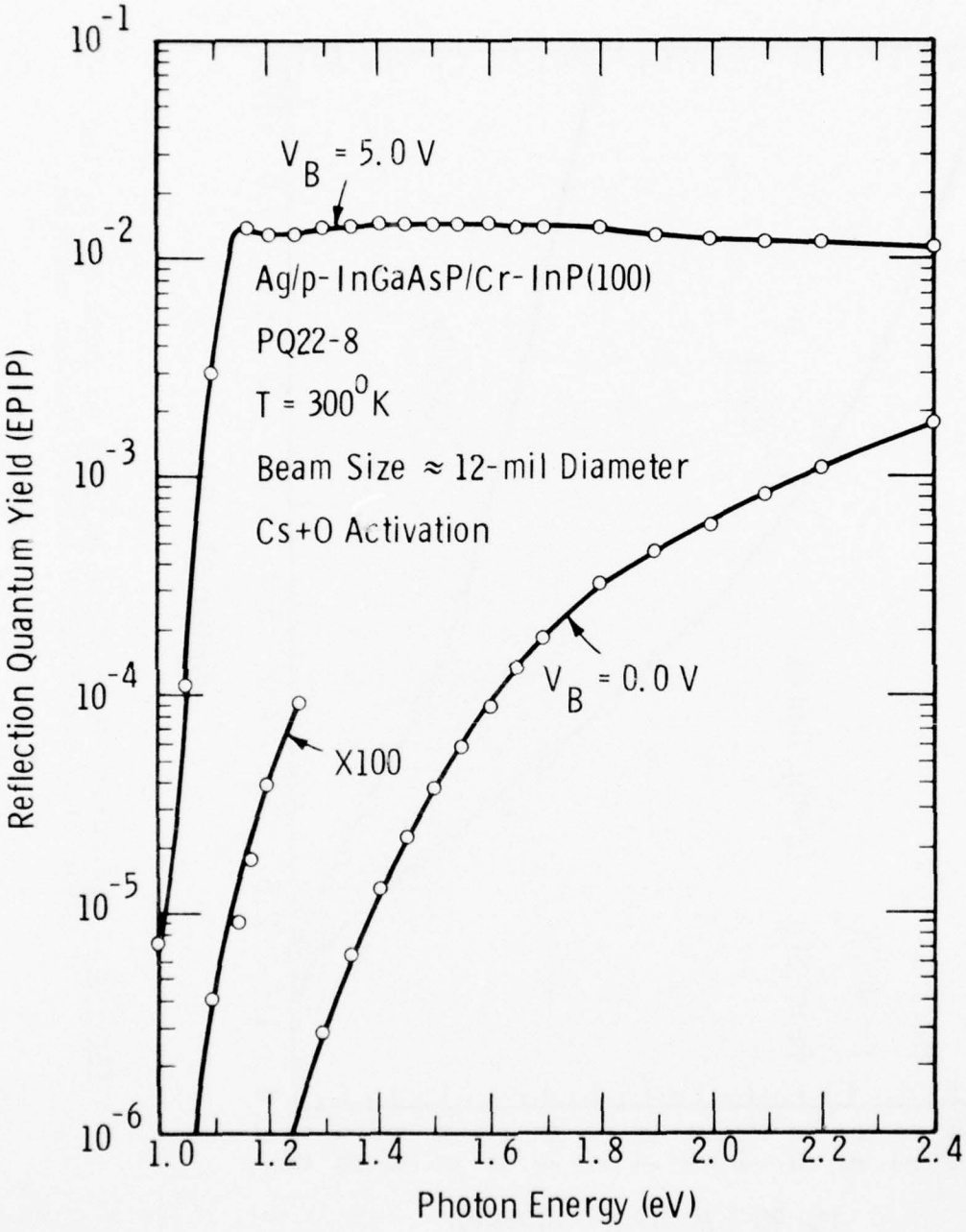

Fig. 42. Reflection-mode quantum yield, Cs+O activation, from a p-InGaAsP direct emitter cathode.

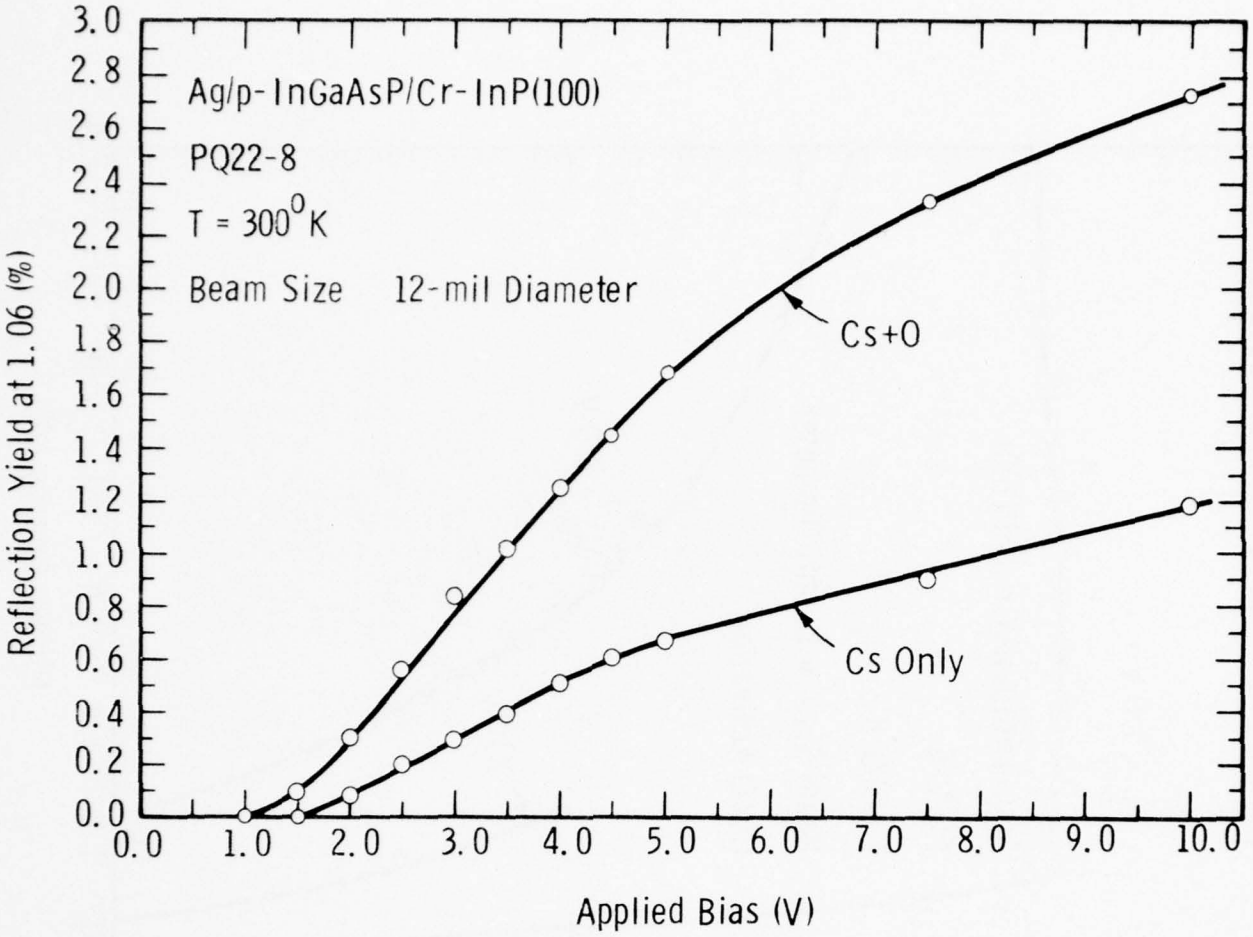

Fig. 43. Reflection-mode yield at 1.06 microns vs applied bias from a p-InGaAsP direct emitter cathode.

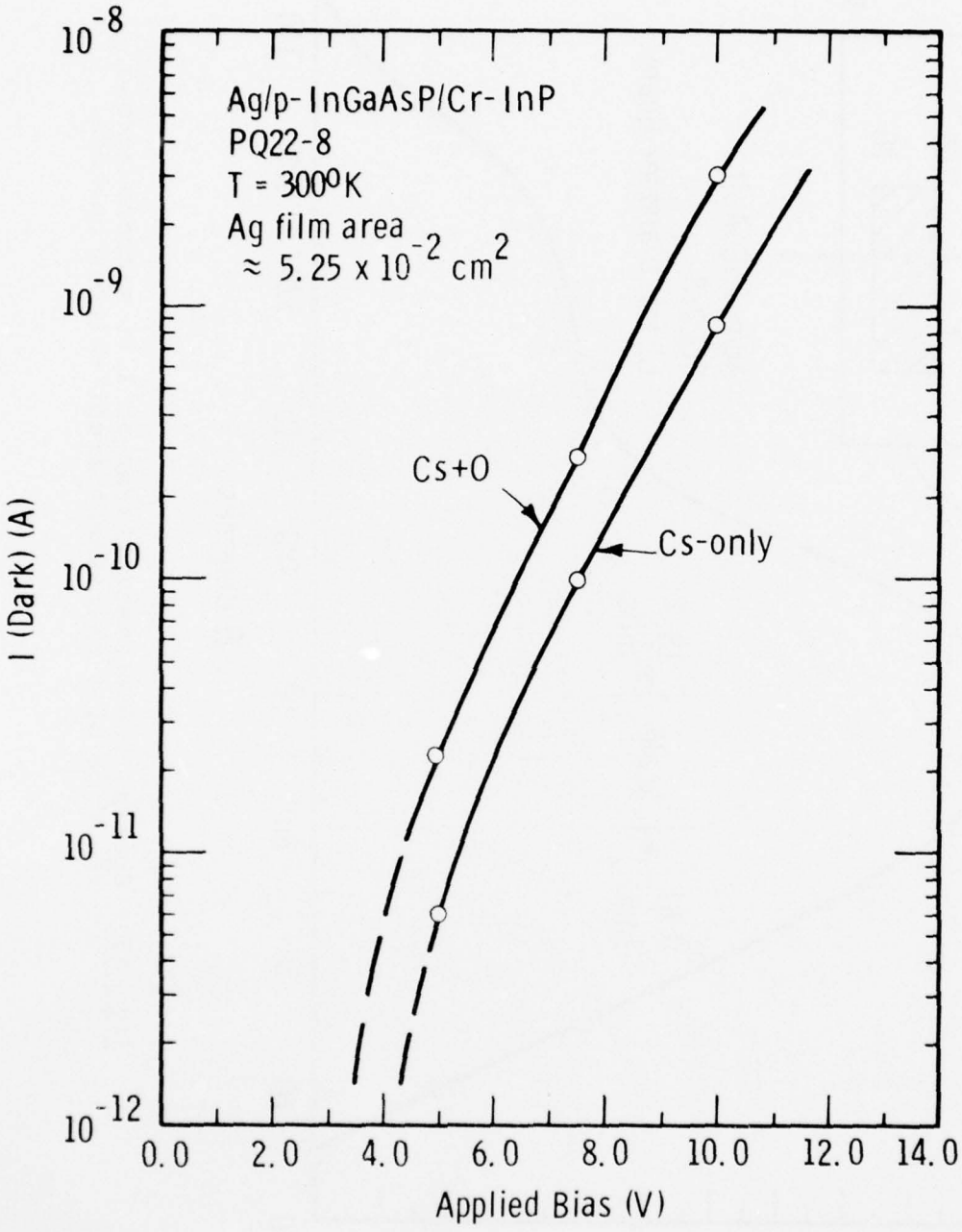

Fig. 44. Dark current emission from a direct emitter cathode at 300°K.

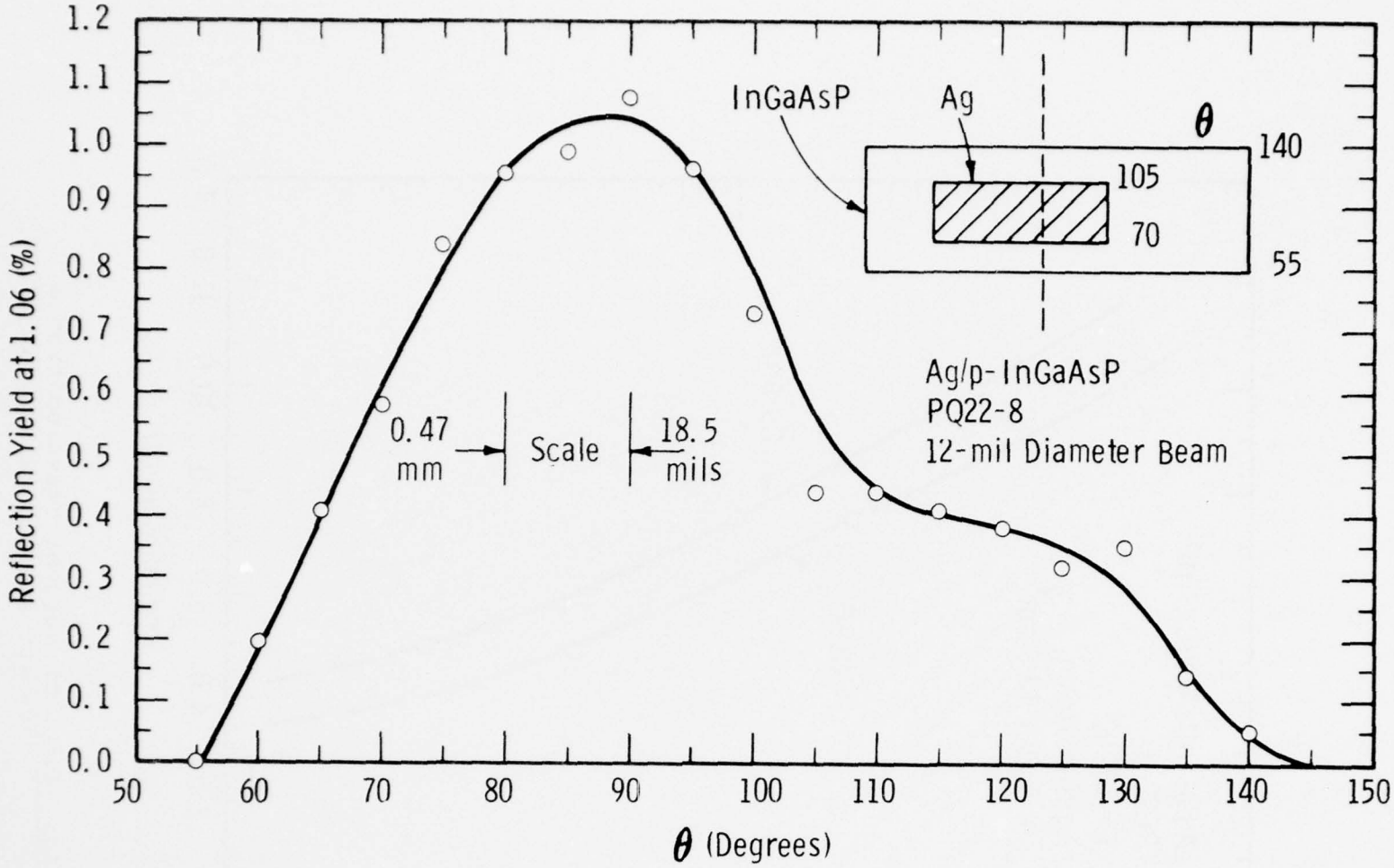

Fig. 45. Spatial photoemission scan at 1.06 microns across the face of a p-InGaAsP direct emitter cathode.

an unusual phenomena. The Cs-O coating has enough conductivity to partially act as a broad area biasing contact as well as a work function lowering layer. The effect is particularly clear if the activation is deliberately made on the Cs-rich side. In this case one often sees the peak TE yield from areas adjacent to the Ag film's edges. Figure 46 shows an extreme example of this behavior for the case of a p-InP emitter cathode with a rather thick (600 Å) Ag film. An interesting related phenomena often observed in those cases where there is significant TE yield from off the Ag film is a pronounced nonlinear behavior in the photoemission signal vs light intensity. Typical incident photon irradiance power densities on the order of 1×10^{-4} W/cm^2 are employed for most yield curve data taking.[63] However a linear photoemission signal vs light intensity behavior often does not occur for power densities a factor of 30-100 times lower. Presumably the reason for this is that the Cs-O activation layer is less effective as a biasing contact at the higher intensity levels. The nonlinear behavior is certainly not a problem under these circumstances and may be an advantage in that the photosignal would be self-limiting at the higher light input intensities.

3.6 Hybrid Heterojunction Photoemission Results from p-InGaAsP/p-InP

2.8% quantum efficiency at 1.06 microns in the reflection mode has been achieved during this reporting period from a hybrid heterojunction TE cathode. This represents the highest 1.06 micron TE photoemission results obtained to date. The earlier progress on the hybrid cathode is outlined in Sec. 2.1 and discussed in some detail in the paper by Escher et al.[30]. The materials growth of the cathode is discussed in Sec. 3.2.

Figure 47 shows the reflection-mode quantum yield from hybrid cathode #2-21B. At first glance the yield shown here seems to be almost a textbook example on how a heterojunction

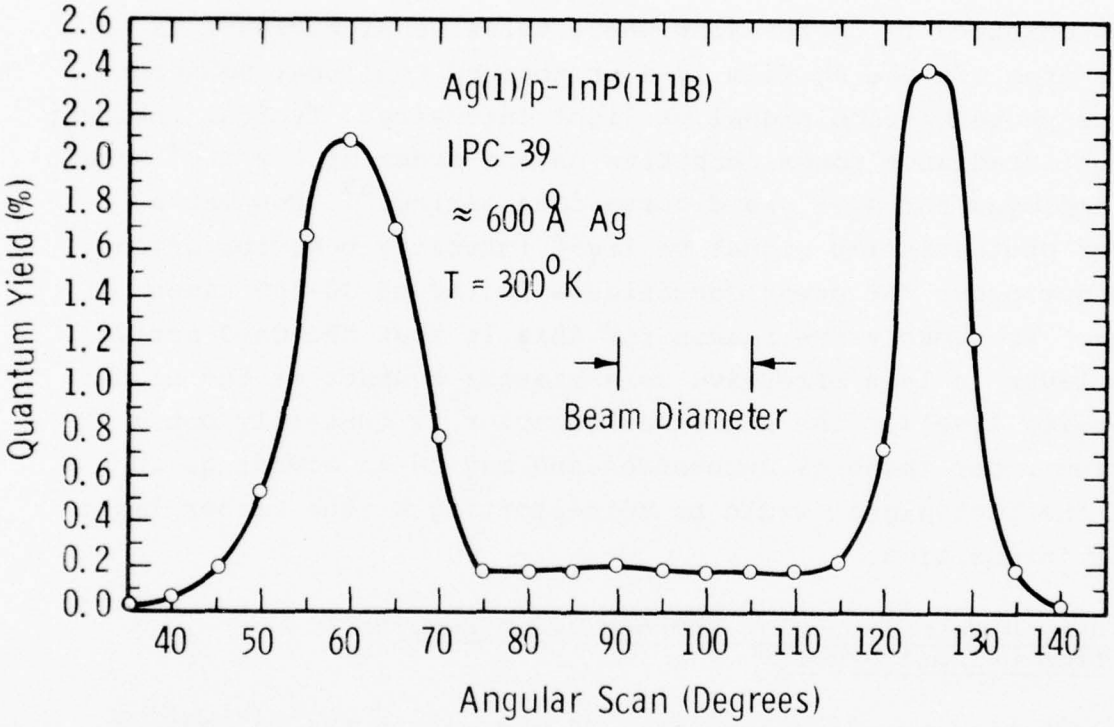

Fig. 46. Spatial photoemission scan across the face of a p-InP TE photocathode.

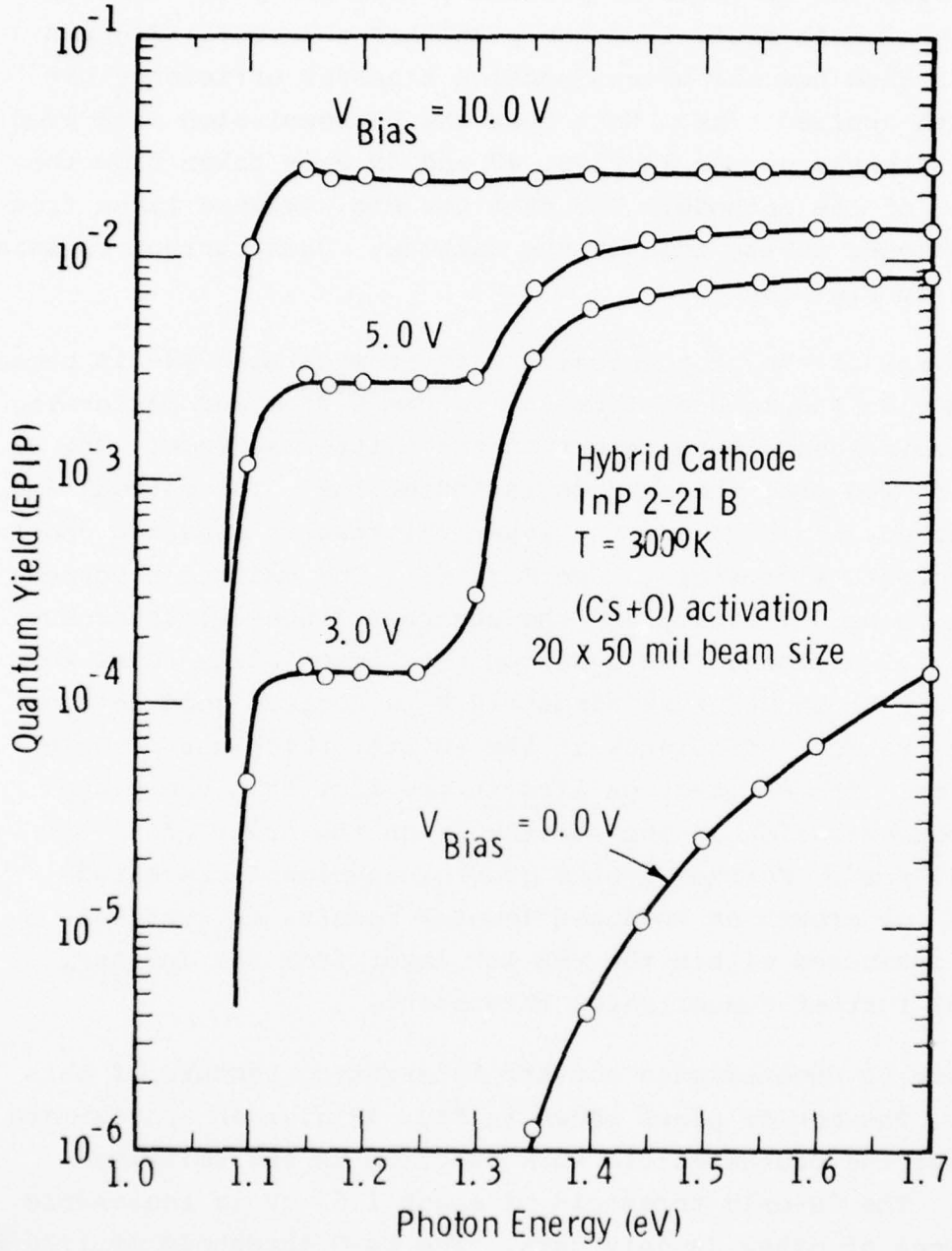

Fig. 47. Reflection-mode quantum yield from a p-InP/p-InGaAsP hybrid heterojunction TE cathode.

cathode should behave. In many ways this is true. For the 3-V applied bias the TE yield is primarily from the p-InP emitter with only a small yield from the p-InGaAsP absorber. Figures 48 and 49 show how the heterojunction transfer efficiency behaves with applied bias. Note that the photoemission data used to calculate the curves in Figs. 47 and 49 were taken from the same area of the cathode. The data for Fig. 48 were taken from an area closer to the edge of the cathode. Dark current emission is shown in Fig. 50.

Analysis of the photoemission data from cathode #2-21B began with removing the cathode from the vacuum system and performing a photoluminescence measurement on the emitter surface. The PL spectra showed that the surface is indeed InP. The cathode was then cleaved, stained, and the layer thicknesses measured under a high-powered microscope. See Fig. 51. The emitter thickness (InP) is about 0.7 micron and the absorber (InGaAsP) thickness is about 1.2 microns. The question that immediately comes to mind is why it should take almost 10 V to achieve good heterojunction transfer efficiency if the emitter thickness is only 0.7 micron. The explanation lies in the fact that the p-type doping concentration in the emitter is on the order of $3\text{-}5 \times 10^{16}/cm^3$. Further hybrid growth experiments revealed that VPE InP growth on Zn-doped InGaAsP results in considerable Zn inclusion within the VPE InP layer from the InGaAsP. Figure 52 further demonstrates this point.

Figure 53 demonstrates another interesting feature of this cathode. The Fowler plots shown in Fig. 53 give an approximate measure of the photoelectric work function on the emitting surface. The Cs-only threshold of about 1.63 eV is reasonable and typical of other Cs-only data. The Cs-O threshold of 1.34 eV however is quite high. A more typical threshold (see, for example, Fig. 35) is 1.0 to 1.2 eV. The reason for the higher threshold is due to a rather low vacuum heat cleaning temperature, 500°C

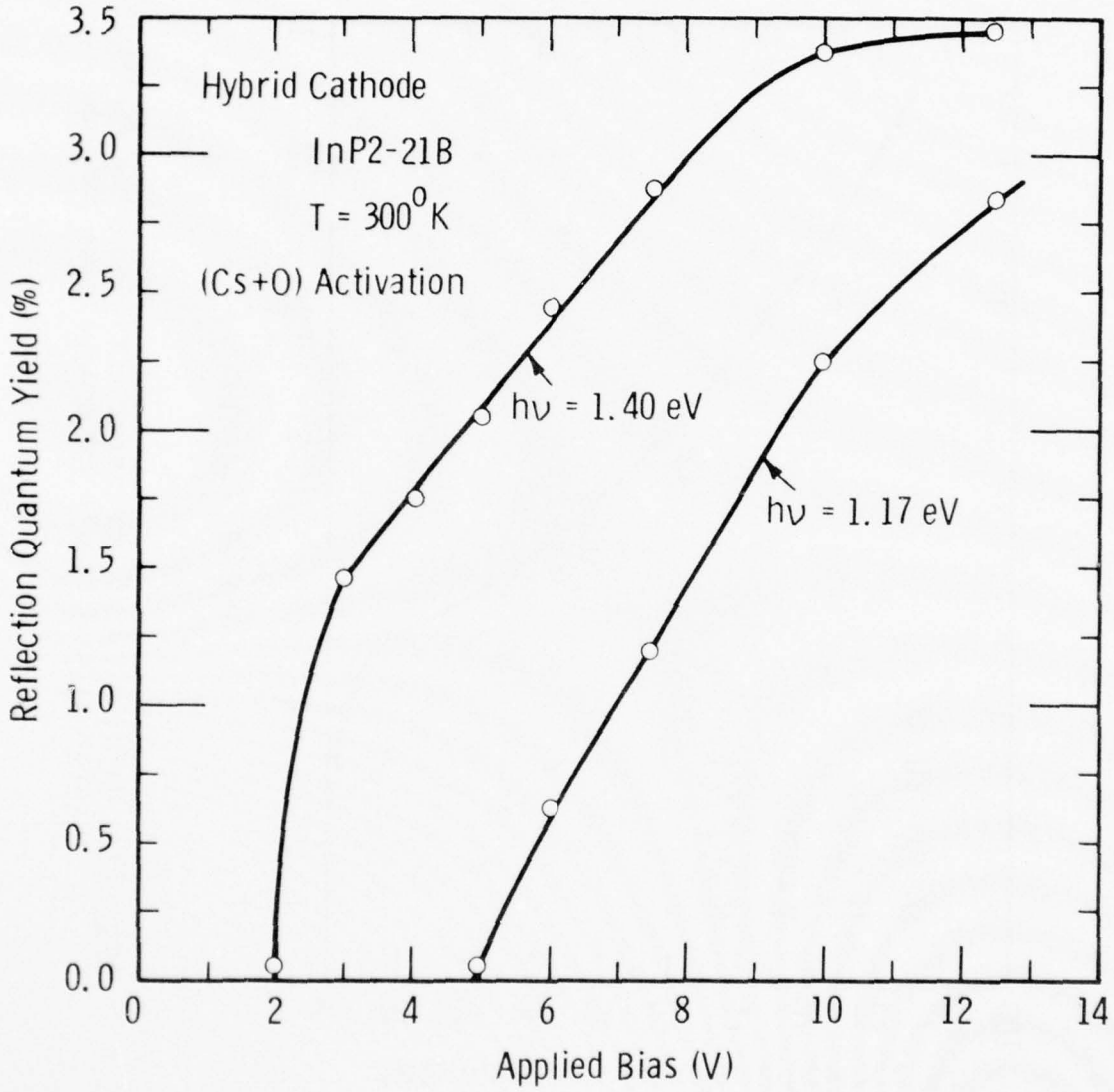

Fig. 48. Reflection-mode yield at 1.40 and 1.17 eV photon energy vs applied bias from a hybrid heterojunction cathode.

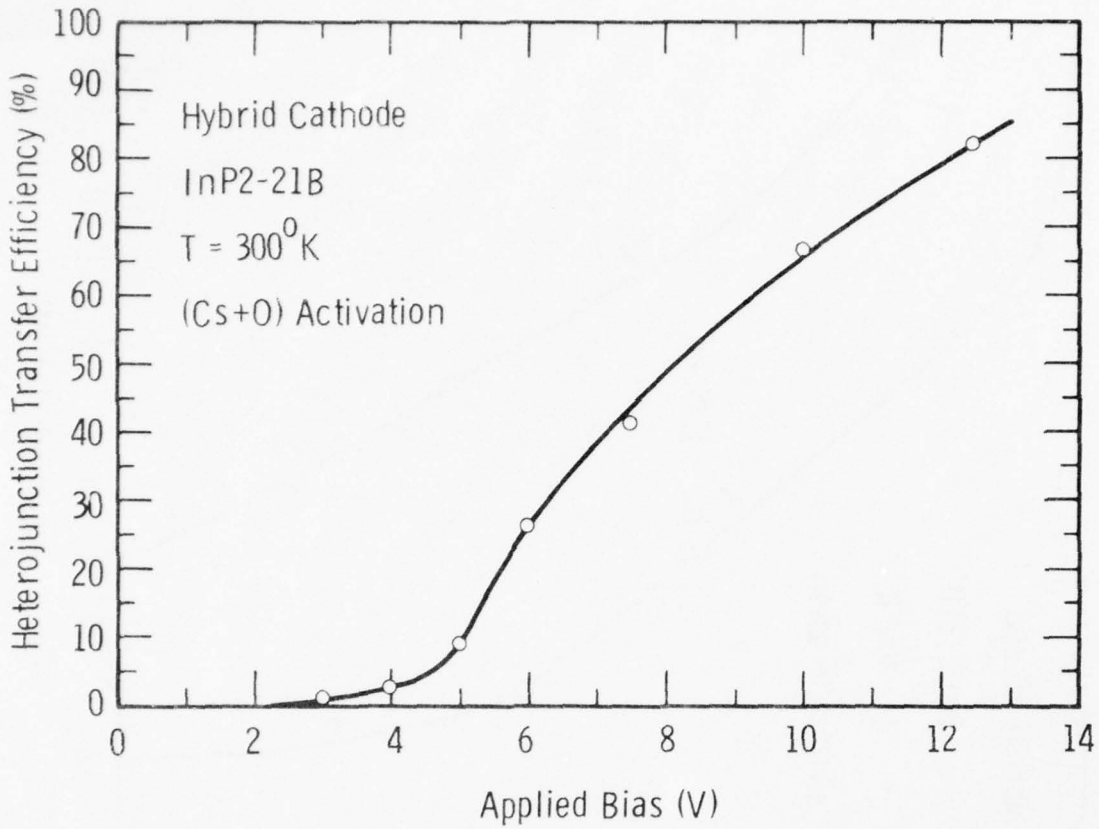

Fig. 49. Heterojunction transfer efficiency vs applied bias from a hybrid heterojunction cathode.

AD-A059 960 VARIAN ASSOCIATES PALO ALTO CALIF F/G 17/5
1.06-MICRON III-V PHOTOCATHODE DEVELOPMENT.(U)
MAY 78 J S ESCHER, P E GREGORY, S B HYDER F33615-76-C-1351
UNCLASSIFIED AFAL-TR-78-78 NL

2 OF 2
ADA
059960

END
DATE
FILMED
12-78
DDC

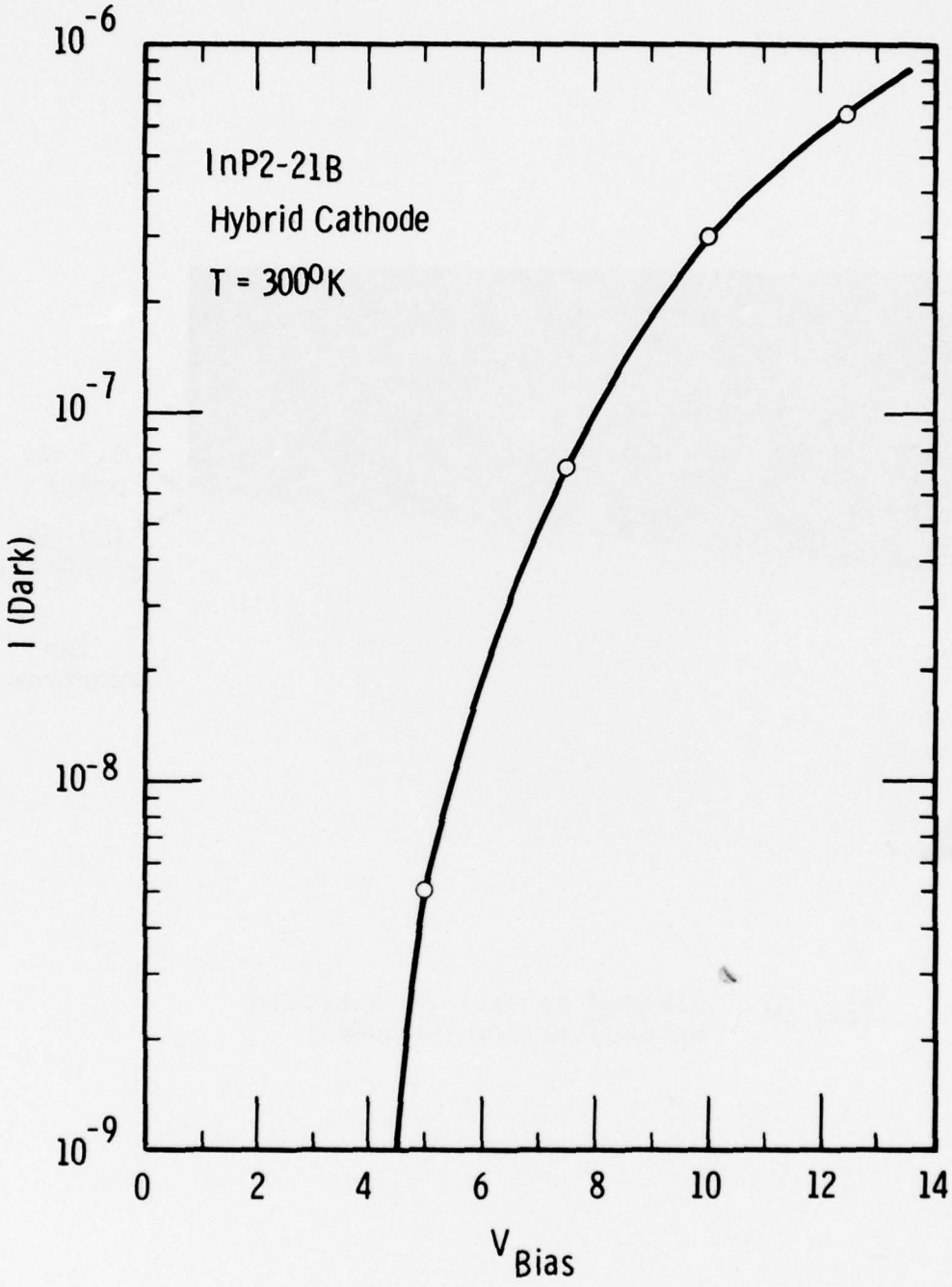

Fig. 50. Dark current emission vs applied bias from a hybrid heterojunction cathode at 300°K.

Fig. 51. Cleaved section of a hybrid heterojunction cathode.

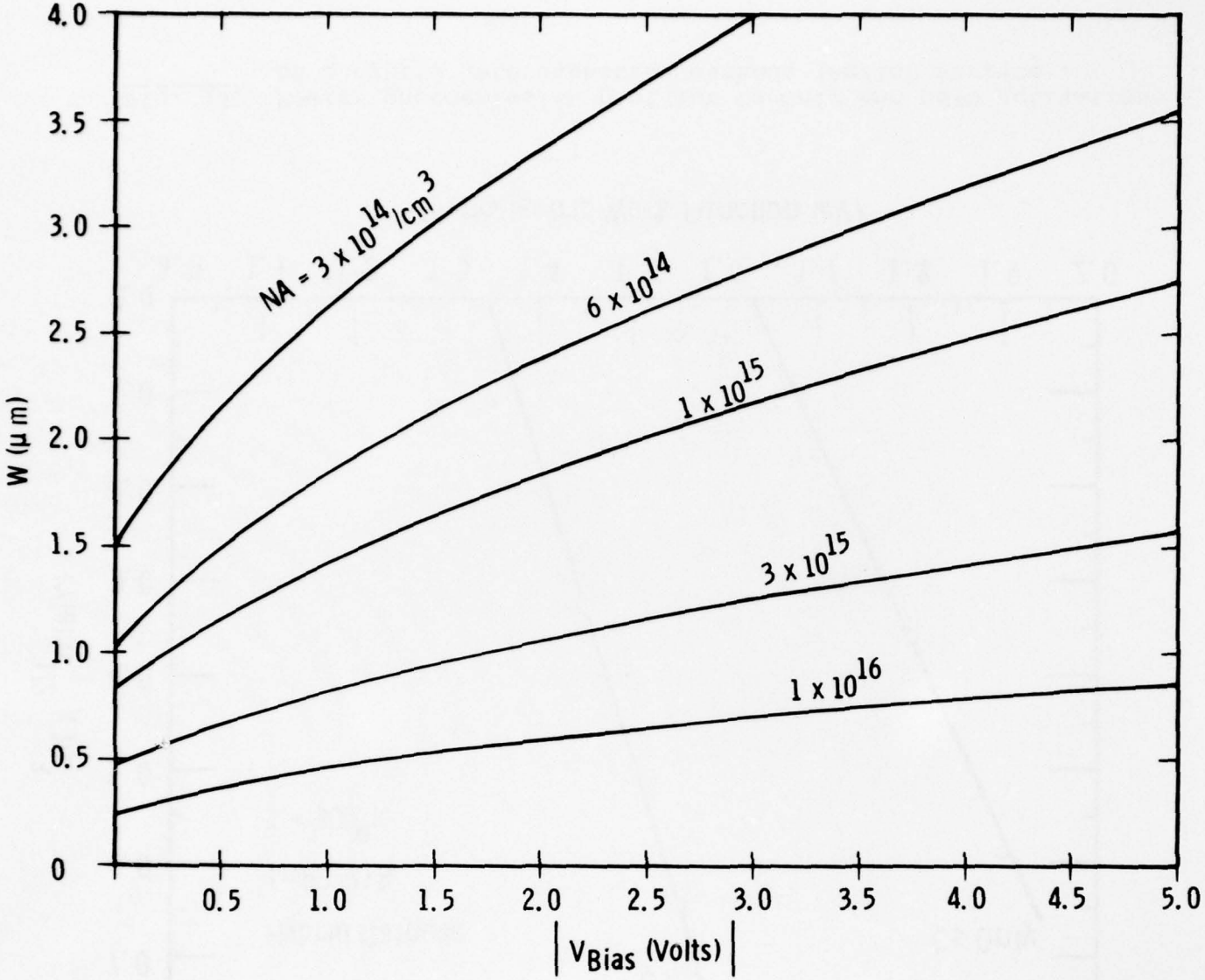

Fig. 52. Depletion layer width, W, versus applied reverse bias, V_{bias}, for an Ag-InP Schottky-barrier contact at various acceptor doping concentrations, N_A.

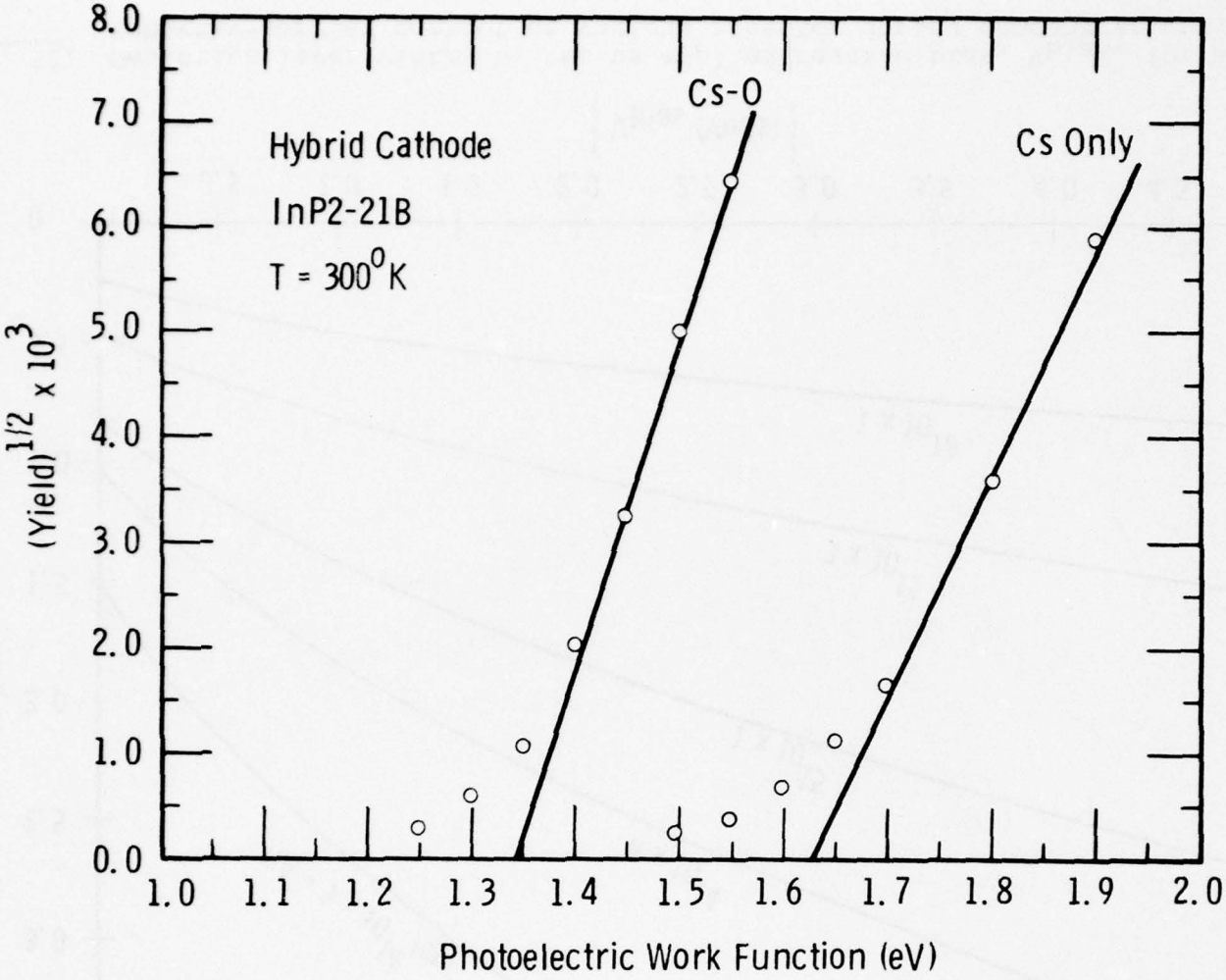

Fig. 53. Fowler photoemission plot for Cs-only and Cs+O activations on a hybrid heterojunction cathode (Ag/InP surface).

vs 610°C normally used. Presumably a slight oxide remained on the surface of this cathode which upset the normal Cs-O activation layer effectiveness. The lower heat cleaning temperature was a deliberate attempt to overcome another phenomenon discussed below.

It was often observed on Auger analysis that a significant Auger In signal could be seen when looking at the Ag film surface. Figure 54 shows an example of this for a relatively thick Ag film on InP. It was further found that the photoelectric threshold on the Cs-O activated Ag film surface was a function of the Ag film thickness. Figure 55 shows this phenomenon in terms of photoelectric threshold vs In/Ag Auger peak height ratio. Auger depth profile analysis through a thin film Ag/InP interface further demonstrates the In outdiffusion process. See Fig. 56.[64] The lower heat cleaning temperature used for cathode #2-21B was an attempt to leave a slight surface oxide layer in order to prevent the In diffusion phenomenon. In practice, the oxide was not successful in lowering the photoelectric work function on the Ag surface. Further work is in progress on different Schottky-barrier metals and activation procedures in order to improve this situation.

Despite a few unusual features, the results from the hybrid heterojunction cathode are extremely important in clearly demonstrating the feasibility and potential of a heterojunction TE cathode. Certainly much of the experience in materials growth and device testing gained from the InP/InGaAsP can be carried over to the InGaP/InGaAs cathode.

3.7 Photoemission Studies on p-InGaP Emitter Cathodes

TE photoemission was successfully achieved from p-InGaP emitter cathodes during this reporting period. A peak reflection mode TE yield of 1% was measured at 300°K.

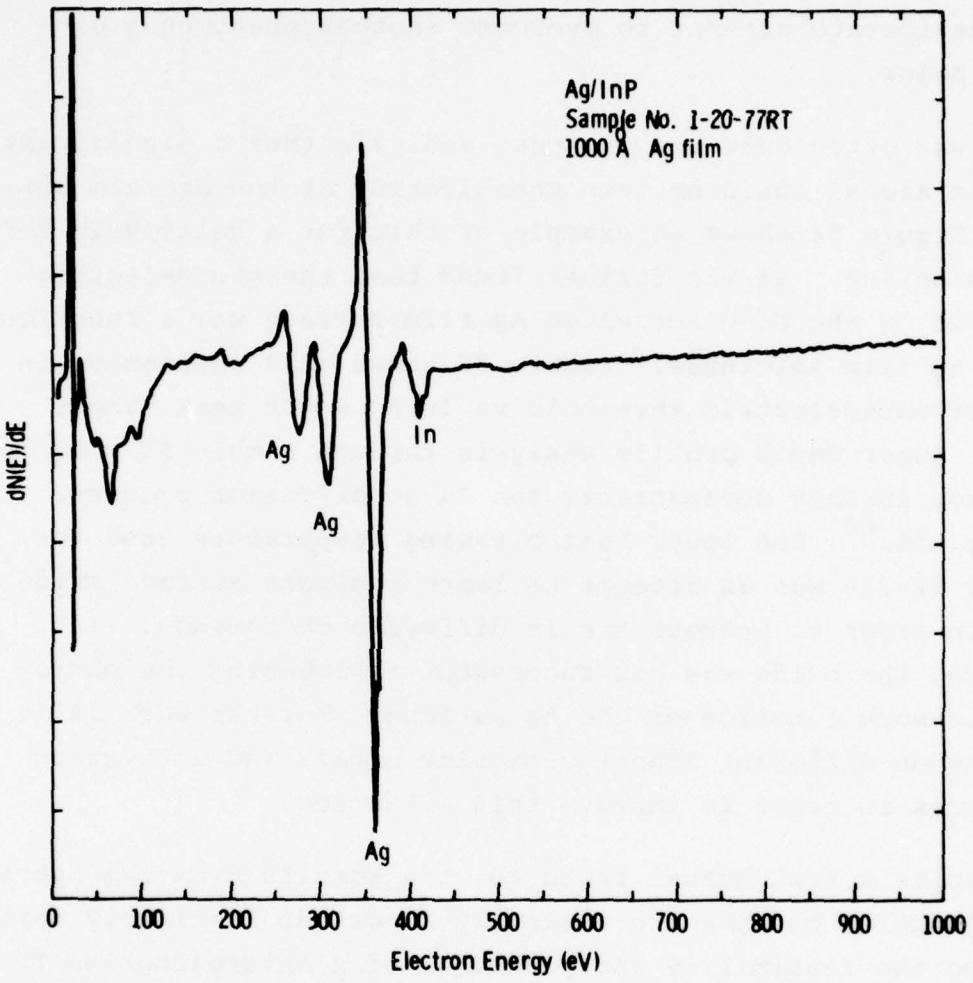

Fig. 54. Auger spectrum from the surface of a Ag/InP cathode showing In on the Ag film surface.

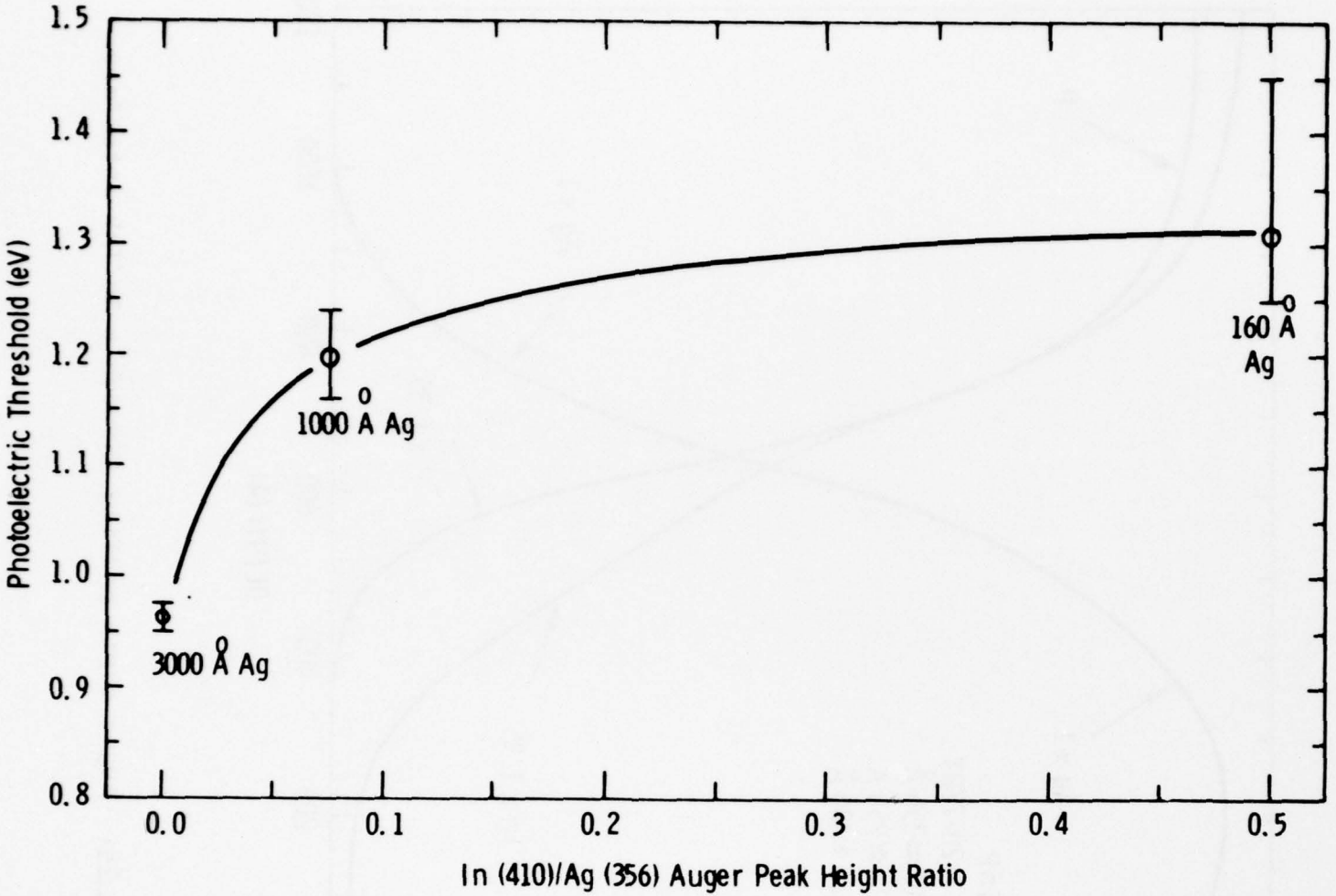

Fig. 55. In/Ag Auger peak height ratio vs photoelectric threshold for 3000, 1000, and 160 Å Ag films on InP.

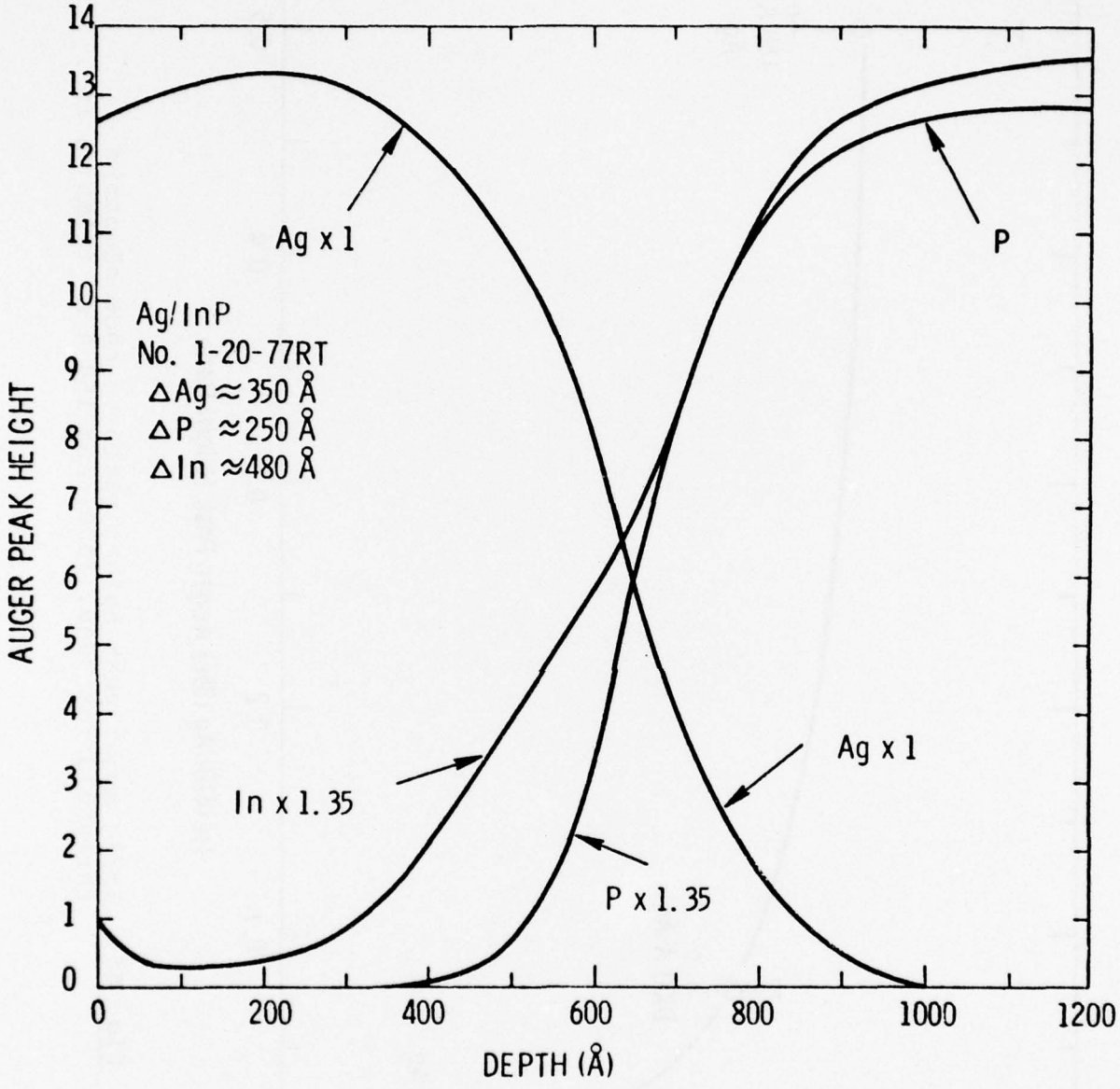

Fig. 56. Auger depth profile through a Ag/InP interface.

A total of 18 p-InGaP cathodes have been vacuum tested since the VPE reactor became fully operational. Four of those cathodes demonstrated some field-assisted photoemission thereby firmly establishing the feasibility of InGaP as a TE emitter. The InGaP emitters tested had direct bandgaps between 1.6 and 1.8 eV and were Zn-doped p-type. Most cathodes tested were grown on (100)-oriented p^+ GaAs substrates. Figures 57 and 58 show field-assisted photoemission from p-InGaP sample #2-17 for Cs-only and Cs+O activation states. A bandgap of approximately 1.7 eV is clearly seen from the yields under bias conditions. The Cs+O yield under bias conditions is somewhat unusual in that the 10-V yield shows a slight bandgap shift to lower energy and the yield for photon energies less than 1.7 eV is field-assisting. The apparent bandgap shift could be due to slight compositional variations within the cathode bulk which become apparent under bias conditions. It is also possible that, inadvertently, the monochromator beam spot had moved to a different position for the no-bias and with-bias yields. The same thing could have happened between taking the 5-V and 10-V yield curves in Fig. 58.

Figures 59 and 60 are reflection-mode yield curves from a p-InGaP emitter cathode for Cs-only and Cs+O activations. These data are quite interesting in that this particular InGaP emitter was grown on a Cr-doped InGaAs layer previously grown in another VPE reactor. The reason for growing on an InGaAs ($\approx$ 1.15 eV) layer was two-fold. The main reason was that it was becoming clear from both the photoemission results and surface Schottky-barrier measurements that InGaP layers grown on the p^+ GaAs substrate material were often coming out much too high p-type for satisfactory TE photoemission experiments. Apparently Zn from the substrate was diffusing rapidly into the InGaP layer during growth. By growing on a thick (10-15 microns) InGaAs/GaAs "substrate" the Zn diffusion problem is much reduced. (Recall that n-type substrates are not a good choice for TE photoemission experiments due to the cold-cathode effect

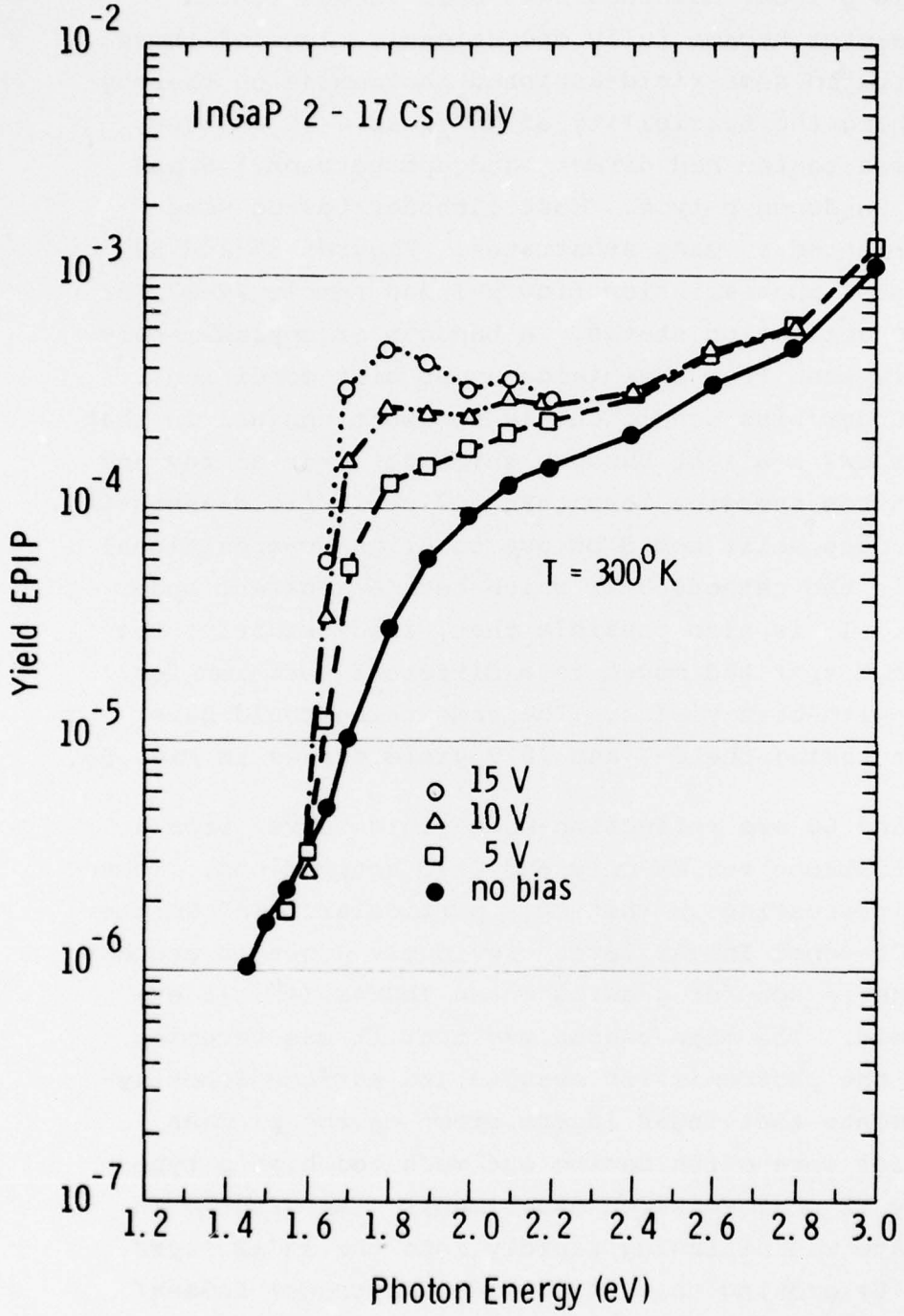

Fig. 57. Reflection-mode quantum yield from a p-InGaP/GaAs direct emitter cathode for Cs-only activation.

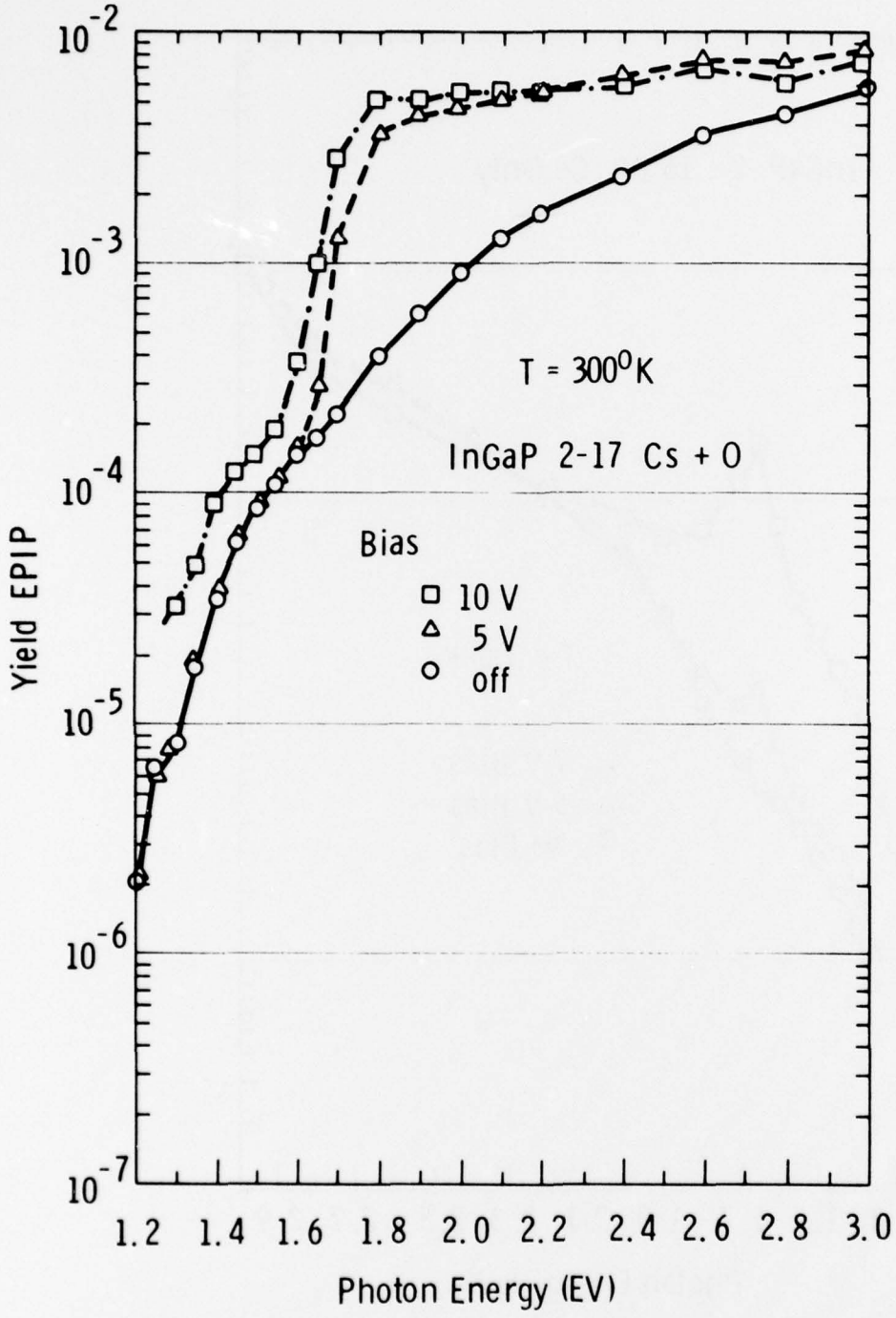

Fig. 58. Reflection-mode quantum yield from a p-InGaP/GaAs direct emitter cathode for Cs+O activation.

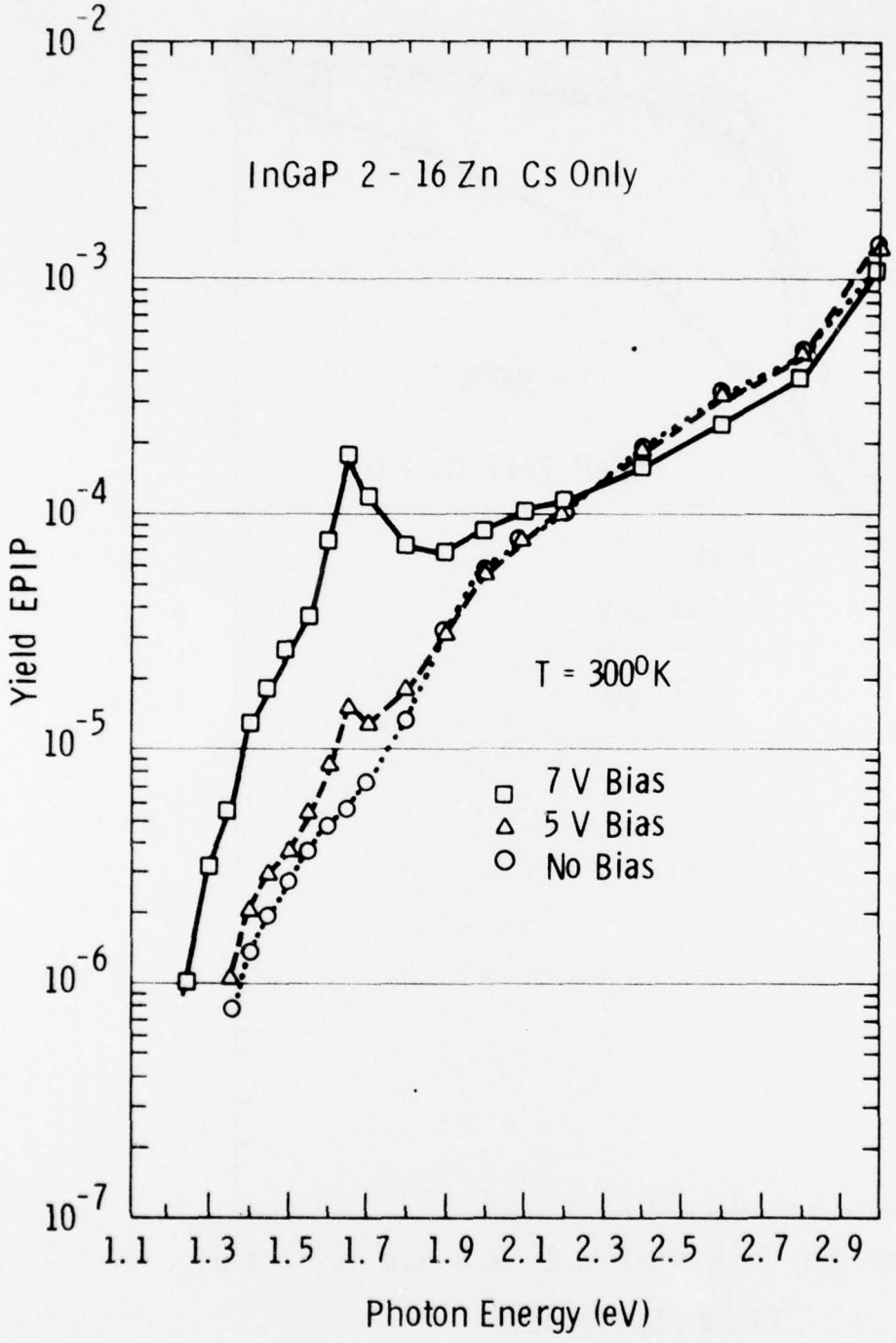

Fig. 59. Reflection-mode quantum yield from a p-InGaP/InGaAs/GaAs cathode for Cs-only activation.

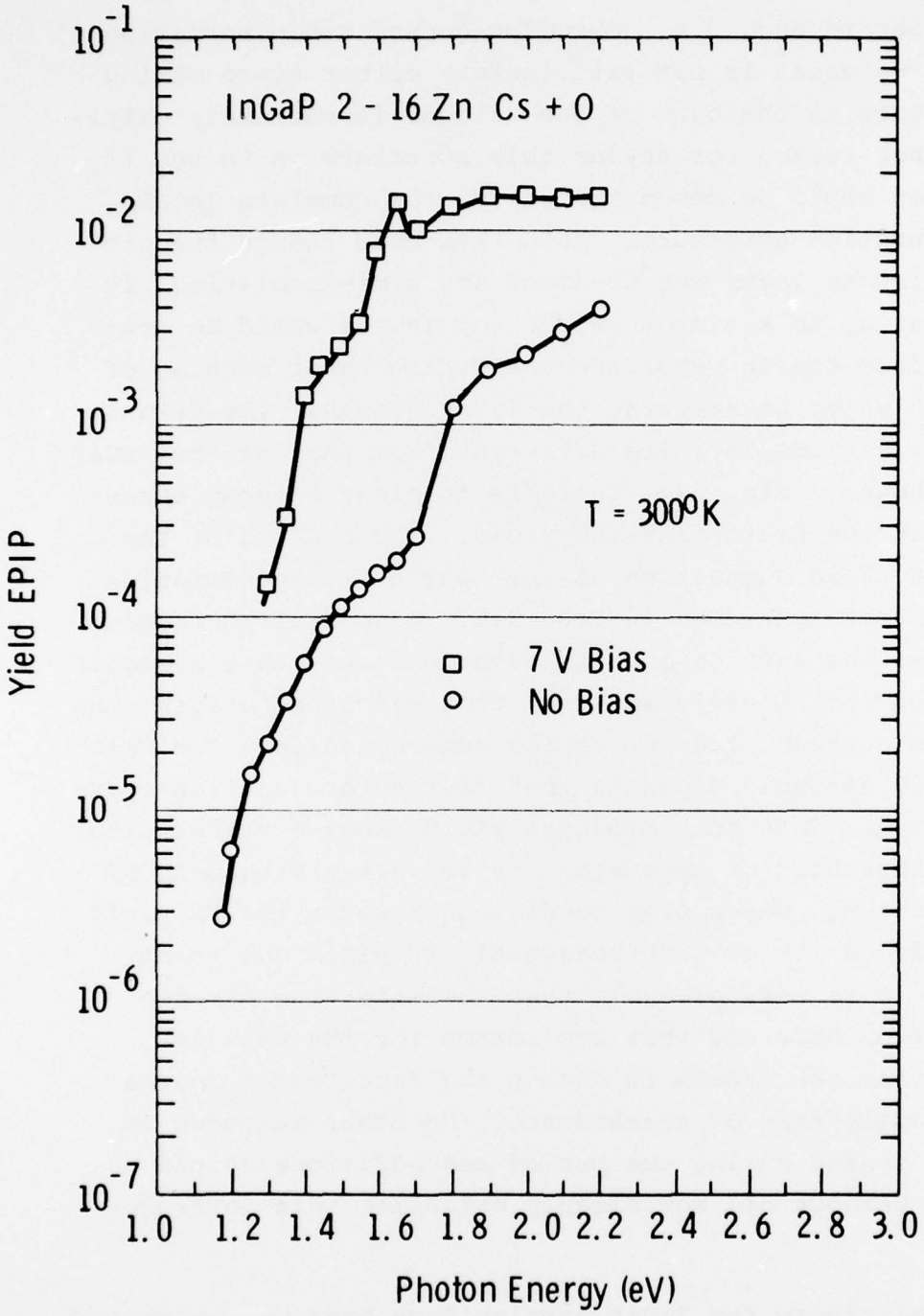

Fig. 60. Reflection-mode quantum yield from a p-InGaP/InGaAs/GaAs cathode for Cs+O activation.

discussed earlier in Sec. 3.5. Chromium-doped, semi-insulating GaAs substrate material is not satisfactory either since making electrical contact to the back of the cathode is extremely difficult.) The other reason for trying this structure is to see if TE photoemission could be demonstrated for the complete InGaP/InGaAs heterojunction structure. Note that even though the previously grown InGaAs layer was Cr-doped and semi-insulating, it is possible that up to a micron of the top InGaAs would be converted p-type from the Zn vapor present during vapor etching of the "substrate" prior to starting the InGaP growth. The Cs-only yield from this cathode is quite different from that of the InGaP/GaAs cathode shown in Fig. 57. There is no clear bandgap threshold apparent in the field-assisted yield. The peaking of the yield near 1.70 eV is suggestive of the nonlinear photoemission vs intensity effect mentioned in Sec. 3.5. A spatial photoemission scan across the surface of this cathode showed that a significant fraction of the TE yield was from photoelectrons originating off the Ag film surface, i.e. primarily edge emission. The Cs+O yield in Fig. 60 strongly suggests that true heterojunction operation is achieved. Note the zero bias yield shows a rather clear photoemission threshold of approximately 1.7 eV--the bandgap of the p-InGaP emitter. Under bias conditions however the TE yield extends well beyond 1.7 eV with reasonable TE yield out to at least 1.4 eV. It is very probable that there is true heterojunction operation here and that the reason for the rapidly falling yield from the InGaAs is due to the fact that p-InGaAs region is extremely thin or nonexistent. No other cathodes of this type were tested during the period and additional yield data from this cathode did not clearly establish this interpretation.

Although relatively few InGaP samples have been vacuum tested to date, the early results are encouraging. There is no doubt that significant improvements will come in the yield from InGaP

emitters with further materials work and optimization of the complete InGaP/InGaAs heterojunction cathode.

3.8 Photoemission from a p-InGaP/p-InGaAs Heterojunction Cathode

In this final section very recent results (January 1978) are presented on a p-InGaP/p-InGaAs TE heterojunction cathode which clearly establishes the feasibility of this cathode design. These post report deadline results are included because of their importance in demonstrating the operation and potential of the InGaP/InGaAs cathode.

The most recent materials work has progressed to growing the complete InGaP/InGaAs/GaAs structure in the same VPE system. Growth of InGaAs/GaAs is a relatively mature technology in this and other laboratories. Therefore once InGaP/GaAs was under reasonable control the final step to growing the complete heterojunction cathode was not too difficult. (The VPE system itself had been designed from the beginning to grow InGaAs as well as InGaP.) A number of complete cathodes have been fabricated and two of these vacuum tested. Both demonstrated TE photoemission and heterojunction operation in that yield from the InGaAs was significant. Results on one of these cathodes (#6-7B) is discussed below.

Figure 61 shows the experimental reflection-mode yield from the second complete p-InGaP/p-InGaAs cathode tested to date. The yield is taken at 300°K and with an O.D. = 1.0 filter in the monochromator due to a nonlinear intensity vs photosignal behavior discussed in Sec. 3.5. There are several features of the yield in Fig. 61 that should be pointed out. First, the most important fact is that for modest bias voltages (i.e. 3-5 V) the heterojunction transfer efficiency for electrons to cross from the InGaAs (absorber) into the InGaP (emitter) is excellent. Therefore, as already seen with the InP/InGaAs heterojunction cathode,

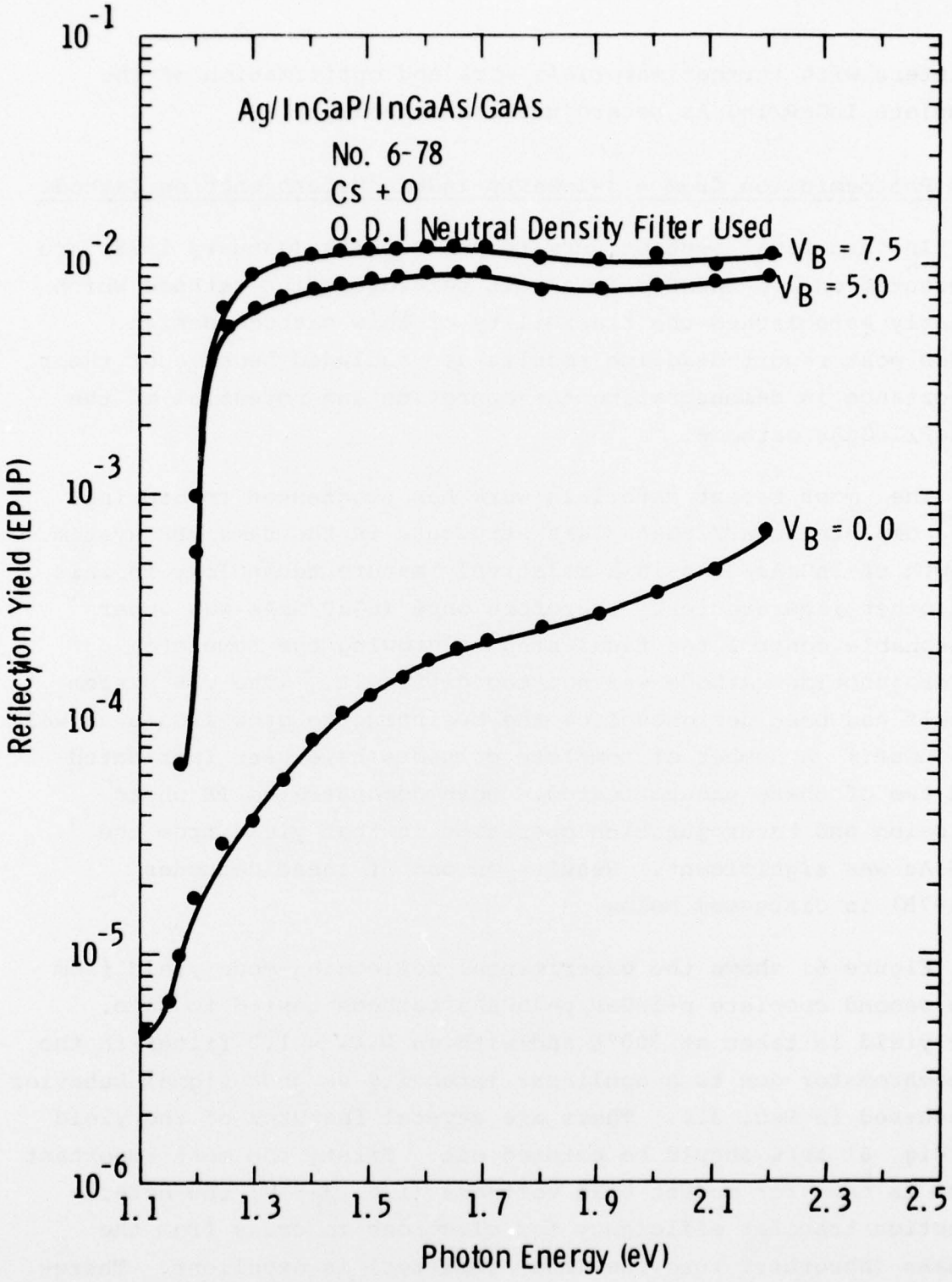

Fig. 61. Recent reflection-mode yield from a p-InGaP/InGaAs/GaAs cathode for Cs+O activation.

the heterojunction operation of the cathode is established. Second, the lower bias yield (not shown in Fig. 61) does not show a clear break at the InGaP bandgap suggesting that even for these lower bias yields the InGaP is fully depleted. (That there is InGaP on the surface has been established both by Auger analysis and subsequent cleaving of the sample.) Third, it is clear that the bandgap of the InGaAs absorber layer is slightly too high for 1.06-micron detection. This is not a problem and can easily be adjusted. Finally, the 1.0% yield from this cathode is quite encouraging. The VPE growth of the complete cathode is coming along well but certainly is not fully optimized yet. As more growth experience is achieved and the cathode optimized in terms of emitter thickness, doping, etc., the overall yield will undoubtedly improve.

4. CONCLUSIONS AND RECOMMENDATIONS

During the first year of effort on this program three different types of TE 1.06-micron photocathodes have been investigated. With a relatively small materials effort, both the p-InGaAsP direct emitter TE cathode and the hybrid p-InP/p-InGaAsP heterojunction TE cathode have demonstrated $\geq$ 2.0% yield in the reflection mode at 1.06 micron in an experimental ultrahigh vacuum system. It is apparent however that in order to achieve even higher 1.06-micron yields, the surface escape probability from the electron emitting surface must be improved. Future work in this area should probably focus on the Schottky-barrier / semiconductor interface. Different Schottky-barrier metals, geometries, etc. should be investigated in addition to trying different crystallographic orientations for the emitting face. Various vacuum heat cleaning procedures, e.g. sputtering vs high temperature heating only, should be evaluated.

Another significant accomplishment during this period is the clear demonstration of the operation of the p-InP/p-InGaAsP TE heterojunction cathode. This combination offers, in principle, a higher performance cathode in that the functions of photogeneration and electron emission are accomplished in two separately grown layers. Engineering the cathode especially for 1.06-micron detection is now a much more realistic concept.

By far the bulk of the materials effort this period has been on the construction and employment of a vapor phase epitaxy InGaP-InGaAs system. Reasonably good-looking InGaP/GaAs structures have been grown in addition to a InGaP/InGaAs/GaAs structure. Vacuum photoemission experiments have clearly demonstrated the feasibility of InGaP as a TE emitter and the only InGaP/InGaAs heterojunction cathode vacuum tested suggested that yield from the InGaAs was being observed. Essentially, the VPE reactor is ready to go on to growth of the complete InGaP/InGaAs hetero-

junction cathode. A fair test of InGaP as a TE emitter is only now becoming possible as the various growth system refinements yield higher and higher quality p-InGaP. A clear demonstration of the InGaP/InGaAs heterojunction cathode, with 1.06-micron response, is very close. (See Sec. 3.8.)

The progress achieved to date is encouraging and a continued research effort concentrating on the p-InGaP/p-InGaAs heterojunction cathode should be pursued.

REFERENCES

1. See, for example, A. H. Sommer, Photoemissive Materials, John Wiley & Sons, Inc. New York, 1968.

2. R. E. Simon and W. E. Spicer, Phys. Rev. 119, 621 (1960).

3. R. E. Simon and W. E. Spicer, J. Appl. Phys. 31, 1505 (1960).

4. P. R. Thornton and D. C. Northrup, Solid State Electron. 8, 437 (1965).

5. I. G. Davies and P. R. Thornton, Appl. Phys. Lett. 10, 249 (1967).

6. S. A. Ward, T. E. Fischer, and W. B. Nowak, CBS Laboratories, Technical Report AFAL-TR-69-161, June 1969, on contract AF33 (615)-3638.

7. R. L. Bell, Negative Electron Affinity Devices, Clarendon Press, Oxford, 1973.

8. J. S. Escher, RCA Laboratories, Final Report, December 1973, contract DAAK02-72-C-0412.

9. F. G. Allen, J. Schwank, I. Shahriary, and K. Venkateswaran, University of California, Los Angeles, Final Report, June 1976, contract DAAK02-72-C-0410.

10. H. G. White and R. A. Logan, J. Appl. Phys. 34, 1990 (1963).

11. T. Itoh, I. Matsuda, and K. Hasegawa, J. Appl. Phys. 38, 3395 (1967). See also, J. Appl. Phys. 41, 1945 (1970).

12. A. L. Musatov and L. N. Shulepov, Sov. Phys. Solid State 12, 2711 (1971).

13. I. J. D'Haenens, J. A. Roth, and C. L. Anderson, Hughes Research Laboratories, Final Technical Report on contract DAAK02-72-C-0442. See also, Final Technical Report on contract DAAK02-72-C-0147.

14. N. A. Foss, J. Appl. Phys. 42, 3762 (1971).

15. A. G. Milnes, D. I. Feucht, and P. K. Govil, Carnegie-Mellon Institute, Final Report, June 1974, on contract DAAK02-72-C-0206. See also Appl. Phys. Lett. 19, 383 (1971).

REFERENCES (Cont.)

16. R. Sahai, J. S. Harris, R. C. Eden, L. O. Bubulac, and J. C. Chu, Crit. Rev. Solid State Sci. 5, 565 (1975). See also, contract reports under ARPA contract DAAK02-73-C-0231.

17. D. K. Schroder, R. N. Thomas, J. Vine, and H. C. Nathanson, IEEE Trans. Electron Devices, ED-21, 785 (1974).

18. P. R. Thorton, Stanford Research Institute, Final Report, December 1973, contract DAAK02-72-C-0149.

19. I. J. D'Haenens, J. A. Roth, and C. L. Anderson, Hughes Research Laboratories, Final Report on contract DAAK02-72-C-0442 (1975). See also, Final Report on contract DAAK02-72-C-0147.

20. See, for example, J. J. Uebbing and L. W. James, J. Appl. Phys. 41, 4505 (1970).

21. See, for example, C. R. Crowell and S. M. Sze, in Physics of Thin Films (Academic Press, New York, 1967), Vol. 4, p. 325.

22. See, for example, R. L. Bell, L. W. James, G. A. Antypas, J. Edgecumbe, and R. L. Moon, Appl. Phys. Lett. 19, 513 (1971); also D. G. Fisher, R. E. Enstrom, J. S. Escher, and B. F. Williams, J. Appl. Phys. 43, 3815 (1972).

23. R. L. Bell, L. W. James, and R. L. Moon, Appl. Phys. Letters, 25, 645 (1974).

24. L. W. James, J. P. Van Dyke, F. Herman, and D. M. Chang, Physical Review B, 1, 3998 (1970).

25. R. H. Fowler, Physical Review, 38, 45 (1931).

26. R. L. Bell and J. J. Uebbing, Appl. Phys. Letters, 12, 76 (1968).

27. G. A. Antypas, R. L. Moon, L. W. James, L. J. Edgecumbe, and R. L. Bell, in Gallium Arsenide and Related Compounds, 1972, (Conf. Series #17, IPPS, London, 1973), p. 48.

28. R. Sankaran, G. A. Antypas, R. L. Moon, J. S. Escher, and L. W. James, J. Vac. Sci. Technol., 13, 932 (1976).

REFERENCES (cont.)

29. G. A. Antypas and L. Y. Shen, in Gallium Arsenide and Related Compounds, 1976, (Inst. Phys. Conf. Ser. #33b, London, 1977), p. 96.

30. J. S. Escher, R. D. Fairman, G. A. Antypas, R. Sankaran, L. W. James, and R. L. Bell, CRC Rev. Solid State Sci. 5, 577 (1975).

31. Work toward a passive night vision imaging device sensitive in the 1-2 micron range is under current investigation in this laboratory. This work is funded by ARPA and is monitored by NVL: contract no. DAAK02-74-C-0132. The hetrojunction cathode is the primary emphasis under this contract.

32. M. T. Pakhomov, A. YE. Melamid, and YA. B. Gerchikov, Radio Eng. and Electron Phys. 20, 147 (1975).

33. Varian LSE, 601 California Avenue, Palo Alto, CA 94304.

34. J. S. Escher, G. A. Antypas, and J. Edgecumbe, Appl. Phys. Letters 29, 153 (1976).

35. J. S. Escher and G. A. Antypas, Appl. Phys. Letters 30, 314 (1977).

36. R. E. Enstrom, D. Richman, M. S. Abrahams, J. R. Alpert, D. G. Fisher, A. H. Sommer, and F. F. Williams, Proceedings of the Third International Symposium on Gallium Arsenide and Related Compounds, IPPS, London (1970).

37. S. B. Hyder, J. Electrochem. Soc. 123, 1503 (1976).

38. J. O. McCaldin, T. C. McGill, and C. A. Mead, Phys. Rev. Lett. 36, 56 (1976).

39. C. A. Mead, Solid-State Electron. 9, 1023 (1966).

40. J. S. Escher, L. W. James, R. Sankaran, G. A. Antypas, R. L. Moon, and R. L. Bell, J. Vac. Sci. Technol. 13, 874 (1976).

41. G. A. Antypas and J. Edgecumbe, J. Crystal Growth 34, 132 (1976).

REFERENCES (Cont.)

42. Note that 1.21 eV at 77°K corresponds to 1.16 eV at 300°K which is nearly ideal for 1.06 micron detection.

43. G. B. Stringfellow, P. F. Lindquist, and R. A. Burmeister, J. Electronic Materials 1, 437 (1972).

44. C. J. Nuese, D. Richman, and R. B. Clough, Met. Trans. 2, 789 (1971).

45. V. S. Ban and M. Ettenberg, J. Phys. and Chem. of Solids 34, 1119 (1973).

46. H. Seki and S. Minegawa, Japanese J. of Phys. 11, 850 (1972).

47. A. G. Sigai, C. J. Nuese, R. E. Enstrom, and T. Zamerowski, J. Electrochem. Soc. 120, 947 (1973).

48. R. E. Enstrom, C. J. Neuse, V. S. Ban, and J. R. Appert, Proc. 4th Symposium on GaAs, 1972, (Institute of Physics, London) p. 37.

49. H. Kressel, C. J. Nuese, and I. Ladany, J. Appl. Phys. 44, 3266 (1973).

50. M. Ettenberg and G. H. Olsen, J. of Appl. Phys 48, 4275 (1977).

51. L. A. Volkov, F. P. Kesamanly, V. F. Kovalenko, I. E. Maronchuk, and L. G. Shepel, Sov. Phys. Semicond. 11, 732 (1977).

52. R. L. Anderson, Solid State Electron. 5, 341 (1962).

53. A. G. Milnes and D. L. Feucht, Heterojunction and Metal-Semiconductor Junctions, (Academic Press, New York, 1972).

54. B. L. Sharma and R. K. Purohit, Semiconductor Heterojunctions, (Pergamon Press, New York, 1974).

55. See, for example, W. R. Frensley and H. Kroemer, J. Vac. Sci. Technol. 13, 810 (1976). W. A. Harrison, J. Vac. Sci. Technol. 14, 1016 (1977). W. R. Frensley and H. K. Kroemer, Phys. Rev. B 16, 2642 (1977).

56. W. G. Oldham and A. G. Milnes, Solid State Electron. 6, 121 (1963).

REFERENCES (Cont.)

57. D. T. Cheung, S. Y. Chiang, and G. L. Pearson, Solid State Electron. 18, 263 (1975).

58. R. Dingle, A. C. Gossard, and W. Wiegmann, Phys. Rev. Lett. 34, 1327 (1975).

59. E. A. Rozek, N. Holonyak, B. A. Vojak, G. E. Stillman, J. A. Rose, D. L. Keune, and J. D. Fairing, Appl. Phys. Lett. 31, 288 (1977).

60. S. M. Sze, Physics of Semiconductor Devices, (John Wiley & Sons, New York, 1969), p. 370.

61. The idea of a "double-transfer" heterojunction TE cathode was discussed in Sec. 3.3.1, Varian Technical Proposal No. 2274, August 1976.

62. J. S. Escher and R. Sankaran, Appl. Phys. Lett. 29, 87 (1976). Also see Appendix B, Varian Technical Proposal No. 2274, August 1976.

63. An incident photon irradiance of $\sim 1 \times 10^{-4}$ W/cm^2 generates only $\sim 10^{-10}$ excess carriers/cm^3. See Ref. 30.

64. Figures 50 and 51 are taken from Semi-Annual Technical Report No. 5, April 1977, and Figure 52 from Quarterly Technical Report No. 7, July 1977, under contract DAAK02-74-C-0132. See Ref. 31.

☆U.S.Government Printing Office: 1978 — 757-080/69